

**NEW DEVELOPMENTS IN THE COORDINATION
CHEMISTRY OF GOLD(I), GOLD(II) AND GOLD(III)
WITH C-, N-, P- AND S-DONOR LIGANDS**

by

JACORIEN COETZEE

THESIS

submitted in fulfilment of the requirements
for the degree of



in the

FACULTY OF SCIENCE

at the

UNIVERSITY OF STELLENBOSCH

SUPERVISOR: DR. S. CRONJE

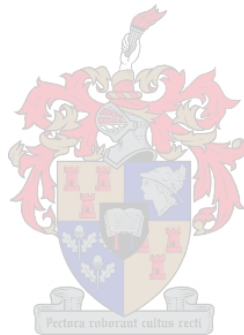
CO-SUPERVISOR: PROF. H.G. RAUBENHEIMER

MARCH 2007

Declaration

I, the undersigned, hereby declare that the work contained in this thesis is my own original work and that I have not previously in its entirety or in part submitted it at any university for a degree.

Signature: .....
Date: 2007-03-01



Copyright © 2007 Stellenbosch University

All rights reserved

SUMMARY

A comprehensive, comparative structural study of gold(I), gold(II) and gold(III) compounds with the general formula $[\text{Au}_x(\text{C}_6\text{F}_5)_y(\text{tht})_z]$ (tht = tetrahydrothiophene) was performed. The series of compounds included the unprecedented dinuclear gold(II) compound, tetrakis(pentafluorophenyl)bis(tetrahydrothiophene)digold(II), which could be prepared in a rational manner. This very unique compound represents the first example of an unbridged dinuclear gold(II) compound in which the gold(II) centres are not stabilised by chelating ligands. Formation of this compound was postulated to have taken place by radical pentafluorophenyl (pfp) ligand migration along with $\text{Au}^{\text{II}}-\text{Au}^{\text{II}}$ bond formation. It may therefore be regarded as a rare example of labile behaviour by a generally inert pfp ligand. In addition to this compound, the crystal and molecular structures of the well-known gold(I) and gold(III) precursor compounds, (pentafluorophenyl)(tetrahydrothiophene)gold(I) and tris(pentafluorophenyl)(tetrahydrothiophene)gold(III) were carried out and are described for the first time. The latter underwent a unique mononuclear ligand rearrangement (metathesis or disproportionation) reaction in solution to yield the novel rearrangement product, bis(pentafluorophenyl)bis(tetrahydrothiophene)gold(III)tetrakis(pentafluorophenyl)gold(III). In all the complexes, the Au–C and Au–S bond lengths displayed a variation which appears to be dependent on the oxidation state of the central gold atom. Both of these bond types were found to decrease in the order $\text{Au(II)} > \text{Au(III)} > \text{Au(I)}$.

In another important focus of the study, ylideneamine functionalised heterocyclic ligands were employed in the preparation of a series of novel gold(I) complexes. No examples of gold(I) compounds derived from this fascinating class of ligands exist in the literature, making the isolation of these compounds a valuable contribution to the field of gold chemistry. In the preparation of the first three members of the series, the important gold(I) precursor compound, (pentafluorophenyl)(tetrahydrothiophene)gold(I), was exploited to prepare the novel compounds, 1,3-dimethyl-1,3-dihydro-benzimidazol-2-ylideneamine(pentafluoro-phenyl)gold(I), 3-methyl-3*H*-benzothiazol-2-ylideneamine(pentafluoro-phenyl)gold(I) and 3,4-dimethyl-3*H*-thiazol-2-ylideneamine(pentafluorophenyl)gold(I). These compounds were fully characterized using standard analytical techniques. Single crystal X-ray structure determinations revealed that coordination of the free ligands to a gold(I) centre does not alter the bond lengths and angles of the ligands significantly. Furthermore, metal coordination does not bring about enhanced electron delocalisation

over the ligand system in the solid state. From the solid state packing of the complexes it was evident that different combinations of intermolecular forces govern the lattice organisation. These included weak aurophilic interactions, π - π interactions and hydrogen bonding.

The series of gold(I) complexes derived from ylideneamine functionalised heterocyclic ligands was further extended by preparing and characterising a number of stable, cationic *N*-coordinated (triphenylphosphine)gold(I) complexes. These complexes are: 1,3-dimethyl-1,3-dihydro-benzimidazol-2-ylideneamine(triphenylphosphine)gold(I) nitrate, 3-methyl-3*H*-benzothiazol-2-ylideneamine(triphenylphosphine)gold(I) nitrate and 3,4-dimethyl-3*H*-thiazol-2-ylideneamine(triphenylphosphine)gold(I) nitrate. Another complement to this unique series, 1,3-dimethyl-1,3-dihydro-benzimidazol-2-ylideneamine-(1,3-di-*tert*-butylimidazol-2-ylidene)gold(I) nitrate, was also prepared and fully characterised. NMR and FT-IR studies of these complexes unearthed interesting phenomena: of all the ligands, 1,3-dimethyl-1,3-dihydro-benzimidazol-2-ylideneamine allows the greatest charge stabilisation through electron delocalisation over the ligand ring system in solution. All complexes however display limited electron delocalisation in the solid state, as was evident from single crystal X-ray structure analysis. Other structural characteristics revealed by these complexes in the solid state included the labilising *trans* influence of the ylideneamines on triphenylphosphine ligands, as was evident from Au-P bond elongation. In addition, the anti-tumour potential of selected compounds against human cervical carcinoma cells was assessed and revealed these compounds to possess limited cytotoxicity. Complexation of the free ligands to (triphenylphosphine)gold(I) however leads to a significant increase in their cytotoxic potency. Finally, deprotonation of the =NH moiety in both neutral free as well as coordinated ylideneamine ligands proved less facile than deprotonation of secondary amine functionalities.

OPSOMMING

'n Omvattende, vergelykende strukturele studie van goud(I)-, goud(II)- en goud(III)-verbindings met die algemene formule $[Au_x(C_6F_5)_y(tht)_z]$ (tht = tetrahydrotiofeen) is uitgevoer. Die reeks van verbindings sluit 'n onbekende dikernige goud(II)verbinding, tetrakis(pentafluorofeniel)bis(tetrahydrotiofeen)digoud(II), wat ook op 'n rasonale wyse berei kon word, in. Hierdie uiters unieke verbinding verteenwoordig die eerste voorbeeld van 'n ongebrugde dikernige goud(II)verbinding waarin die goudkerne nie deur middel van chelerende ligande gestabiliseer word nie. Die vorming van hierdie verbinding vind waarskynlik plaas by wyse van radikaal pentafluorofeniel (pff) migrasie wat gepaardgaan met die vorming van 'n Au^I-Au^I binding. Dit kan derhalwe beskou word as 'n seldsame voorbeeld van labiele gedrag deur die, normaalweg inerte, pff-ligand. Terselfdetyd is die kristal en molekulêre strukture van die welbekende goud(I) en goud(III) uitgangstowwe (pentafluorofeniel)(tetrahydrotiofeen)goud(I) en tris(pentafluorofeniel)(tetrahydrotiofeen)-goud(III) vir die eerste keer beskryf. Laasgenoemde ondergaan 'n ongewone monokernige, ligandherranskikking (metatese of disproporsionering) in oplossing om die nuwe ioniese produk bis(pentafluorofeniel)bis(tetrahydrotiofeen)goud(III)tetrakis(pentafluorofeniel)goud(III) te lewer. Die Au-C en Au-S bindingslengtes in al die komplekse toon 'n variasie wat afhanklik is van die oksidasie toestand van die sentrale goud atoom. Beide hierdie bindingslengtes neem af in die volgorde $Au(II) > Au(III) > Au(I)$.

Ilideenamien-gefunksionaliseerde heterosikliese ligande is as ander hooffokus van hierdie studie gebruik om 'n reeks nuwe goud(I)komplekse te berei. Geen voorbeelde van goud(I)verbindings van hierdie fassineerende klas ligande is nog voorheen gerapporteer nie. Die isolasie van sulke voorbeelde maak dus 'n waardevolle bydrae tot die veld van goudchemie. Die reeds genoemde goud(I) uitgangstof, (pentafluorofeniel)(tetrahydrotiofeen)goud(I), is aangewend in die sintese van die eerste drie lede van die reeks, 1,3-dimetiel-1,3-dihidro-bensimidiasool-2-ilideenamien(pentafluorofeniel)goud(I), 3-metiel-3*H*-bensotiasool-2-ilideenamien(pentafluorofeniel)goud(I) en 3,4-dimetiel-3*H*-tiasool-2-ilideenamien(pentafluorofeniel)goud(I). Hierdie verbindings is volledig gekarakteriseer met behulp van standaard analitiese tegnieke. Enkelkristal X-straaldiffraksie struktuurbepalings van hierdie verbindings onthul dat koördinasie van die ligande aan goud(I)kerne nie tot noemenswaardige veranderinge in die bindingslengtes en bindingshoeke van die ligande aanleiding gee nie. Verder bring metaalkoördinasie ook nie

verhoogde elektrondelokalisering oor die ligandsisteem in die vaste toestand mee nie. Vanuit die pakking van die komplekse in die vaste toestand het dit geblyk dat verskillende kombinasies van intermolekulêre kragte die kristalrooster organiseer. Dit sluit swak ourofiliese interaksies, π - π interaksies en waterstofbindings in.

Die reeks van goud(I)komplekse gemaak uit ilideenamien-gefunksionaliseerde heterosikliese ligande is verder uitgebrei deur 'n aantal stabiele, kationiese *N*-gekoördineerde (trifenielfosfien)goud(I) komplekse te berei en karakteriseer. Dit sluit in: 1,3-dimetiel-1,3-dihidro-bensimidiasool-2-ilideenamien(trifenielfosfien)goud(I) nitraat, 3-metiel-3*H*-bensotiasool-2-ilideenamien(trifenielfosfien)goud(I) nitraat en 3,4-dimetiel-3*H*-tiasool-2-ilideenamien(trifenielfosfien)goud(I) nitraat. Nog 'n toevoeging tot hierdie reeks, 1,3-dimetiel-1,3-dihidro-bensimidiasool-2-ilideenamien(1,3-di-*ters*-butielimidiasol-2-ilideen)goud(I) nitraat, is geïsoleer en ten volle gekarakteriseer. KMR en IR studies van hierdie komplekse het interessante verskynsels na vore gebring: 1,3-dimetiel-1,3-dihidro-bensimidiasool-2-ilideenamien toon die beste ladingstabilisering in oplossing, deur middel van elektron delokalisering oor die ligandring sisteem. Alle komplekse het egter beperkte elektron delokalisering in die vaste toestand soos blyk uit X-straal struktuur analise. In die vaste toestand is 'n labiliserende *trans* invloed van die ilideenamiene op trifenielfosfien ligande duidelik – hierdie verskynsel word gemanifesteer deur Au-P bindingsverlengings. Verder is die anti-tumor potensiaal van geselekteerde verbindings teen menslike servikale kankerselle bepaal. Die bepaling het getoon dat hierdie verbindings oor beperkte sitotoksisiteit beskik. Koördinasie van die vry ligande aan (trifenielfosfien)goud(I) lei egter wel tot 'n noemenswaardige verhoging in hulle sitotoksiese eienskappe. Ten slotte het deprotonering van die =NH eenheid in beide die vry sowel as gekoördineerde ligand moeiliker geblyk as deprotonering van 'n sekondêre amien funksionaliteit.



ACKNOWLEDGEMENTS

There are several people that have meant a great deal to me during the execution of this study and whom have made this a very rewarding and enriching experience on so many levels. I would however like to thank a few people in particular:

First of all I would like to thank my parents for their sustained love and support throughout my studies and for always providing me with an endless sea of opportunities.

My brother and sister, Johannes and Karolien, as well as their spouses, Natasha and Francois: for all your love, support and encouragement.

William for your unconditional love, support and the three wonderful years together. Also, for your endless enthusiasm with regards to this study, constructive criticism and valuable contributions.

All my friends for providing support and healthy distractions.

Dr. Cronje, for your important contribution to this study, all your support, good advice and proof reading. Prof. Raubenheimer, for your kind interest in this study as well as your indispensable advice, suggestions and ideas. All the members of the organometallic chemistry group for creating a stimulating and pleasant working environment. Anneke, for being my partner in crime these last two years, for all your motivational peptalks and comradeship - it was priceless. Elzet, for your friendship, all the good laughs, drama and for teaching me that you can always "*Blame it on the boogie!*" Gerrit for being an excellent instructor. Christoph, for being my own personal encyclopaedia, it was a pleasure sharing an aisle with you. Ulrike for all your crazy stories and always providing never-ending laughter. Magda, for being the funniest person I have ever met! Tesfamariam for being the definition of kindness, thank you for your constant encouragement. Adèle for always providing updates on all the latest series episodes and celebrities gossip. Oliver and Stefan, for your friendship and meticulous care in X-ray data collections and refinements.

Jean and Elsa for excellent NMR services and kindness. Mr. Ward for your speedy service, friendly smiles and interesting conversations in the passage. Mrs. May for your

kindness and patience. Stefan Louw and Tommie van der Merwe for collection of mass spectrometry data. Margo Nell for performing the cytotoxicity assays.

Finally, for financial support, I would like to thank the National Research Foundation and Stellenbosch University.

Different aspects of the work in this study have been presented in the form of:

- A communication accepted for publication: J. Coetzee, W. F. Gabrielli, K. Coetzee, O. Schuster, S. D. Nogai, S. Cronje, H. G. Raubenheimer, entitled “Comprehensive structural studies of gold(I), (II) and (III) with pentafluorophenyl and tetrahydrothiophene ligands” *Angew. Chem. Int. Ed.*, **2007**, 10.1002/anie.200604592
- A lecture presented by Dr. William F. Gabrielli at Gold 2006, September 2006, Limerick Ireland, titled “Utilisation of various bonding modes of N-rich heterocycles in gold(I) chemistry”.
- A poster presentation by the author at the Organometallics and their Applications (OATA) symposium, 11th August 2006, Cape Town, South Africa, titled “Crystallising gold(I), (II) and (III) with pentafluorophenyl and tetrahydrothiophene ligands.”
- A lecture presented by Dr. William F. Gabrielli at the South African Chemical Institute (SACI) Young Chemist Symposium, 5th July 2005, Stellenbosch South Africa, titled “Unusual modifications to simple carbene complexes”.
- A series of lectures presented by Prof. Helgard G. Raubenheimer at various European Universities during 2005 and 2006.

“.....volmaaktheid is een beperkte voorstelling van die werkelijkheid...”

– Stef Bos –



CONTENTS

SUMMARY	iii
OPSOMMING	v
ACKNOWLEDGMENTS	viii
CONTENTS	xi
ABBREVIATIONS	xiii

CHAPTER 1

General Introduction

1.1	Brief introduction to gold chemistry	1
1.2	Recent developments in gold chemistry	2
1.2.1	Carbon donor ligands in gold chemistry	2
1.2.2	Nitrogen donor ligands in gold chemistry	3
1.2.3	Phosphorus donor ligands in gold chemistry	4
1.2.4	Sulphur donor ligands in gold chemistry	5
1.3	Medicinal applications of gold compounds	6
1.4	Research objectives and thesis outline	7

CHAPTER 2

A Comprehensive Structural Study of Gold(I), (II) and (III) with Pentafluorophenyl and Tetrahydrothiophene Ligands

2.1	Introduction	10
2.2	Results and discussion	16
2.2.1	Gold(I), gold(II) and gold(III) complexes with tetrahydrothiophene and pentafluorophenyl ligands	16
2.2.2	Spectroscopic characterisation of ligand I and complexes 1 – 4	20
2.2.3	Structure determinations of compounds I and 1 – 5	24
2.3	Conclusions	33
2.4	Experimental	33
2.4.1	General procedures and instruments	33
2.4.2	Preparations and procedures	34
2.4.3	X-ray structure determinations	36

CHAPTER 3

Utilisation of $[\text{Au}(\text{C}_6\text{F}_5)(\text{tht})]$ in the Preparation of Novel Imidazolin- and Thiazolin-2-ylideneamine Gold(I) Complexes

3.1	Introduction	40
3.2	Results and discussion	44
3.2.1	Ylideneamine functionalised heterocyclic ligands and their corresponding (pentafluorophenyl)gold(I) complexes	44
3.2.2	Spectroscopic characterisation of compounds III – V and 5 – 7	48
3.2.3	Structure determinations of compounds III – V and 5 – 7	55
3.3	Conclusions	70
3.4	Experimental	71
3.4.1	General procedures and instruments	71
3.4.2	Preparations and procedures	72
3.4.3	X-ray structure determinations	75

CHAPTER 4

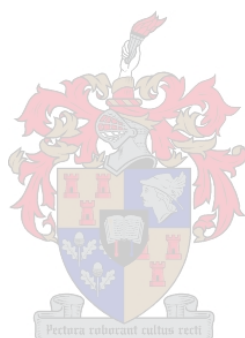
Preparation and Characterisation of Novel Ylideneamine Gold(I) Complexes with Phosphine or Carbene (NHC) Ancillary Ligands

4.1	Introduction	79
4.2	Results and discussion	83
4.2.1	Cationic ylideneamine coordinated (triphenylphosphine)gold(I) complexes	83
4.2.2	Spectroscopic characterisation of compounds 8 – 11	87
4.2.3	Structure determinations of compounds 8a – 11	95
4.2.4	Cytotoxicity assays of compounds 8 – 11	103
4.2.5	Deprotonation studies	104
4.2.6	Spectroscopic characterisation of compounds 12 – 14	107
4.2.7	Structure determinations of compounds 8b and 15	111
4.3	Conclusions	116
4.4	Experimental	118
4.4.1	General procedures and instruments	118
4.4.2	Preparations and procedures	119
4.4.3	X-ray structure determinations	121

ABBREVIATIONS

Å	Ångstrom (10^{-10} m)
Ar	Aromatic
Bu	Butyl
Bz	Benzyl
Bzim	Benzimidazole
Cy	Cyclohexyl
DFT	Density functional theory
DMF	<i>N,N'</i> -dimethylformamide
DMSO	Dimethyl sulfoxide
dppe	1,2-bis(diphenylphosphino)ethane
dppn	1,8-bis(diphenylphosphino)naphthalene
Eq	Equation
Et	Ethyl
FT	Fourier Transform
Hhpp	1,3,4,6,7,8-hexahydro-2 <i>H</i> -pyrimido[1,2 <i>a</i>]pyrimidine
Im	Imidazole
ⁱ Pr	Isopropyl
IR	Infrared
M_f	Molecular formula
M_r	Molecular weight
Me	Methyl
m.p.	Melting point
MS	Mass spectrometry
n.a.	Not applicable
n.o.	Not observed
NHC	<i>N</i> -heterocyclic carbene
NMR	Nuclear Magnetic Resonance
pcp	Pentachlorophenyl
pfp	Pentafluorophenyl
Ph	Phenyl
PPh ₃	Triphenylphosphine
PPN	Bis(triphenylphosphine)iminium
Pr	Propyl
R	Alkyl, aryl or hydrogen group
r.t.	Room temperature
^t Bu	Tertiary butyl
^t BuIm	Tertiary butylimidazole
THF	Tetrahydrofuran
tht	Tetrahydrothiophene
∠	Angle
NMR bs	Broad singlet
d	Doublet
dd	Doublet of doublets
ddd	Doublet of doublets of doublets
δ	Chemical shift (ppm)
<i>J</i>	Coupling constant (Hz)
m	Multiplet
ppm	Parts per million

	q	Quartet
	s	Singlet
	t	Triplet
	Δ	difference
MS	FAB-MS	Fast atom bombardment mass spectrometry
	EI-MS	Electron impact mass spectrometry
	M^+	Molecular ion
	m/z	Mass/charge ratio
IR	ν	Stretching vibration
	δ^b	bending vibration
	st	Strong
	w	weak
	m	medium
	δ^b_{oop}	out of plane bending



CHAPTER 1

General Introduction

1.1 Brief introduction to gold chemistry

Gold is known to display very unique chemical behaviour compared to other transition metals. It not only possesses the highest oxidation potential, but also the highest electron affinity of all metal atoms. These distinctive characteristics have been rationalised through the concept of relativistic effects, which reaches a maxima for this noble metal. Relativistic effects can be explained as a concurrent s-orbital contraction and d-orbital expansion and thus provide a qualitative insight into the electronic states of the valence orbitals. The resulting smaller energy gap between the 5d and 6s orbital allows for the construction of hybrid orbitals suitable for the formation of linear and square planar gold(I) complexes and complexes with square planar or octahedral geometries containing gold centres of higher oxidation states (Au^{III} and Au^{V}). In addition, the unique colour of bulk gold has also been ascribed to this small separation between the contracted 5d and expanded 6s orbitals. Another feature of gold chemistry that has attracted particular interest over the years is the interatomic attractive forces between gold(I) centres. These attractive forces are known as aurophilic interactions and have now become the prototype for metallophilic bonding.^{1,2} Pyykö has attributed these interactions to correlation effects enhanced by relativistic effects.³ The strength of aurophilic interactions have been estimated by NMR experiments to be in the same order of magnitude as that of a typical hydrogen bond (29-33 kJ/mol).⁴ These interactions also often play a determining role in the molecular configurations and crystal lattice organisation of gold(I) complexes.⁵

The chemistry of gold is dominated by the typically linear gold(I) and square-planar gold(III) derivatives. Interest in gold(II) derivatives has however increased significantly over the years and dinuclear diamagnetic gold(II) derivatives in particular have developed an equally rich chemistry.⁶ Unsupported $\text{Au}^{\text{II}}\text{-Au}^{\text{II}}$ bonds are however seldom observed.

¹ H. Schmidbaur, S. Cronje, B. Djordjevic, O. Schuster, *Chem. Phys.* **2005**, *311*, 151-161.

² M. C. Gimeno, A. Laguna in: *Comprehensive Coordination Chemistry II, Vol. 6* (Eds. J. A. McCleverty and T. J. Meyer), Elsevier Pergamon, Oxford **2004**, p911.

³ P. Pyykkö, *Angew. Chem. Int. Ed. Engl.* **2004**, *43*, 4412-4156.

⁴ H. Schmidbaur, W. Graf, W. Müller, G. Müller, *Angew. Chem. Int. Ed. Engl.* **1988**, *27*, 417-419.

⁵ M. C. Gimeno, A. Laguna, *Gold Bull.* **2003**, *36*, 83-92.

⁶ K. A. Barakat, T. R. Cundari, H. Rabaâ, M. A. Omary, *J. Phys. Chem. B* **2006**, *110*, 14645-14651.

Among the gold complexes, those with gold(I) centres are the most widespread and will also be the focus of the larger part of this study.

This chapter does not constitute a comprehensive overview of the vast literature accessible on the topic of gold chemistry, but presents some recent advances in gold derivatives with C-, N-, P- and S-donor ligands. Furthermore, a brief overview of the donor properties of the relevant ligand types is included. Although gold chemistry has made advances in catalysis, nanotechnology, electronics, liquid crystals, vapour depositions and medicine, this chapter will only focus on its medicinal applications. Additional information on the relevant topics appears in the introduction section to each chapter.

1.2 Recent developments in gold chemistry

1.2.1 Carbon donor ligands in gold chemistry

Organogold derivatives have been known for almost a century and date back to as early as 1908.⁷ Although the development of this class of compounds was slow at first it has matured considerably after the 1970's, and is now a solid established field of research. Organogold compounds may be broadly divided into compounds that contain formally either one- or two-electron carbon-donor ligands. One electron carbon-donor ligands include alkyl, aryl and alkynyl ligands while two electron carbon-donors include ligands such as carbon monoxide, isocyanides, alkenes and carbenes.⁸ The majority of gold complexes with carbon donor ligands, however, contain alkyl or aryl ligands. The use of polyhalophenyl ligands in particular is very common since these ligands are known to enhance the stability of gold compounds. Laguna and co-workers have made several valuable contributions to the field of arylgold(I) chemistry and have recently published a comprehensive review on the topic.⁹ In one such contribution they report the preparation and structural characterisation of the gold(I) complex, $[\text{Au}(\text{C}_6\text{F}_5)(\text{HN}=\text{CR}_2)]$. This compound represents the only known example of an ylideneamine gold(I) complex with a pentafluorophenyl ancillary ligand. Furthermore, this compound exhibits an interesting molecular packing, which contains both aurophilic interactions as well as N–H \cdots F hydrogen bonds. Differences observed in the molecular packing of this compound and the

⁷ W. J. Pope, C. S. Gibson, *J. Chem. Soc.* **1908**, 295, 2061-2066.

⁸ R. J. Puddephatt in: *Comprehensive Organometallic Chemistry I, Vol. 2* (Eds. E.J. Abel, F.J. Stone, G. Wilkinson) 2nd edition, Pergamon Press, Oxford, **1982**, p765-756.

⁹ E. J. Fernández, A. Laguna, E. Olmos in: *Organometallic Chemistry, Vol. 52* (Eds. R. West, A. F. Hill, F. G. A. Stone) 1st edition, Elsevier, London, **2005**, p77-141.

silver(I) analogue have been interpreted on the basis of *ab initio* calculations and is due to competition between the intermolecular forces present in the crystal lattice. In the solid state packing of the silver(I) complex, argentophilic interactions are of a weaker nature than hydrogen bonding. The latter, therefore, acts as the chief director of the molecular organisation. In the gold(I) complex intermolecular forces however compete with each other, due to the comparable strength of hydrogen bonds and aurophilic interactions.¹⁰

The two-electron donor *N*-heterocyclic carbene (NHC) ligands have received increasing attention over the last decade and are primarily regarded as strong σ -donor ligands with structural studies indicating M–C_{carbene} distances to be comparable to M–C_{alkyl} distances for similar complexes.¹¹ Although photoelectron spectroscopy and DFT calculations on bis(carbene)Pd and Pt complexes have indicated π -backbonding to be negligible in such complexes, other computational studies suggest that M–C_{carbene} bonds possess in the order of 20% π -character.^{12,13,14} A comprehensive overview of recent highlights in the area of Au(I)-NHC chemistry has been published by Lin and Vasam¹⁵ in the form of a review article. These recent developments include several significant contributions by Baker and co-workers. They have recently demonstrated for the first time the anti-mitochondrial activity of a family of dinuclear cationic NHC gold(I) complexes.¹⁶ In addition, they have now extended their study by reporting the anti-mitochondrial activity of a series of cationic linear NHC gold(I) complexes.¹⁷



1.2.2 Nitrogen donor ligands in gold chemistry

Gold(I) complexes with N-donor ligands have not been studied extensively, probably due to their supposed limited stability arising from the incompatibility of the soft gold(I) centre and hard to borderline-hard nitrogen donors.¹⁸ Owing to this limitation, the majority of amine complexes derived from aliphatic and aromatic amines, azoles and others,

¹⁰ A. Codina, E. J. Fernández, P. G. Jones, A. Laguna, J. M. López-de-Luzuriaga, M. Monge, M. E. Olmos, J. Pérez, M. A. Rodríguez, *J. Am. Chem. Soc.* **2002**, *124*, 6781-6786.

¹¹ W. A. Herrmann, C. Köcher, *Angew. Chem. Int. Ed. Engl.* **1997**, *36*, 2162-2187.

¹² J. C. Green, R. G. Scurr, P. L. Arnold, F. G. N. Cloke, *Chem. Commun.* **1997**, 1963-1964.

¹³ D. Nemesok, K. Wichmann, G. Frenking, *Organometallics* **2004**, *23*, 3640-3646.

¹⁴ S. K. Schneider, P. Roembke, G. R. Julius, C. Loschen, H. G. Raubenheimer, G. Frenking, W. A. Herrmann, *Eur. J. Inorg. Chem.* **2005**, 2973-2977.

¹⁵ I. B. Lin, C. S. Vasam, *Can. J. Chem.* **2005**, *83*, 812-825.

¹⁶ P. J. Barnard, M. V. Baker, S. J. Berners-Price, D. A. Day, *J. Inorg. Biochem.* **2004**, *98*, 1642-1647.

¹⁷ M. V. Baker, P. J. Barnard, S. J. Berners-Price, S. K. Brayshaw, J. L. Hickey, B. W. Skelton, A. H. White, *Dalton Trans.* **2006**, 3708-3715.

¹⁸ M. C. Gimeno, A. Laguna in: *Comprehensive Coordination Chemistry II, Vol. 6* (Eds. J. A. McCleverty, T. J. Meyer), Elsevier Pergamon, Oxford **2004**, p1034-1039.

described in literature, are stabilised by inert phosphine ligands. In many complexes secondary stabilisation in the solid state is provided by intermolecular bonding, i.e. aurophilic interactions of gold centres or hydrogen bonding in the presence of N–H groups. These interactions may either co-exist to synergistically stabilise the nitrogen coordinated gold(I) system, or compete against each other, as was recently concluded by Laguna and co-workers (discussed in section 1.2.2).¹⁹ Although, several reports of gold complexes that contain naturalazole ligands, such as imidazoles, thiazoles and tetrazoles exist, gold compounds derived from ylidenamine ligands remain largely unexplored. In particular, gold complexes derived from ylidenamine functionalised heterocyclic ligands have not been explored yet. A few ylidenamine gold(I) compounds of the type $[\text{Au}(\text{Cl})(\text{HN}=\text{CR}_2)]$, $[\text{Au}(\text{HN}=\text{CR}_2)_2][\text{AuCl}_2]$ and $[\text{Au}(\text{PR}_3)(\text{HN}=\text{CR}_2)]$ have been reported by Schmidbaur and co-workers.^{20,21} The complexes of the form $[\text{Au}(\text{X})(\text{HN}=\text{CR}_2)]$ (where X = Cl or Br), however, display limited stability in solution and decompose at room temperature within a few hours. In addition, from NMR experiments it is evident that these complexes undergo ligand redistribution in solution to form homoleptic rearrangement products of the general form $[\text{Au}(\text{HN}=\text{CR}_2)_2][\text{AuX}_2]$.

1.2.3 Phosphorus donor ligands in gold chemistry

Phosphine ligands form kinetically stable complexes with metal centres in both high and low oxidation states, reflecting the electronic versatility thereof. Owing to their versatile nature, a great variety of gold complexes of the general form $[\text{Au}(\text{X})(\text{PR}_3)]$ have been described. Although these types of complexes have been known for years there has been a revival of interest in them after the discovery of their medicinal potential. Recent research efforts in this field include a valuable contribution from our group in which a series of unique gold(I) trithiophosphite complexes were prepared and fully characterised.²² These complexes display interesting solid state organisation and tend to aggregate in infinite chains *via* aurophilic interactions. Laguna and co-workers²³ have also recently exploited the ability of gold(I) centres to participate in aurophilic interactions by preparing gold(I) complexes that contain a phosphinothioformamide ligand (Scheme 1.1). This

¹⁹ A. Codina, E. J. Fernández, P. G. Jones, A. Laguna, J. M. López-de-Luzuriaga, M. Monge, M. E. Olmos, J. Pérez, M. A. Rodríguez, *J. Am. Chem. Soc.* **2002**, *124*, 6781-6786.

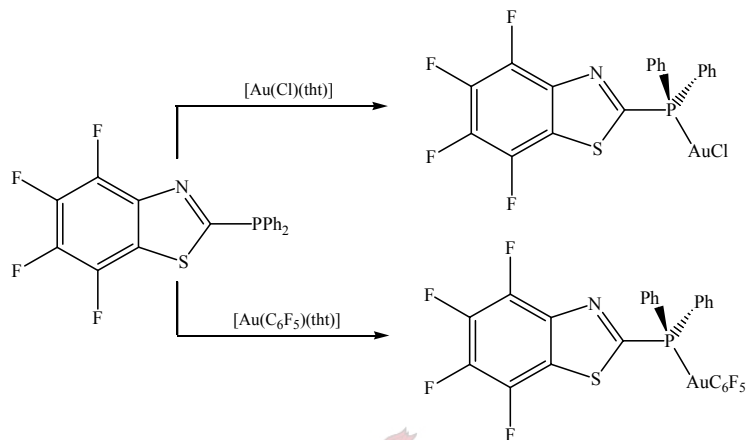
²⁰ W. Schneider, A. Bauer, A. Schier, H. Schmidbaur, *Chem. Ber./Recueil* **1997**, *130*, 1417-1422.

²¹ W. Schneider, A. Bauer, A. Schier, H. Schmidbaur, *J. Chem. Soc., Dalton Trans.* **1997**, *130*, 415-420.

²² C. E. Strasser, S. Cronje, H. Schmidbaur, H. G. Raubenheimer, *J. Organomet. Chem.* **2006**, *691*, 4788-4796.

²³ E. J. Fernández, A. Laguna, J. M. López-de-Luzuriaga, M. Monge, M. Montiel, M. E. Olmos, M. A. Rodríguez-Castillo, *Dalton Trans.* **2006**, 3672-3677.

polyfunctional ligand, which bears P-, N- and S-donor centres, coordinates *via* the phosphorus atom and is suitable for coordination to various metal centres. It may be utilised in the preparation of homo- and heteronuclear complexes with interesting structural arrangements. In addition, X-ray structure determinations of various gold(I) complexes of this ligand display weak interactions between the gold(I) centres and endocyclic sulphur atoms.



Scheme 1.1 Preparation of gold(I) complexes that contain a phosphinothioformamide ligand

Bidentate phosphines are useful as bridging ligands between gold(I) centres. Dinuclear (chloro)gold(I) complexes of ditertiary phosphine ligands, where the phosphorus atoms are bridged by alkyl chains of varied lengths, are often used as precursors in the preparation of complexes with interesting structural patterns directed by the formation of Au...Au interactions.²⁴ Finally, the bis-chelated diphosphine gold(I) complex [Au(dppe)₂]Cl, [dppe = 1,2-bis(diphenylphosphino)ethane], is known to possess anti-tumour activity against a broad range of tumour models.²⁵

1.2.4 Sulphur donor ligands in gold chemistry

Of all the gold complexes with sulphur donor ligands, phosphine gold(I) thiolate complexes have been of particular interest owing to their relation to the gold-based drug Auranofin, which is utilised in the treatment of rheumatoid arthritis.²⁶ In addition, the photophysical properties of these complexes earmark them as suitable candidates for

²⁴ M. C. Gimeno, A. Laguna: in *Comprehensive Coordination Chemistry II, Vol. 6* (Eds. J. A. McCleverty and T. J. Meyer), Elsevier Pergamon, Oxford **2004**, p1042-1075.

²⁵ P. J. Barnard, M. V. Baker, S. J. Berners-Price, B. W. Skelton, A. H. White, *Dalton Trans.* **2004**, 1038-1047.

²⁶ M. Bardají, M. J. Calhorda, P. J. Costa, P. G. Jones, A. Laguna, M. R. Pérez, M. D. Villacampa, *Inorg. Chem.* **2006**, *45*, 1059-1068.

utilisation in optical materials and sensors.²⁷ Thioethers, such as dimethylsulfide and tetrahydrothiophene, are another class of sulphur donor ligands that has found an important application in gold chemistry. These ligands, which are weak σ -donors, are readily displaced by ligands with superior donor abilities. Owing to this property, gold thioether complexes such as $[\text{Au}(\text{Cl})(\text{SMe}_2)]$, $[\text{Au}(\text{C}_6\text{F}_5)(\text{tht})]$ and $[\text{Au}(\text{C}_6\text{F}_5)_3(\text{tht})]$, are most often employed as valuable precursor compounds in various synthetic pathways that involve ligand substitution.

Although the generalisation that gold(I) prefers S-donor to N-donor ligands are sometimes made, Cronje and co-workers²⁸ have recently shown that gold(I) centres, when provided with a choice between borderline-hard imine and soft endo- and exocyclic thioether ligands, prefer imine coordination. This finding is confirmed by the many gold(I) imine and amine complexes reported in literature, prepared by substitution of thioether ligands.

1.3 Medicinal applications of gold compounds

Gold drugs find clinical use in the treatment of rheumatoid arthritis and are classified as disease-modifying anti-rheumatic drugs (DMARDs). DMAR drugs slow down the biological process of the disease and are some of a few drugs which steer inflammatory diseases into remission.²⁹ In addition to this application, gold compounds also display tremendous potential as anti-malarial, anti-HIV and anti-cancer agents. Gold-based drugs are regarded as pro-drugs which are believed to undergo rapid substitution reactions with sulphur containing biomolecules following administration.³⁰ Due to similarities in the electronic configuration and structural characteristics of gold(III) and the most widely used anti-cancer drug cisplatin, several gold(III) compounds have been investigated for potential antitumour activity. The gold(III) complexes receiving serious attention can be divided into three classes. These classes are 1) complexes with incorporated biologically active ligands, 2) complexes with imine donor atoms and 3) complexes that contain carbon donor ligands.³¹ Of all the gold(I) complexes explored, the gold(I) phosphine complexes show the most promise for application as anti-tumour agents.³¹ Two classes of gold(I)

²⁷ V. W. Yam, *Pure Appl. Chem.* **2001**, 73, 543-548.

²⁸ S. Cronje, H. G. Raubenheimer, H. S. C. Spies, C. Esterhuysen, H. Schmidbaur, A. Schier, G. J. Kruger, *Dalton Trans.* **2003**, 2859-2866.

²⁹ A. A. Mohamed, H. E. Abdou, J. Chen, A. E. Bruce, M. R. M. Bruce, *Comments Inorg. Chem.* **2002**, 23, 321-334.

³⁰ E. R. T. Tiekink, *Crit. Rev. Oncol. Hematol.* **2002**, 42, 225-248.

³¹ E. R. T. Tiekink, *Gold Bull.* **2003**, 36, 117-124.

phosphines have been considered for their anti-tumour activity, they are 1) the neutral, two-coordinate gold(I) complexes (e.g. Auranofin) and 2) the cationic tetrahedral bischelated gold(I) complexes related to $[\text{Au}(\text{dppe})_2]^+$ [dppe = (diphenylphosphino)ethane]. Both these classes of complexes display enormous potential as anti-tumour compounds and may assist in overcoming the two overriding impediments in cancer chemotherapy, i.e. drug-resistant tumour cells and low-tumour selectivity of cancer drugs. Mitochondrial membrane permeability, which plays a fundamental role in the regulation of programmed cell death (apoptosis), seems to be the key to selectively target carcinoma cells. The elevated mitochondrial membrane potentials observed for the mitochondria of carcinoma cells allow rapid accumulation of lipophilic cationic complexes in the mitochondrial plasma. The selectivity of cationic gold(I) complexes for fast proliferating cells over normal cells can therefore be fine-tuned by adjusting their lipophilic/hydrophilic balance through ligand design²⁵.

1.4 Research objectives and thesis outline

The serendipitous discovery of a very unique unbridged, unchelated gold(II) complex that contained only pentafluorophenyl and tetrahydrothiophene ligands, initiated the first part of the study which will be described in **Chapter 2**. An additional incentive came from the observation that no structural studies of the important gold(I) and gold(III) analogues of this compound are listed in Cambridge Crystallographic Database. With these factors in mind, this part of the reasearch was aimed at:

- 1) performing a comprehensive structural study of gold(I), (II) and (III) compounds with pentafluorophenyl and tetrahydrothiophene ligands;
- 2) evaluating the effect that variation in oxidation state of the central gold atom has on the bonding parameters of these analogous compounds;
- 3) exploring whether preparation of the unique unbridged, unchelated gold(II) compound in a rational manner was feasible. If possible, this compound may act as valuable precursor compound to other unbridged gold(II) compounds in future, and finally,
- 4) investigating the formation pathway of this gold(II) compound.

A comprehensive literature search of gold complexes containing ylideneamine ligands revealed that very few examples of such compounds have been described. Furthermore, of

the few ylideneamine gold complexes known, only one contains a pentafluorophenyl group as an ancillary ligand. Metal complexes of ylideneamine functionalised heterocyclic ligands are rare in particular, and no such complexes with gold centres have been reported to date. The second part of the study, described in **Chapter 3**, was therefore aimed at rectifying this shortcoming and once again emphasizing the importance of the gold(I) precursor compound studied in the first part, by:

- 1) preparing and fully characterising a series of ylideneamine-functionalised heterocyclic ligands;
- 2) utilising these ligands by preparing and fully characterising their corresponding neutral (pentafluorophenyl)gold(I) complexes; and
- 3) determining the structural changes in the free ligand upon metal coordination.

The final part of the study was inspired by the biological activity displayed by various ylideneamine metal complexes together with the known anti-cancer potential of gold(I) complexes with phosphine and N-heterocyclic carbene (NHC) ligands.^{31,32,33} Although the biological activity of ylideneamine ligands and metal complexes thereof have been explored in great detail, very little information on their potential as anti-tumour agents exist in the literature. In addition, no ylideneamine gold complexes with NHC ancillary ligands have been described and reports of ylideneamine gold(I) complexes with phosphine ligands are limited. Ylideneamide metal complexes are also very rare with no ylideneamide gold complexes described to date. Recent findings that lipophilic cationic gold(I) complexes show enormous potential as anti-tumour agents which are able to selectively target carcinoma cell mitochondria gave the final encouragement to venture into the final part of this study described, in **Chapter 4**, which was aimed at:

- 1) expanding the family of gold(I) complexes with ylideneamine-functionalised heterocyclic ligands by preparing and fully characterising a series of related lipophilic cationic gold(I) phosphine and NHC complexes;
- 2) evaluating the influence of ligand variation on the structural parameters of the complexes;
- 3) determining whether a possible synergism between these ligands exists by assessing their anti-tumour potential;

³² P. Morain, C. Abrahams, B. Portevin, G. De Nanteuil, *Mol. Pharmacol.* **1994**, *46*, 732-742.

³³ A. J. J. Wood, C. J. Bailey, R. C. Turner, *New England J. Med.* **2003**, *334*, 574-228.

- 4) preparing a related series of cationic gold(I) phosphine complexes with guanidine and biguanidine type ligands;
- 5) exploring whether deprotonation of the neutral ylideneamine-functionalised heterocyclic ligands prior to or after coordination is feasible in order to generate neutral ylideneamide gold(I) complexes;
- 6) attempting deprotonation of the central NH functionality in biguanide gold(I) phosphine complexes.

To summarise the thesis outline: In **Chapter 2** the different pathways to the formation of gold(II) and gold(III) complexes, that contain only pentafluorophenyl and/or tetrahydrothiophene ligands, from a common gold(I) precursor are explored. The structural characteristics of these compounds are then assessed in a comparative study. The value of the common gold(I) precursor compound, (pentafluorophenyl)(tetrahydrothiophene)gold(I), introduced in **Chapter 2** is further accentuated in **Chapter 3** by the employment thereof in the preparation of a series of novel (pentafluorophenyl)gold(I) compounds with ylideneamine functionalised heterocyclic ligands. This series is extended in **Chapter 4** with the introduction of lipophilic cationic phosphine and NHC gold(I) complexes that contain ylideneamine-functionalised heterocyclic ligands. The potential of these compounds as anti-tumour agents are then assessed by the determination of their cytotoxic potency and tumour selectivity against cervical carcinoma cells. In addition to these research efforts, the deprotonation of various phosphine gold(I) complexes with ylideneamine ligands are explored in this chapter.

CHAPTER 2

A Comprehensive Structural Study of Gold(I), (II) and (III) with Pentafluorophenyl and Tetrahydrothiophene Ligands

2.1 Introduction

The first tetrahydrothiophene (tht) complex of gold was reported by Cattalini and co-workers¹ in 1968, whereas Vaughan and Sheppard² were the first to obtain a gold complex that contained the pentafluorophenyl (pfp) group as a ligand two years later. Since then and mainly up to the 1980's, Uson and co-workers – with the Laguna brothers and Vicente prominent – have developed the chemistry of such compounds. Tht, which behaves as a labile ligand in gold(I), (II) and (III) chemistry, is now commonly employed for allowing substitution reactions whereas pfp is utilized as a robust and generally inert group (compared to other aryls).^{3,4,5} These ligands are most often employed in the preparation of gold(I) and (III) complexes, with the two most widely used precursor complexes being (pentafluorophenyl)(tetrahydrothiophene)gold(I), $[\text{Au}(\text{C}_6\text{F}_5)(\text{tht})]$, and tris(pentafluorophenyl)(tetrahydrothiophene)gold(III), $[\text{Au}(\text{C}_6\text{F}_5)_3(\text{tht})]$. Several synthetic procedures involving these ligands are described in two books edited by King and Eisch⁶ and later applications are described in various books and review articles.⁷

Although pfp and tht containing gold(II) precursor compounds exist, their numbers are limited compared to the more abundant gold(I) and gold(III) derivatives.^{8,9} This is due to their low redox stability and the strong tendency of Au^{II} to disproportionate to Au^{I} and Au^{III} . Their instability can in part be ascribed to the unfavourable energy of the odd

¹ L. Cattalini, M. Martelli, G. Marangoni, *Inorg. Chem.* **1968**, 7, 1492–1495.

² L. G. Vaughan, W. A. Sheppard, *J. Organomet. Chem.* **1970**, 22, 739-742.

³ F. Mohr, E. Cerrada, M. Laguna, *Organometallics* **2006**, 25, 644-648.

⁴ S. Cronje, H.G. Raubenheimer, H. S. C. Spies, C. Esterhuysen, H. Schmidbaur, A. Schier, G. J. Kruger, *Dalton Trans.* **2003**, 14, 2859-2866.

⁵ E. J. Fernandez, A. Laguna, J. M. Lopez-de-Luzuriaga, M. Monge, M. Montiel, E. M. Olmos and M. Rodriguez-Castillo, *Dalton Trans.* **2006**, 30, 3672-3677.

⁶ a) R. Usón, A. Laguna in: *Organometallic Synthesis, Vol. 3* (Eds. R. B. King, J. J. Eisch) Elsevier, Amsterdam, **1986**, p322-323, b) R. Usón, A. Laguna in: *Organometallic Synthesis, Vol. 4* (Eds. R. B. King, J. J. Eisch) Elsevier, Amsterdam, **1988**, p342-353.

⁷ For example see: a) M. C. Gimeno, A. Laguna in: *Comprehensive Coordination Chemistry II, Vol. 6* (Eds. J. A. McCleverty, T. J. Meyer) 1st edition, Elsevier, Oxford, **2004**, p990-1145, b) A. Grohmann, H. Schmidbaur in: *Comprehensive Organometallic Chemistry II* (Eds. E. W. Abel, F. G. A. Stone, G. Wilkinson) 1st edition, Elsevier Science, Oxford, **1995**, p1-56.

⁸ H. H. Murray, J. P. Fackler Jr., L. C. Porter, D. A. Briggs, M.A. Guerra, R. J. Lagow, *Inorg. Chem.* **1987**, 26, 357-363.

⁹ A. Laguna, M. Laguna, J. Jimenez, F. J. Lahoz, E. Olmos, *J. Organometallic Chem.* **1992**, 435, 235-247.

electron which is located in the d_{x²-y²} orbital in square planar d⁸ metal complexes.¹⁰ The formation of a gold(II)–gold(II) bond, resulting in a dinuclear diamagnetic complex, is common and provides the much needed stabilisation. Most known gold(II) complexes, formally contain an [Au₂]⁴⁺ core stabilised by two equal bridging ligands (typically organophosphines, ylides or organothiolates) retaining the gold centres in close proximity to afford a diauracycle. Some diauracycles with two different bridging ligands or one bridging ligand have been reported but only four dinuclear gold(II) complexes devoid of any bridging ligands have been described.¹⁰ However, in all four of these complexes, each of the gold centres are stabilised by a chelating ligand. The first example of such an unbridged dinuclear gold(II) complex, [Au₂(dppn)₂Cl₂][PF₆]₂ (dppn = 1,8-bis(diphenylphosphino)naphthalene), was reported by Yam and co-workers in 1996.¹¹ Five years later they extended their work by reporting the structurally related halo analogues, [Au₂(dppn)₂Br₂][PF₆]₂ and [Au₂(dppn)₂I₂][PF₆]₂ [Figure 2.1(a)].¹² Two years later Yurin *et al.* obtained a similar unbridged complex, bis(quinolin-8-ylthio)digold dichloride [Figure 2.1 (b)], by reacting tetrahydrothiophenogold(I) chloride, [Au(Cl)(tht)], with di(8-quinoly) disulfide in the presence of a mixture of chlorinated solvents.¹³

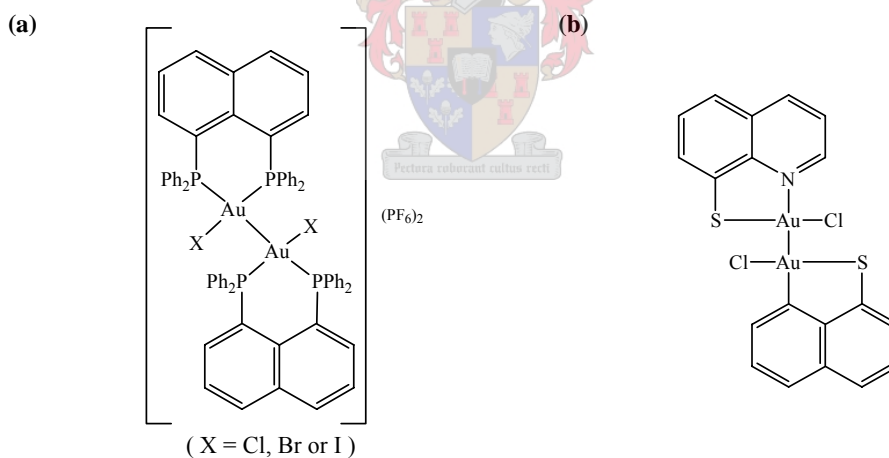


Figure 2.1 (a) Structure of [Au₂(dppn)₂X₂][PF₆]₂, where X = Cl, Br or I (b) Structure of bis(quinolin-8-ylthio)digold dichloride.

Most bridged gold(II) complexes are readily derived from their dinuclear gold(I) precursors by oxidative addition of halogens or pseudohalogens (some selected examples

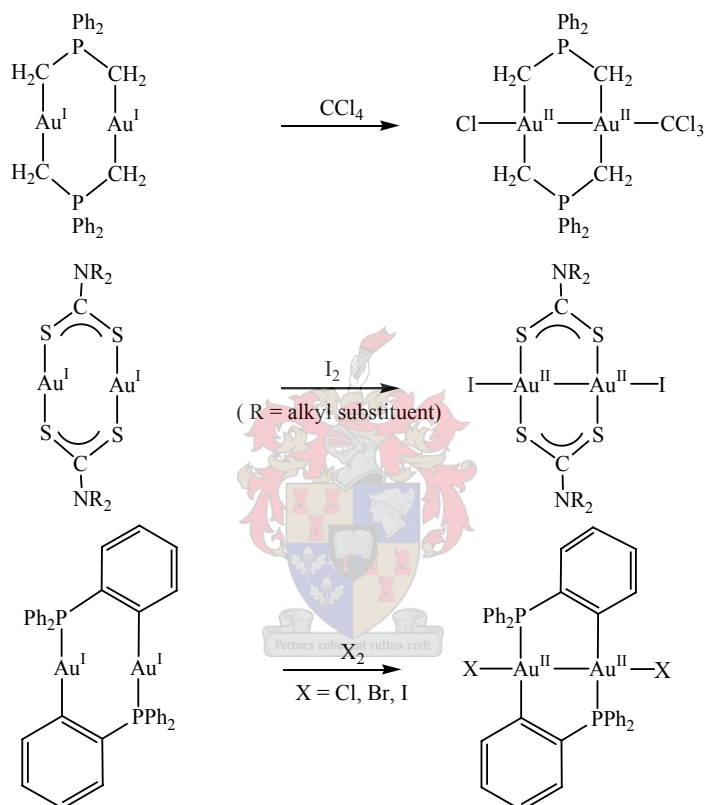
¹⁰ A. Laguna, M. Laguna, *Coord. Chem. Rev.* **1999**, 193-195, 837-856.

¹¹ V. W. Yam, S. W. Choi, K. Cheung, *Chem. Commun.* **1996**, 10, 1173-1174.

¹² V. W. Yam, C. K. Li, C. L. Chan, K. Cheung, *Inorg. Chem.* **2001**, 40, 7054-7058.

¹³ S. A. Yurin, D. A. Lemenovskii, K. I. Grandberg, I. G. Ll'ina, L. G. Kuz'mina, *Russ. Chem. Bull., Int. Ed.* **2003**, 52, 2752-2753.

are shown in Scheme 2.1). Murray and Fackler¹⁴ established that halomethanes of the form CH_3X_{4-y} ($y = 3, 2, 1, 0$ and $X = Cl, Br, I$), but with the exception of methylchloride, are able to react with the dinuclear gold(I) precursors, $[Au(CH_2)_2PPh_2]_2$ by oxidative addition across the carbon-halogen bond. This leads to the formation of initial gold(II) adducts of the general form $[Au(CH_2)_2PPh_2]_2(CH_3X_{3-y})X$ ($y = 3, 2, 1, 0$). The reactivity of these halomethanes is inversely related to the carbon-halogen bond dissociation energy which follows the order $I > Br > Cl$.



Scheme 2.1 Selected examples of gold(II) complexes prepared from their corresponding dinuclear gold(I) precursor complexes by oxidative addition of halogens.

Other oxidants employed in the preparation of gold(II) complexes from their gold(I) diauracycle precursor complexes, include $[Hg(CN)_2]$,¹⁵ nitroalkanes, N_2O_4 ,¹⁶ tetraethylthiurium,¹⁷ $[Ti(C_6F_5)_2Cl]_2$ and $[Ag(MeCN)(PF_6)_4]$.¹¹

¹⁴ H. H. Murray, J. P. Fackler, Jr., *Inorg. Chim. Acta* **1986**, 115, 207-209.

¹⁵ H. H. Murray, A. M. Manzany, J. P. Fackler, Jr., *Organometallics* **1985**, 4, 154-157.

¹⁶ B. Trzcinska-Bancroft, M. N. I. Kahn, J. P. Fackler, Jr., *Organometallics* **1988**, 7, 993-996

¹⁷ D. D. Heinrich, R. J. Staples, J. P. Fackler, Jr., *Inorg. Chim. Acta* **1995**, 229, 61-75.

A number of polynuclear gold(II) complexes which contain gold–gold bonds between gold centres of different formal charge, have been described in the literature (Figure 2.2). Most of these compounds contain pfp ligands and are prepared by reacting gold(II) derivatives with an $[Au_2]^{4+}$ core and two equal bridging ligands, with gold(I) or gold(III) compounds. Although the complexes shown in Figure 2.2 (a) and (b) seem, by inspection, to contain formal covalent $Au^{II}-Au^I$ bonds,^{18,19,20} extended Hückel calculations have indicated the formal charges of the involved gold centres to be best described as $Au^{III}-Au^I-Au^I-Au^I-Au^{III}$ and $Au^{III}-Au^I-Au^I-Au^I-Au^I-Au^{III}$ respectively.^{21,22} The shortest gold-gold bond known to date is located between the gold centres of a dinuclear gold(II) compound and has been reported by Irwin and co-workers.²³ This dinuclear gold(II) complex is doubly bridged by a guanidinate-type ligand, Hhpp (1,3,4,6,7,8-hexahydro-2H-pyrimido[1,2-*a*]pyrimidine), and presents an $Au^{II}-Au^{II}$ bond of 2.4752(9) Å.

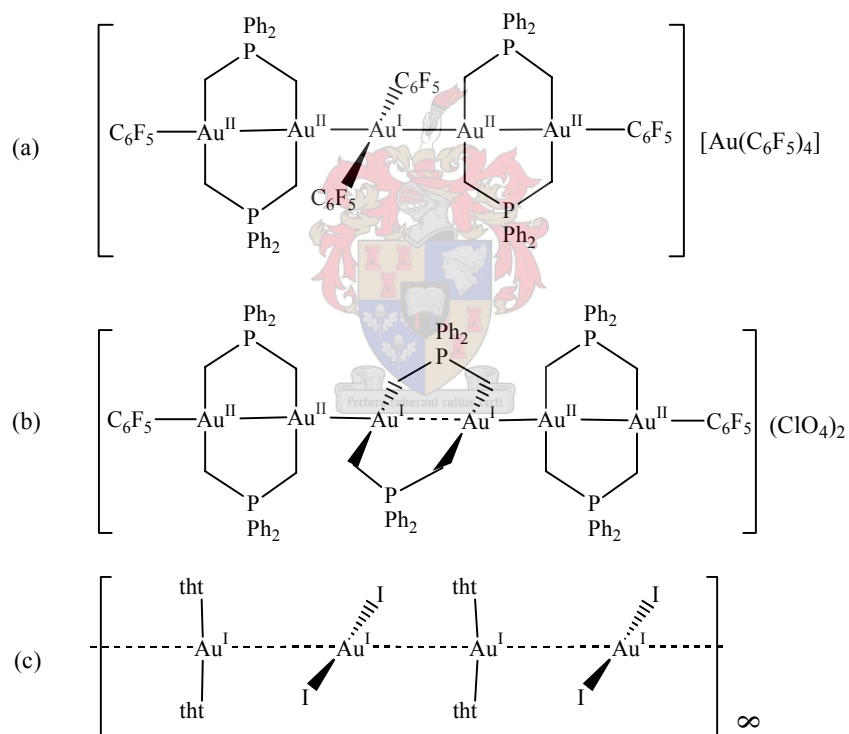


Figure 2.2 (a) and (b) Selected examples of polynuclear gold(II) compounds containing gold–gold bonds between gold centres with different formal charges, (c) A polynuclear chain involving gold(I) centres linked by aurophilic interactions.

¹⁸ R. Usón, A. Laguna, M. Laguna, J. Jiménez, P. G. Jones, *Angew. Chem. Int. Ed. Engl.* **1991**, *30*, 198-199.

¹⁹ A. Laguna, M. Laguna, J. Jiménez, F. J. Lahoz, E. Olmos, *Organometallics* **1994**, *13*, 253-257.

²⁰ M. C. Gimeno, J. Jiménez, P. G. Jones, A. Laguna, M. Laguna, F. J. Lahoz, E. Olmos, *Organometallics* **1994**, *13*, 2508-2511.

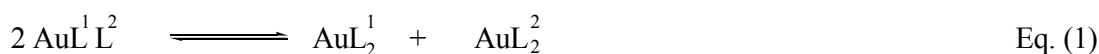
²¹ M. J. Calhorda, L. F. Veiros, *J. Organomet. Chem.* **1994**, *478*, 37-44.

²² L. F. Veiros, M. J. Calhorda, *J. Organomet. Chem.* **1996**, *510*, 71-81.

²³ M. D. Irwin, H. E. Abdou, A. A. Mohamed, J. P. Fackler, Jr., *Chem. Commun.* **2003**, 2882-2883.

Despite these interesting examples of compounds containing a gold-gold bond, the most studied gold-gold interactions are those exhibited by linear gold(I) centres. Gold(I) compounds are known to associate in dimers, oligomers or polymers by short inter- and/or intramolecular Au^I...Au^I aurophilic interactions [for an example see Figure 2.2 (c)].^{24,25,26,27} The presence of these aurophilic interactions not only contributes to the overall stability of the system [as was confirmed with by DFT (density functional theory) calculations] but also, in part, direct the molecular configuration and assembly of the molecules in the crystal lattice.²⁸

Well documented ligand rearrangements of gold(I) take place according to Eq. 1 (charges omitted), where L¹ and L² correspond to two different, normally soft, ligands.^{29,30}



Although these ligand rearrangement reactions are fairly common for gold(I), reports of such reactions for mononuclear gold(III) complexes are extremely rare. Note, however, that Fackler and Schmidbaur³¹ have independently described the ligand dynamics (involving isomerisations and rearrangements) in various polynuclear ylide-bridged gold(III) complexes. In another example of such a related rearrangement the anionic gold(I) complex, [Au(C₆F₅)₂]⁻ is reacted with the gold(III) complex, [Au(C₆F₅)₃·OEt₂] in an attempt to achieve Au^I-Au^{III} bond formation. However, instead of Au^I-Au^{III} bond formation, pfp ligand migration proceeds to yield the monomeric homoleptic rearrangement product, [Au(C₆F₅)₄]⁻.³² Although some examples of such homoleptic tetra-substituted aurates exist, they are not common. Furthermore, all other known examples have been prepared *via* a rational synthetic approach and were not facilitated by spontaneous ligand scrambling reactions. Most of these complexes are tetra-arylaaurates

²⁴ S. L. Zheng, C. L. Nygren, M. M. Messerschmidt, P. Coppens, *Chem. Commun.* **2006**, 3711-3713.

²⁵ D. Schneider, O. Schuster, H. Schmidbaur, *Organometallics* **2005**, *24*, 3547-3551.

²⁶ H. Ehlich, A. Schier, H. Schmidbaur, *Organometallics* **2002**, *21*, 2400-2406.

²⁷ S. Ahrland, B. Norèn, A. Oskarsson, *Inorg. Chem.* **1985**, *24*, 1330-1333.

²⁸ J. E. Aquado, M. J. Calhorda, M. Concepción Gimeno, A. Laguna, *Chem. Commun.* **2005**, 3355-3356.

²⁹ S. Ahmad, *Coord. Chem. Rev.* **2004**, *248*, 231-243.

³⁰ S. Onaka, Y. Katsukawa, M. Shiotsuka, O. Kanegawa, M. Yamashita, *Inorg. Chim. Acta* **2001**, *312*, 100-110.

³¹ a) S. Wang, J. P. Fackler, Jr. in: *The chemistry of organic derivatives of gold and silver Vol. 6* (Eds. S. Patai and Z. Rappoport) 2nd edition, John Wiley & Sons Ltd., Chichester, **1999**, p431-450, b) H. Schmidbaur, A. Grohmann, M. E. Olmos, A. Schier in: *The chemistry of organic derivatives of gold and silver Vol. 6* (Eds. S. Patai and Z. Rappoport) 2nd edition, John Wiley & Sons Ltd., Chichester, **1999**, p271-272.

³² R. Usón, A. Laguna, M. Laguna, M. T. Tartón, P. G. Jones, *J. Chem. Soc., Chem. Commun.* **1988**, 740-741.

and even though Markwell³³ successfully prepared the complex $[\text{Au}(\text{C}_6\text{H}_5)_4]^-$, the majority of these complexes include polyhalophenyl ligands, with the pfp and pcp (pentachlorophenyl) ligands most prominent. More research efforts have, however, been devoted to pfp complexes rather than to their pcp counterparts, since their greater stability renders them easier to isolate. The incorporation of halogenated aryl ligands are believed to stabilise the Au^{III} metal centre, owing to the electron-withdrawing nature of the halogen atoms.³⁴

In most gold(III) complexes of the general form $[\text{AuR}_2\text{L}_2]$ antisymbiosis prevails with the ligands arranged in a square planar fashion about the central gold atom, displaying equal ligands in positions *cis* to each other. This is coherent with the Pearson π -competition theory which states that in such four-coordinate complexes, two soft ligands in mutual *trans* positions, when attached to class B (soft) metal atoms, will have a destabilising effect on each other.³⁵ Only a few exceptions to this rule have been reported. Some examples of these include *trans*- $[\text{Au}(\text{C}_6\text{F}_5)_2(\text{tht})_2][\text{CF}_3\text{SO}_3]$, *trans*- $[\text{Au}(\text{C}_6\text{F}_5)_2(\text{C}_6\text{F}_3)_2]-[\text{N}(n\text{-Bu})_4]$ and *trans*- $[\text{Au}(\text{C}_6\text{F}_5)_2(\text{Cl})_2][\text{N}(n\text{-Bu})_4]$ with the latter representing the only example where the structure of the compound has been confirmed by crystal and molecular structure determination.^{3,36,37}

Although many tht- and pfp-containing gold compounds exist, it is surprising that no crystal structure determinations of complexes that include both of these important ligands coordinated to a gold centre have been performed. This observation together with the serendipitous discovery of a very interesting unbridged, unchelated dinuclear gold(II) compound, containing only these ligands inspired us to launch a study aimed at rectifying this shortcoming. The goal of this study was therefore to perform a comprehensive comparative structural study of gold(I), gold(II) and gold(III) complexes which contained only pfp and tht ligands. In addition to this, the study was aimed at exploring whether the unique gold(II) compound could be prepared in higher yields by other, more rational approaches. If such a synthetic procedure could be developed, this compound can act as a valuable starting material for the preparation of other gold(II) compounds in future.

³³ A. J. Markwell, *J. Organomet. Chem.* **1985**, 293, 257-263.

³⁴ J. A. Schlueter, U. Geiser, H. H. Wang, M. L. Van Zile, S. B. Shannon, J. M. Williams, A. Laguna, M. Laguna, D. R. T. Naumann, *Inorg. Chem.* **1997**, 36, 4265-4269.

³⁵ R. G. Pearson, *Inorg. Chem.* **1973**, 12, 721-713.

³⁶ R. Usón, A. Laguna, M. Laguna, J. Jiménez, P. G. Jones, *Angew. Chem. Int. Ed. Engl.* **1991**, 30, 198-199.

³⁷ P. G. Jones, E. Bembenek, *Z. Kristallogr.* **1993**, 208, 362-365.

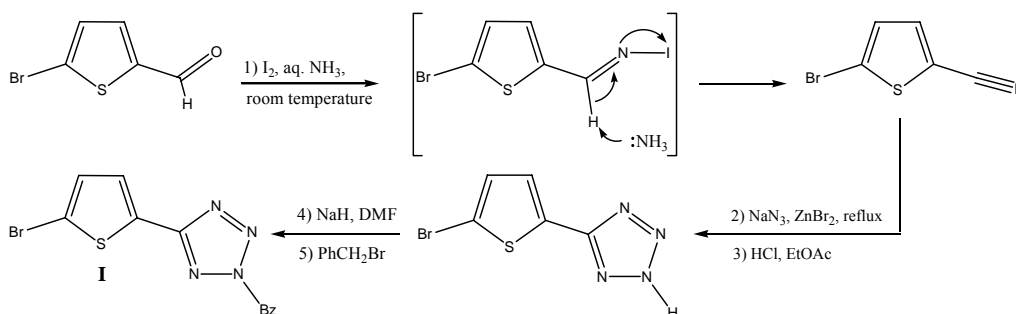
2.2 Results and discussion

2.2.1 Gold(I), gold(II) and gold(III) compounds with tetrahydrothiophene and pentafluorophenyl ligands

Section 2.2.1.1 describes the preparation and isolation of the various gold(I), gold(II) and gold(III) compounds, while section 2.2.2 is devoted to the spectroscopic characterisation of these compounds. In section 2.2.3 the crystal structures of both (pentafluorophenyl)-(tetrahydrothiophene)gold(I), **1**, and tris(pentafluorophenyl)(tetrahydrothiophene)gold(III), **3**, are described. The latter compound could be obtained in two true polymorphic forms (compounds **3a** and **3b**). Furthermore, the molecular structure of the very unique dinuclear unbridged gold(II) compound, tetrakis(pentafluorophenyl)bis(tetrahydrothiophene)digold(II), **2**, is also described in section 2.2.3. In addition, this section includes the molecular structure of an unique ionic rearrangement product of **3**, [bis(pentafluorophenyl)bis(tetrahydrothiophene)gold(III)][tetrakis(pentafluorophenyl)gold(III)], **4**.

2.2.1.1 Preparation of 2-benzyl-5-(5-bromothiophen-2-yl)-2H-tetrazole, **I** and compounds **1** – **4**

As part of an ongoing investigation of preferential gold coordination to various *N*-heterocycles³⁸, [Au(C₆F₅)(tht)], **1**, was treated with the organic bromide, 2-benzyl-5-(5-bromothiophen-2-yl)-2H-tetrazole, **I**, in a 1:1 molar ratio. The latter novel compound was prepared from 5-bromo-thiophene-2-carbaldehyde according to the procedure summarised in Scheme 2.2.



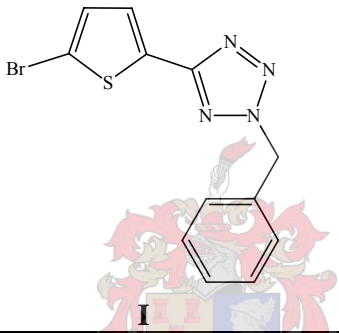
Scheme 2.2 Reaction scheme for the preparation of **I** showing the mechanism of formation for the nitrile derivative from the aldehyde precursor via a *N*-iodo aldimine intermediate.

The first part of the preparation involved the transformation of the aldehyde, into the corresponding nitrile by treatment with an iodine and ammonia water mixture for 1h at

³⁸ W. F. Gabrielli, *PhD Dissertation 2005*, University of Stellenbosch.

room temperature. This step was followed by the addition of an azide ion, in the presence of a zinc salt, and subsequent heating for 14h to afford the resultant tetrazole, 5-bromo-2-(2-*H*-tetrazol-5-yl)thiophene. In this transformation iodine is utilised as an oxidant to effect the nitrile derivative *via* an *N*-iodo alidimine intermediate.³⁹ Benzoylation of the tetrazole precursor was readily achieved by deprotonation of the nitrogen in the 2-position of the tetrazole ring with sodium hydride, subsequent alkylation with benzylbromide and quenching of the reaction with a copious amount of water.⁴⁰ Purification of **I** was performed by means of column chromatography [ether/hexane (1:1) as eluent] and recrystallisation from ether, prior to reaction with **1**. Analytical data for **I** are summarised in Table 2.1.

Table 2.1 Physical properties and analytical data of compound **I**.

Complex	 <p style="text-align: center;">I</p>
m.p (°C)	96
Colour	yellow
Yield (%)	61
<i>M_r</i>	321.20
Analysis (%)*	C ₁₂ H ₉ BrN ₄ S
C	44.99 (44.87)
H	2.73 (2.82)
N	17.55 (17.44)

* Required calculated values given in parenthesis. The product was powdered and evacuated for 10h prior to elemental analysis.

Treatment of the gold(I) compound **1** with the organic bromide, **I**, (molar ratio 1:1) in ether did not furnish the desired nitrogen coordinated gold(I) derivative. Instead, a reaction mixture that contained gold in various oxidation states was obtained. From this mixture

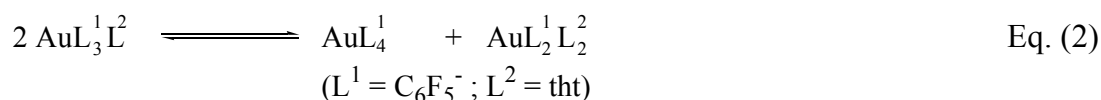
³⁹ J. J. Shie, J. M. Fang, *J. Org. Chem.* **2003**, *68*, 1158-1160.

⁴⁰ D. P. Matthews, J. R. McCarthy, J. P. Whitten, P. R. Kastner, C. L. Barney, F. N. Marshall, M. A. Ertel, T. Burkhard, P. J. Shea, T. Kariya, *J. Med. Chem.* **1990**, *33*, 317-327.

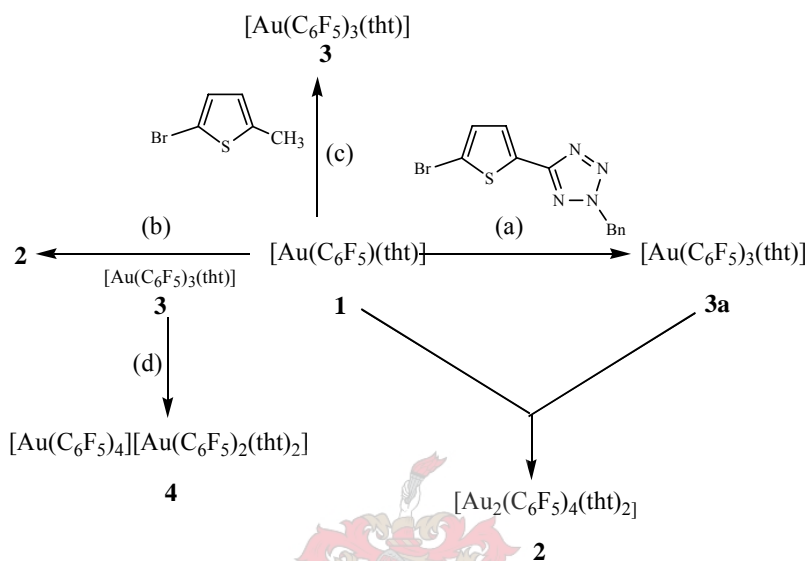
the unprecedented dinuclear gold(II) compound [Au₂(C₆F₅)₄(tht)₂], **2**, was isolated. This compound is very unique since it represents the first example of an unbridged gold(II) complex with a formal [Au₂]⁴⁺ core in which the gold centres are not stabilised by any chelating ligands. In addition, this mixture also afforded crystals of the well-known gold(III) complex [Au(C₆F₅)₃(tht)], **3a**. Upon standing (*ca.* 24h), metallic gold was visible in the form of a gold mirror on the walls of the Schlenk tube.

In a similar reaction, performed to establish the nature of the gold(I) interaction with the organic bromide **I**, **1** was treated with 2-bromo-5-methylthiophene, **II**. This again resulted in the oxidation of gold(I) to eventually furnish crystals of [Au(C₆F₅)₃(tht)], **3a**. The gold(II) compound, **2**, was however not isolated from this reaction mixture. Compound, **2**, was subsequently also prepared *via* an extremely slow redox reaction between equimolar quantities of compounds **1** and **3** in ether. The formation of compound **2** in this reaction was confirmed by unit cell determinations of various yellow crystals isolated from this mixture by single crystal X-ray diffraction. All determined unit cells had exactly the same dimensions as was previously determined during the full data collection of **2**. This result proved that the gold(II) compound **2** can be attained in a rational manner in the absence of any organic halides. It, however, does not rule out the possibility of **2** forming first during the oxidation of **1** to **3**. The formation of the dinuclear compound **2** from **1** and **3** can be interpreted in terms of C₆F₅ radical transfer from the gold(III) to the gold(I) with simultaneous Au–Au bond formation; it thus represents a rare example of labile C₆F₅ behaviour.⁴

In addition to the crystallisation of **2**, unreduced [Au(C₆F₅)₃(tht)] crystallised unaltered from the reaction mixture, with the polymorphic structure **3b** while, some of it underwent spontaneous ligand rearrangement to afford the ionic compound, [Au(C₆F₅)₄]-[Au(C₆F₅)₂(tht)₂], **4**, that consists of two gold(III) complexes. As was mentioned in the introduction to this chapter, well documented homoleptic rearrangements of gold(I) occur according to Eq.(1) (see section 2.1). This result, has now established that ligand scrambling also takes place for a mononuclear organogold(III) compound according to Eq.(2) and almost certainly other examples will be discovered in future.



The reactions that lead to the formation of the unusual crystalline products are summarised in Scheme 2.3. The elemental analysis of compounds **2** and **4** and the melting point of **4** could not be determined due to an insufficient amount of sample material as a result of the low yield procedures. Physical and analytical data for compounds **1** – **4** are summarised in Table 2.2.



Scheme 2.3 Crystalline products **2** and **3a** prepared according to reaction (a) (assuming **2** formed from **1** and **3**), **2** prepared according to reaction (b) and **3** according to reaction (c). In reaction (d), **3** rearranged to form **4** and also crystallised as **3b**.

Table 2.2 Physical and analytical data for complexes **1** – **4**.

Complex				
	1	2	3	4
m.p. (°C)*	106-109 (109) (decomp)	104-107 (decomp)	190-191 (190)	–
Colour	colourless	yellow	colourless	colourless
Yield (%)	80	± 3%	78	± 1%
<i>M_r</i>	452.20	1238.50	786.31	1572.62
Analysis (%)*	C ₁₀ H ₈ AuF ₅ S	C ₃₂ H ₁₆ Au ₂ F ₂₀ S ₂	C ₂₂ H ₈ AuF ₁₅ S	C ₄₄ H ₁₆ Au ₂ F ₃₀ S ₂
C	26.32 (26.56)	– (31.03)	32.91 (33.60)	– (33.60)
H	1.74 (1.78)	– (1.30)	1.22 (1.03)	– (1.03)

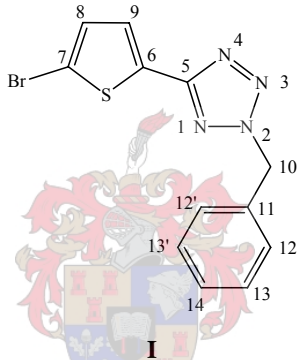
* Literature m.p. values and values calculated for elemental analysis are given in parenthesis. The products were powdered and evacuated for 10h prior to elemental analysis.

2.2.2 Spectroscopic characterisation of ligand I and complexes 1 – 4

2.2.2.1 Nuclear magnetic resonance spectroscopy

The ¹H and ¹³C NMR spectroscopic data for compound **I** are summarized in Table 2.3. In the ¹H NMR spectrum the protons in the 9- and 8-position on the thiazole ring, resonate as doublets due to mutual coupling, with the chemical shift of the latter appearing more downfield. Furthermore, the CH₂ proton of the benzyl substituent resonates as a singlet at δ 5.77, while the aromatic protons give rise to an unresolved multiplet in the region δ 7.37-7.44.

Table 2.3 ¹H and ¹³C NMR spectroscopic data of compound **I**.

Ligand	 <p style="text-align: center;">I</p>
Solvent	Dichloromethane-d ₂
Temperature (°C)	25
Assignment	Chemical shift (ppm)
¹ H NMR (300 MHz)	
H ⁸	7.53 (d, 1H, ¹ J = 4.0 Hz)
H ⁹	7.12 (d, 1H, ¹ J = 3.9 Hz)
H ¹⁰	5.77 (s, 2H)
H ¹² , H ^{12'} , H ¹³ , H ^{13'} , H ¹⁴	7.37-7.44 (m, 5H)
¹³ C NMR (75 MHz)	
C ⁵	161.2 (s)
C ⁶	133.9 (s)
C ⁷	115.6 (s)
C ⁸	131.5 (s)
C ⁹	128.5 (s)
C ¹⁰	57.2 (s)
C ¹¹	131.3 (s)
C ¹² , C ^{12'} , C ¹³ , C ^{13'}	129.5 (s)
C ¹⁴	129.0 (s)

In the ¹³C NMR spectrum of **1** the signal that appears most downfield can be assigned to the highly deshielded C-atom in the 5-position on the tetrazole ring. The resonance is detected as a singlet of low intensity (due to the absence of NOE enhancement during the decoupling process) at δ 161.2. The *ortho*- and *meta*-carbon atoms of the aromatic ring are rendered equivalent by their chemical environment and resonate as an intense singlet at δ 129.5. The low intensity resonance at δ 131.3 and medium intensity resonance at δ 129.0 can be ascribed to the *ipso*- and *para*-carbon atoms respectively. The most upfield of the signals in the unsaturated sp² carbon region (δ 115.6), can be assigned to the rather shielded C-atom in the 7-position of the thiophene ring, while the C-atom in the 6-position resonates significantly more downfield at δ 133.9. The NMR spectroscopic data of **1** compares favorably to related compounds reported in the literature.

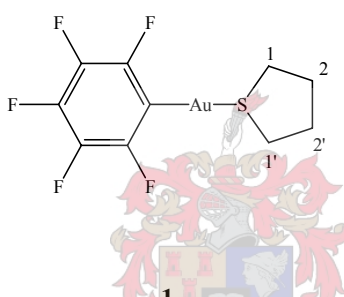
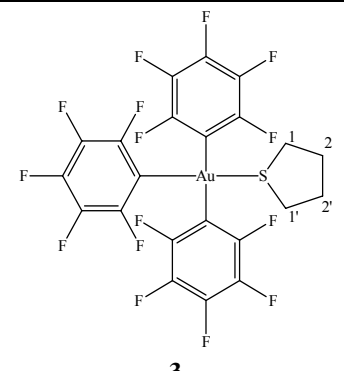
Due to very low yields, compound **4** could not be characterized by means of NMR spectroscopy. The low resonance intensities of the pfp ligands in ¹³C NMR and the broad signals for the tht ligands in the ¹H NMR would not allow for unambiguous characterization and assignments. All attempts to obtain ¹H, ¹³C and ¹⁹F spectra of compound **2**, using high resolution (400 MHz and 600 MHz) instruments, failed. In the crystal batches used during these attempts, the distinctive yellow crystals of compound **2** were clearly visible amongst the other colourless crystals of **1** and **3**. NMR spectra of these mixtures however only contained the diagnostic signals for the starting materials **1** and **3**. From this it could be concluded that the concentration of compound **2** in these solutions was too low for detection or compound **2** is unstable in solution and reverts back to **1** and **3**. The latter explanation is however currently favoured. The ¹H, ¹³C and ¹⁹F NMR spectroscopic assignments for compounds **1**, **3** are summarised in Table 2.4.

The ¹H NMR spectra offer limited information as to the structures of complexes **1** and **3**, with only the two broad singlet signals of more or less equal intensity, observed for the tht ligands, prominent. As one would expect, the signal for the H-atoms bonded to the C-atoms α to the sulphur atom emerge more downfield from the signal observed for the H-atoms bonded to the carbon atoms further removed from this deshielding atom.

In the high resolution ¹³C NMR spectra of both complex **1** and **3**, resonance signals assigned to the tht C-atoms α to the S-atoms are detected at δ 39.3 and δ 40.6, respectively. These broad resonances are less intense and more downfield from the

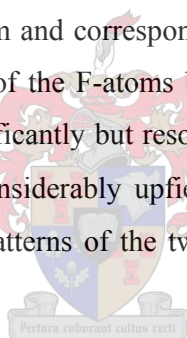
resonances observed for the C-atoms β to the S-atom which emerge at δ 31.4 for **1** and δ 31.7 for **3**. The presence of Au(C₆F₅) moieties is confirmed by the distinctive C–F and F–F coupling patterns found in the ¹³C and ¹⁹F NMR spectra of these complexes. In the ¹³C NMR spectrum of **1**, a triplet of unresolved multiplets is detected at δ 126.4 (²J = 58.0 Hz) and can be assigned to the *ipso*-carbon atom which couples to F-atoms over 2, 3 and 4 bonds. C–F coupling of the *ortho*-carbon atoms results in a doublet of doublets of multiplets at δ 149.4 (¹J = 226.6 Hz, ²J = 27.6 Hz) whereas the two doublets of multiplets sets detected at δ 137.6 (¹J = 248.8 Hz) and δ 139.5 (¹J = 243.7 Hz) can be assigned to the C–F coupled *meta*- and *para*-carbon atoms respectively.

Table 2.4 ¹H, ¹³C and ¹⁹F NMR spectroscopic data of complexes **1** and **3**.

Complex		
Solvent	Acetone-d ₆	Acetone-d ₆
Temperature (°C)	25	25
Assignment	Chemical shift (ppm)	
¹ H NMR δ (ppm) (300/400 MHz)	H ¹ , H ^{1'} 3.50 (s, 4H) H ² , H ^{2'} 2.21 (s, 4H)	3.39 (s, 4H) 2.92 (s, 4H)
¹³ C NMR δ (ppm) (75/100 MHz)	C ¹ , C ^{1'} 39.3 (s) C ² , C ^{2'} 31.4 (s) C ₆ F ₅ -C ^{<i>ipso</i>} 126.4 (tm, ² J = 58.0 Hz) C ₆ F ₅ -C ^{<i>ortho</i>} 149.4 (ddm, ¹ J = 226.6 Hz, ² J = 27.6 Hz) C ₆ F ₅ -C ^{<i>meta</i>} 137.6 (dm, ¹ J = 248.8 Hz) C ₆ F ₅ -C ^{<i>para</i>} 139.5 (dm, ¹ J = 243.7 Hz)	40.6 (s) 31.7 (s) 106.8 (tm, ² J = 54.3 Hz,), 118.1 (tm, ² J = 44.8 Hz) 144.2 (dm, ¹ J = 234.8 Hz), 145.9 (dm, ¹ J = 234.1 Hz), 137.1 (dm, ¹ J = 214.7 Hz), 138.0 (dm, ¹ J = 252.2 Hz) 139.8 (dm, ¹ J = 244.6 Hz), 140.6 (dm, ¹ J = 234.7 Hz)
¹⁹ F NMR δ (ppm) (376 MHz)	F ^{<i>ortho</i>} -112.8 (m) F ^{<i>meta</i>} -157.9 (t) F ^{<i>para</i>} -161.1 (m)	121.9 (m), -122.1 (m) -157.1 (t, ³ J = 19.7 Hz), -158.0 (t, ³ J = 19.7 Hz) -161.4 (m), -162.4 (m)

In the ¹³C NMR spectrum of **3**, two sets of resonances, portraying a similar coupling pattern to that noticed for **1**, are observed for each of the *ipso*-, *ortho*-, *meta*- and *para*-carbon atoms. These sets consist of a less intense upfield set and a more intense slightly downfield set corresponding to the pfp entities *trans* and *cis* to the tht ligand respectively. Assignments of ¹³C-resonances and calculation of coupling constants were made only tentatively, due to the presence of severe long range coupling resulting in heavy multiplicity along with a moderate degree of overlap. The chemical shifts of the resonances are comparable to those of **1**, with the greatest discrepancies detected for the *ipso*- and *ortho*-carbon atom resonances.

In the ¹⁹F NMR spectrum of **1** the the F-atoms bonded to the *ortho*- and *para*-carbon atoms resonate as multiplets at δ 112.8 and δ 161.1 respectively, while the triplet observed at δ 157.9 can be ascribed to the F–F coupled F-atom bonded to the *meta*-carbon atom. As was noticed in the ¹³C NMR spectrum of **3**, two sets of resonances are observed for the pfp groups in the ¹⁹F NMR spectrum and correspond to the pfp moieties *cis* and *trans* to the tht ligand. The chemical shifts of the F-atoms bonded to the *meta*- and *para*-carbon atoms of **1** and **3** do not differ significantly but resonances for the F-atoms bonded to the *ortho*-carbon atoms of **3** appear considerably upfield (δ 121.9 and δ 122.1) from those observed in **1**. The F–F coupling patterns of the two complexes are comparable and no distinctive differences exist.



2.2.2.2 Mass spectrometry

Electron impact mass (EI-MS) spectral data for compound **I** are summarised in Table 2.5 with mass to charge ratios (m/z) of the isotope peaks corresponding to fragments containing ⁷⁹Br or ⁸¹Br, separated by a backslash. The EI-MS spectrum of **I** reveals two distinctive molecular ion (M^+) isotope peaks (m/z 320/322). Diagnostic fragmentation patterns include the loss of molecular nitrogen (m/z 292/294) and a further loss of two CH fragments from the remaining cation (m/z 264/266). The loss of two nitrogen molecules together with a benzyl group result in fragments with m/z ratios of 173 (⁷⁹Br) and 175 (⁸¹Br).

Attempts to obtain the fast atom bombardment mass spectrum (FAB-MS) of **2**, were unsuccessful. Again it is possible that the compound decomposed in solution prior to analysis.

Table 2.5 Mass spectrometric data of compound **I**

Fragment	<i>m/z</i> (I in %)*
{[M]} ⁺	320 (33) / 322 (36)
{[M]-N ₂ } ⁺	292 (8) / 294 (10)
{[M]-N ₂ -2CH} ⁺	264 (64) / 266 (57)
{[M]-(Br)(S)C=CH} ⁺	184 (55)
{[M]-benzyl-2N ₂ } ⁺	173(4) / 175 (5)
{[M]-benzyl-Br} ⁺	152 (33)
{Benzyl} ⁺	91 (100)
{Tetrazole} ⁺	69 (28)

* *m/z* values separated by / refers to isotope peaks of ⁷⁹Br and ⁸¹Br respectively

2.2.3 Structure determinations of compounds **I** and **1 – 5**

The crystal and molecular structures of compounds **I**, **1**, **2**, **3** (**3a** and **3b**) and **4** were determined by single crystal X-ray diffraction. The bond lengths and angles of the pfp ligands in complexes **1 – 4**, do not show any variation with changes in the oxidation state of the central gold atom. All pfp ligands display C–C bond lengths in the order of 1.35 – 1.39 Å and C – F bond lengths within the range 1.34 – 1.37 Å. These values also compare favourably to pfp bonds lengths and angles reported for related compounds and will therefore not be discussed in more detail.^{3,4}

2.2.3.1 Crystal and molecular structure of 2-benzyl-5-(5-bromo-thiophen-2-yl)-2H-tetrazole, **I**

Compound **I** crystallises from diethyl ether in the monoclinic space group *P*2₁/*n* with only one unique molecule in the asymmetric unit and *Z* = 4 molecules in the unit cell. The molecular structure of **I** is depicted in Figure 2.3 and selected bond lengths and angles are summarised in Table 2.6. Within the molecular structure, the thiophene, tetrazole and benzylic CH₂ moieties, all lie within the same plane with the phenyl ring positioned at an angle of 111.5(1)° to this plane. The bond lengths and angles of the thiophene and tetrazole rings are comparable to those observed for similar compounds, 2-(2-bromothiophen-5-yl)-5,6-dimethyl-1,3,6-triazolebicyclo(3.1.0)-hexane and N-acetyl-(1-1-benzyl-1*H*-tetrazol-5-yl)ethylamine.^{41,42}

⁴¹ A. V. Shevtsov, V. Yu. Petukhova, N. N. Makhova, K. A. Lyssenko, *Russ. Chem. Bull. Int. Ed.* **2002**, *51*, 1497-1503.

⁴² A. Le Tiran, J. P. Stables, H. Kohn, *Bioorg. Med. Chem.* **2001**, *9*, 2693-2708.

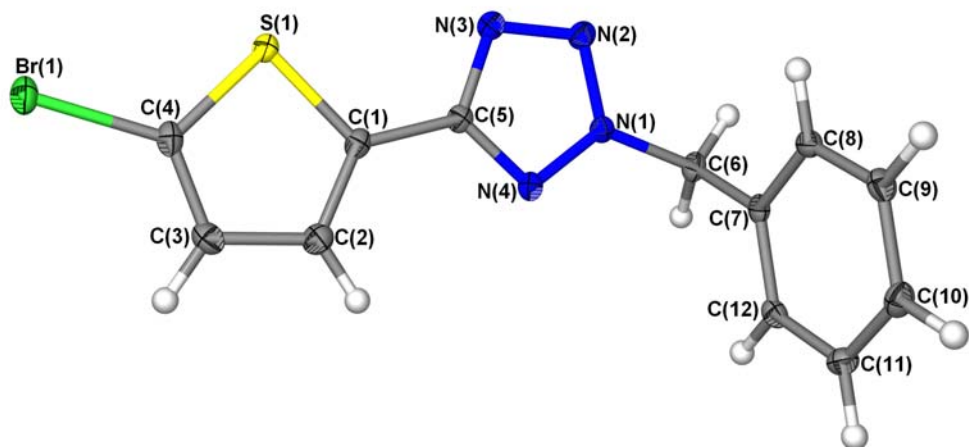


Figure 2.3 Molecular structure of **I** showing the numbering scheme. Thermal ellipsoids are set at 50% probability.

Table 2.6 Selected bond lengths (Å) and angles (°) of **I** with estimated standard deviations in parenthesis.

<i>Bond lengths</i> (Å)			
C(4)–Br(1)	1.875(2)	C(1)–C(2)	1.360(3)
C(4)–S(1)	1.723(2)	C(2)–C(3)	1.419(3)
C(1)–S(1)	1.729(2)	N(1)–N(2)	1.323(2)
C(1)–C(5)	1.453(2)	N(2)–N(3)	1.325(2)
C(5)–N(3)	1.350(2)	N(1)–N(4)	1.328(2)
C(5)–N(4)	1.338(2)	N(1)–C(6)	1.469(2)
C(4)–C(3)	1.350(3)	C(6)–C(7)	1.512(2)
<i>Bond angles</i> (°)			
Br(1)–C(4)–S(1)	119.7(1)	C(5)–N(4)–N(1)	101.1(1)
C(4)–S(1)–C(1)	90.26(9)	N(1)–N(2)–N(3)	105.7(1)
S(1)–C(1)–C(5)	120.3(1)	N(2)–N(1)–N(4)	114.6(1)
C(1)–C(5)–N(3)	123.9(2)	N(2)–N(1)–C(6)	122.1(2)
C(1)–C(5)–N(4)	123.6(2)	N(4)–N(1)–C(6)	123.3(2)
N(3)–C(5)–N(4)	112.5(2)	N(1)–C(6)–C(7)	111.5(1)
C(5)–N(3)–N(2)	106.2(2)		

The well-organised molecular packing of **I** is largely directed by π – π stacking of the thiophene rings along the a-axis. The molecules assemble in repeating box-like pairs along the b-axis, with each of the molecules within a pair related to each other *via* a two-fold rototranslation followed by an n-glide (Figure 2.4). Apart from the π – π interactions, no other noteworthy interactions are observed.

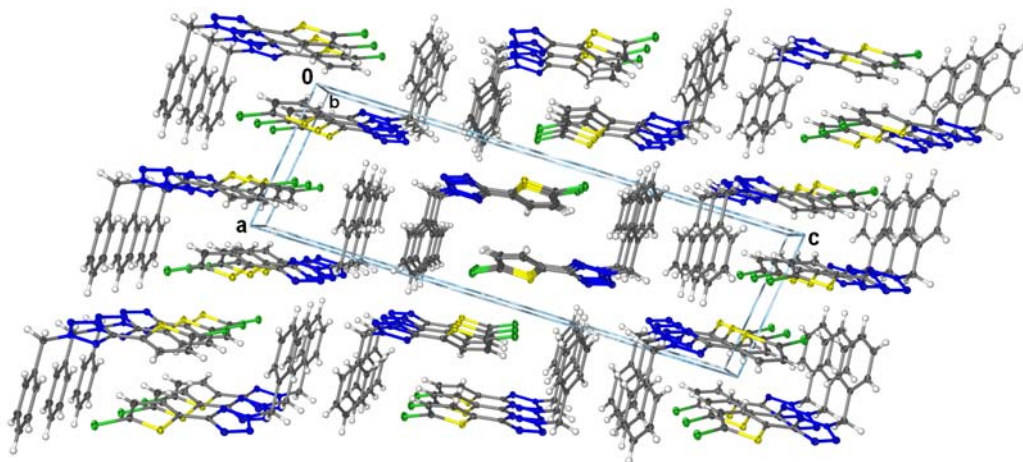


Figure 2.4 Perspective drawing of the box-like molecular packing of **I** viewed along the b-axis.

2.2.3.2 Crystal and molecular structure of tetrakis(pentafluorophenyl)bis(tetrahydrothiophene)digold(II)

The most spectacular of the crystalline pfp-tht complex products, $(C_6F_5)_2(tht)Au-Au(tht)(C_6F_5)_2$, **2**, forms tetragonal crystals within the space group $P4_12_12$ with $Z = 4$ molecules in the unit cell. The gold atoms occur in two distorted square planar configurations, featuring a linear S–Au–Au–S axis and two orthogonally oriented $(C_6F_5)Au(C_6F_5)$ moieties with all aromatic rings in parallel planes (Figure 2.5).

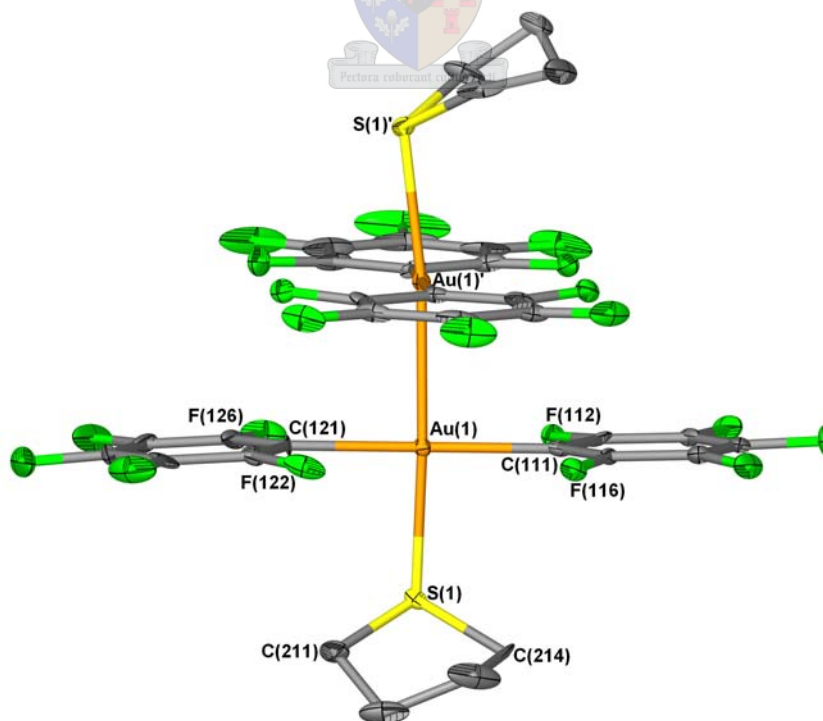


Figure 2.5 Molecular structure of **2** showing the numbering scheme. Thermal ellipsoids are set at 25% probability and hydrogen atoms are omitted for clarity.

Selected bond lengths and angles are summarized in Table 2.7. The tht ligands are situated at a torsion angle of 93° to each other, on either side of the essentially linear S1–Au1–Au1'–S1' backbone. The Au^{II}–Au^{II} bond length of 2.5679(7) Å is within the range of bond lengths displayed by the only other reported examples of unbridged, but chelated, Au^{II}–Au^{II} compounds, namely: bis(quinolin-8-ylthio)digold dichloride [2.5355(5) Å],¹³ [Au₂(dppn)₂Cl₂][PF₆]₂ [2.6112(7) Å],¹¹ [Au₂(dppn)₂Br₂][PF₆]₂ [2.6035(8) Å] and [Au₂(dppn)₂I₂][PF₆]₂ [2.6405(8) Å].¹² The Au–C bonds [2.110(2) and 2.078(2) Å] are significantly longer than those observed for the anionic gold(I) compound [n-Bu₄N][Au(C₆F₅)₂] [2.044(4) Å],^[43] possibly reflecting the higher s-character of the overlapping orbitals in gold(I) compared to gold(II).^[44]

Table 2.7 Selected bond lengths (Å) and angles (°) of **2** with estimated standard deviations in parenthesis.

<i>Bond lengths (Å)</i>			
C(111)–Au(1)	2.110(2)	S(1)–Au(1)	2.418(3)
C(121)–Au(1)	2.078(2)	Au(1)–Au(1)'	2.5679(7)
<i>Bond angles (°)</i>			
S(1)–Au(1)–Au(1)'	173.58(7)	C(111)–Au(1)–Au(1)'	91.53(6)
C(111)–Au(1)–S(1)	90.7(1)	C(121)–Au(1)–Au(1)'	88.14(7)
C(121)–Au(1)–S(1)	89.9(1)	C(111)–Au(1)–C(121)	177.6(2)

2.2.3.3 Crystal and molecular structure of tris(pentafluorophenyl)(tetrahydrothiophene)gold(III), **3a** and **3b**

Crystals of the gold(III) compound, **3**, were obtained in two polymorphic forms, space groups *Pbca*, **3a**, and *P2₁/n*, **3b**, and are orthorhombic and monoclinic respectively. The asymmetric unit of both forms contain only one independent molecule while the unit cells consist of *Z* = 8 (**3a**) and 4 (**3b**) molecules. The crystals feature similar, equivalent molecules with the donor atoms of the ligands arranged in a square planar manner about the central gold atoms. Figure 2.6 shows the molecular structures of **3a** and **3b** with details on selected bond lengths and angles summarised in Table 2.8 and 2.9. The only obvious difference between the two polymorphs appears to be the orientation of the tht ligand. Owing to the large mutual *trans* influences of the two opposing pfp ligands, their Au–C bond distances [2.060(6) Å - 2.075(6) Å] are longer than when such a ligand appears *trans*

⁴³ P. G. Jones, *Z. Kristallogr.* **1993**, 208, 347-350.

⁴⁴ L. E. Orgel, *J. Am. Chem. Soc.* **1958**, 4186-4190.

to the tht ligand [2.035(5) / 2.031(3) Å]. Similar results have been reported for [Au(C₆F₅)₃(S₂CPEt₃)]⁴⁵ and [Au(Me)₃(PPh₃)]⁴⁶. The Au–C and Au–S bond lengths agree with those observed in [Au(C₆F₅)₃(S₂CPEt₃)] [Au–C: 2.067(4) Å / 2.076(4) Å / 2.037(3) Å and Au–S: 2.366(1) Å]. Furthermore, it is noteworthy that the Au–C and Au–S bonds of both polymorphs are significantly shorter and hence stronger than those of the analogous gold(II) compound, **2**.

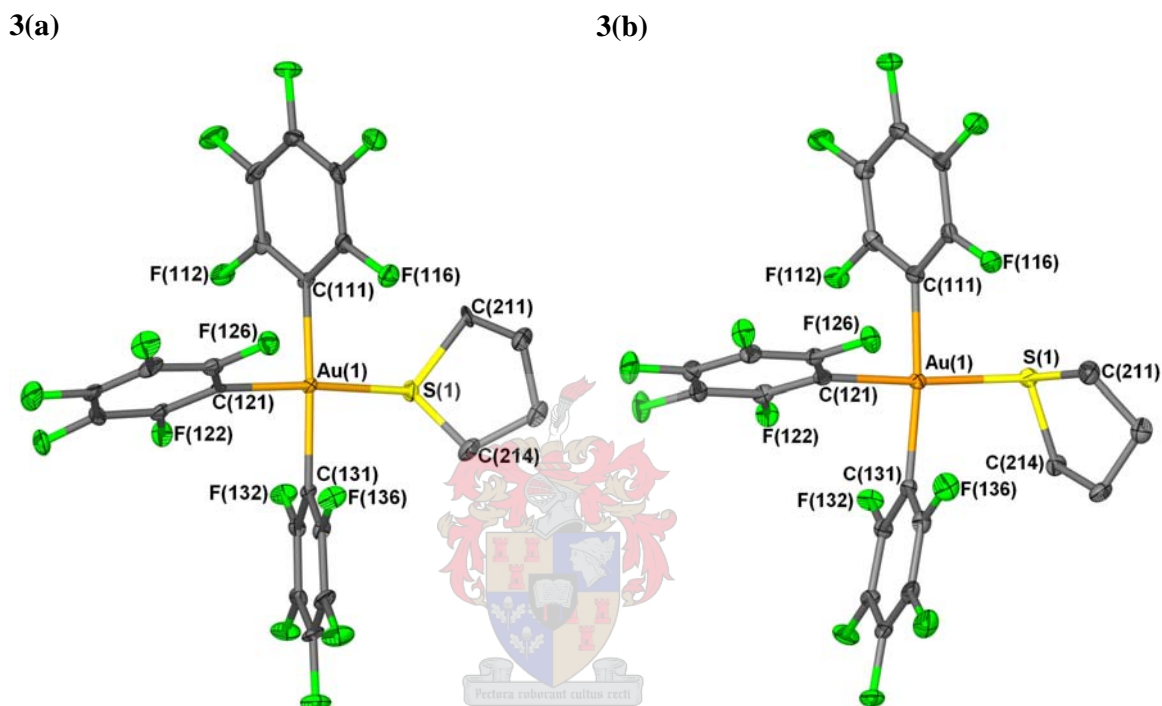


Figure 2.6 Molecular structures of compounds **3a** (left) and **3b** (right). Thermal ellipsoids are set at 50%. H-atoms are omitted for clarity.

Table 2.8 Selected bond lengths (Å) and angles (°) for **3a** with estimated standard deviations in parenthesis.

<i>Bond lengths</i> (Å)			
C(111)–Au(1)	2.060(6)	C(131)–Au(1)	2.075(6)
C(121)–Au(1)	2.035(5)	S(1)–Au(1)	2.362(2)
<i>Bond angles</i> (°)			
C(111)–Au(1)–S(1)	95.93(15)	C(111)–Au(1)–C(121)	88.3(2)
C(121)–Au(1)–S(1)	174.4(2)	C(121)–Au(1)–C(131)	88.4(2)
C(131)–Au(1)–S(1)	87.4(2)	C(111)–Au(1)–C(131)	176.6(2)

⁴⁵ R. Usón, A. Laguna, M. Laguna, M. L. Castilla, P. J. Jones, C. Fittschen, *J. Chem. Soc., Dalton Trans.* **1987**, 3017-3022.

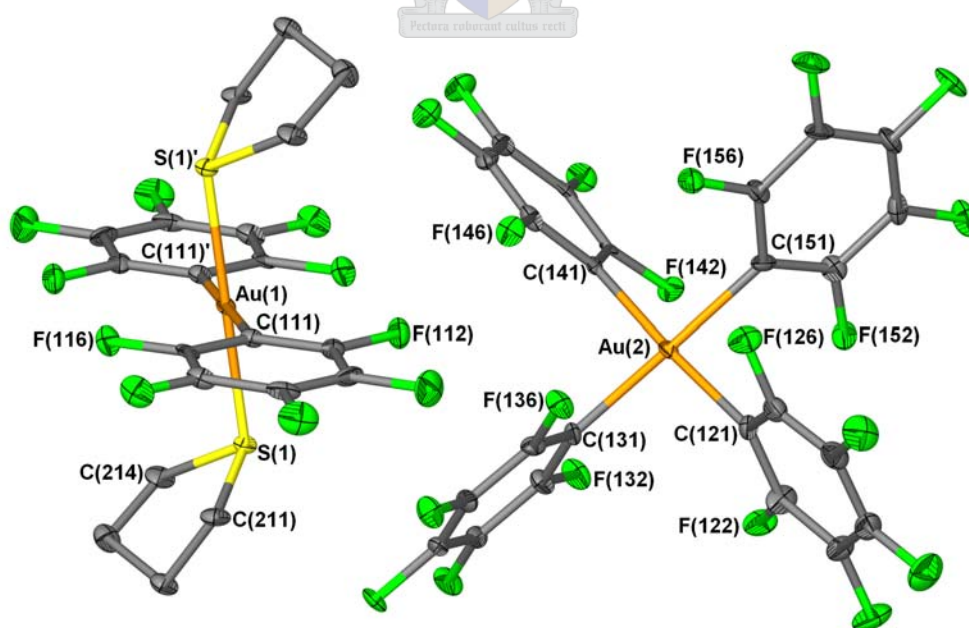
⁴⁶ J. Stein, J. P. Fackler, Jr., C. Papparizos, H. W. Chen, *J. Am. Chem. Soc.* **1981**, *103*, 2192-2198.

Table 2.9 Selected bond lengths (Å) and angles (°) for **3b** with estimated standard deviations in parenthesis.

<i>Bond lengths (Å)</i>			
C(111)–Au(1)	2.067(3)	C(131)–Au(1)	2.067(3)
C(121)–Au(1)	2.031(3)	S(1)–Au(1)	2.3794(9)
<i>Bond angles (°)</i>			
C(111)–Au(1)–S(1)	89.12(9)	C(111)–Au(1)–C(121)	87.1(1)
C(121)–Au(1)–S(1)	176.19(9)	C(121)–Au(1)–C(131)	86.5(1)
C(131)–Au(1)–S(1)	97.31(9)	C(111)–Au(1)–C(131)	173.6(1)

2.2.3.4 Crystal and molecular structure of [bis(pentafluorophenyl)bis(tetrahydrothiophene)gold(III)][tetrakis(pentafluorophenyl)gold(III)]

The ionic compound [Au(C₆F₅)₂(tht)₂][Au(C₆F₅)₄], **4**, (the result of a ligand scrambling reaction) represents the first gold(III) compound to contain pfp and/or tht ligands in both of the composite ions. The compound crystallises from a pentane layered solution of diethyl ether as colourless needles in the triclinic space group *P* $\bar{1}$. The asymmetric unit consists of one unique molecule of each of the ions and one molecule of pentane with *Z* = 8 molecules in the unit cell. Figure 2.7 depicts the molecular structure, indicating the numbering scheme, and details on selected bond lengths and angles are summarised in Table 2.10.

**Figure 2.7** Molecular structure of **4** showing the numbering scheme. Thermal ellipsoids are set at 50% probability. Hydrogen atoms and pentane molecule are omitted for clarity.

The coordination geometry of both gold atoms is square planar with the homoleptic anion adopting the same propeller-like D₄ symmetry as reported for [Ph₃P=N=PPh₃]-[Au(C₆F₅)₄]⁴⁷ with comparable Au–C bond lengths, ranging from 2.050(6) to 2.065(6) Å. To meet the steric constraints and avoid repulsive F···F interactions, the planes of the pfp rings are twisted with respect to the central coordination sphere. The cation, on the other hand, contains an Au^{III} centre of the type *trans*-[AuR₂L₂] (R = organic ligand, L = neutral ligand) comparable to the complex [Au(C₆F₅)₂(tht)₂][CF₃SO₃].³ This complex does not comply with the normal anti-symbiosis prevalent in most square planar complexes. It thus represents an example of a gold(III) complex where two pfp ligands occur in a symbiotic *trans* relationship. Furthermore, the very strong preference for *cis* isomers in [AuR₂X₂] compounds (according to the Tobias orbital rationalisation)^[48] is thrown overboard. All Au–C bond lengths compare well to the separation measured for the Au–C bonds *trans* to the tht ligand in compound **3**. The Au–S bond [2.335(1) Å], is on the other hand, significantly shorter than the corresponding bonds in compound **3** [2.362(2) Å and 2.3794(9) Å].

Table 2.10 Selected bond lengths (Å) and angles (°) of **4** with estimated standard deviations in parenthesis.

<i>Bond lengths</i> (Å)			
C(111)–Au(1)	2.066(6)	C(131)–Au(2)	2.050(6)
S(1)–Au(1)	2.335(1)	C(141)–Au(2)	2.065(6)
C(121)–Au(2)	2.051(6)	C(151)–Au(2)	2.055(7)
<i>Bond angles</i> (°)			
C(111)–Au(1)–S(1)	91.1(2)	C(121)–Au(2)–C(151)	87.8(3)
C(111)–Au(1)–S(1)'	88.9(2)	C(121)–Au(2)–C(141)	176.5(3)
C(111)–Au(1)–C(111)'	180.000	C(131)–Au(2)–C(141)	92.3(2)
S(1)–Au(1)–S(1)'	180.000	C(131)–Au(2)–C(151)	176.4(3)
C(121)–Au(2)–C(131)	91.2(3)	C(141)–Au(2)–C(151)	88.8(2)

2.2.3.4 Crystal and molecular structure of (pentafluorophenyl)(tetrahydrothiophene)gold(I)

To complete a series of [Au_x(C₆F₅)_y(tht)_z] gold(I), gold(II) and gold(III) compounds, the important starting compound, **1**, was crystallised from diethyl ether as orthorhombic

⁴⁷ a) P. G. Jones, E. Bembenek, *Z. Kristallogr.* **1994**, *209*, 690-692, b) H. H. Murray, J. P. Fackler, L. C. Porter, D. A. Briggs, M. A. Guerra, R. J. Lagow, *Inorg. Chem.* **1987**, *26*, 357-363.

⁴⁸ a) R. J. Puddephatt in: *Comprehensive Organometallic Chemistry I, Vol. 2* (Eds. E. J. Abel, F. J. Stone, G. Wilkinson) 2nd edition, Pergamon Press, Oxford, **1982**, p762; p789; p801, b) R. S. Tobias, *Inorg. Chem.* **1970**, *9*, 1296-1298.

crystals, space group $Pbnb$, with $Z = 16$ molecules in the unit cell. The structural elucidation of this compound was first reported by another member of our group and is included, in the interest of completeness, with courtesy of K. Coetzee.⁴⁹ Selected bond lengths and angles are given in Table 2.11. The asymmetric unit contains two independent monomers with similar paddle-like geometries and one half of an ether molecule (Figure 2.8).

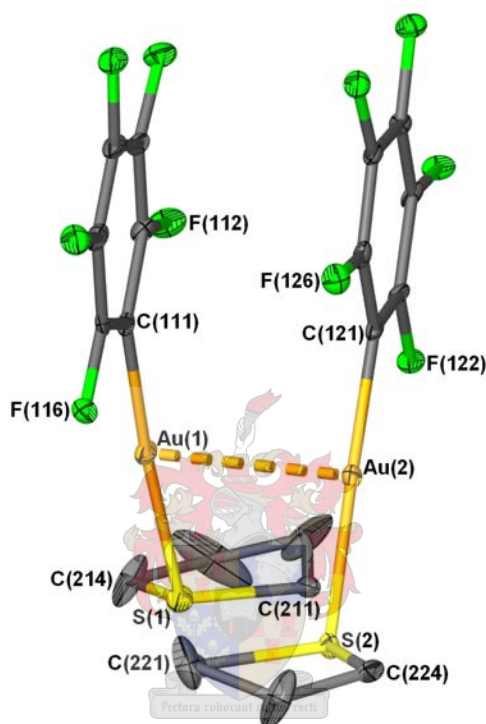


Figure 2.8 Representation of the asymmetric unit of **2** showing the aurophilic interaction between the two unique gold centres. Thermal ellipsoids are set at 25% probability. Hydrogen atoms and the solvent molecule are omitted for clarity.

These monomers associate *via* alternating long (3.306 Å) and two different short (3.191 Å, 3.128 Å) aurophilic interactions (Figure 2.9) to form an infinite chain along the *a*-axis. All of these distances fall within the range of typically observed distances for aurophilic interactions between gold(I) centres.^{3,50} Identical pairs of molecules are alternatingly rotated by 180°. Wide angles (142.8°, 139.2°) between symmetry-related molecules and small torsion angles (42.85°) between the independent monomers are observed. The small torsion angles of the latter result in greater steric hindrance and weaker Au⋯Au interactions as is evident from the observed bond distances. The Au–S bond lengths

⁴⁹ K. Coetzee, *MSc Thesis* **2003**, University of Stellenbosch, p112-115.

⁵⁰ H. Schmidbaur, *Chem. Soc. Rev.* **1995**, 24, 391-400.

present in the structure [2.317(3) and 2.320(3) Å] do not deviate significantly from those observed for $[Au(tht)_2](C_6H_4NO_4S_2)$ [2.2948(14) Å] and $[Au(tht)_2][Au_2]$ [2.306(7) and 2.335(6) Å].^{51,27} The observed Au–C bond lengths [2.014(9) and 2.03(1)] can be compared to that of $[Au(C_6F_5)\{S=CN(H)C(CH_3)=C(H)S\}]$ [2.06(1) Å].⁴ Furthermore, it is noteworthy that the average Au–C and Au–S bonds are significantly shorter, and therefore much stronger, than those observed for compounds **2**, **3** and **4**.

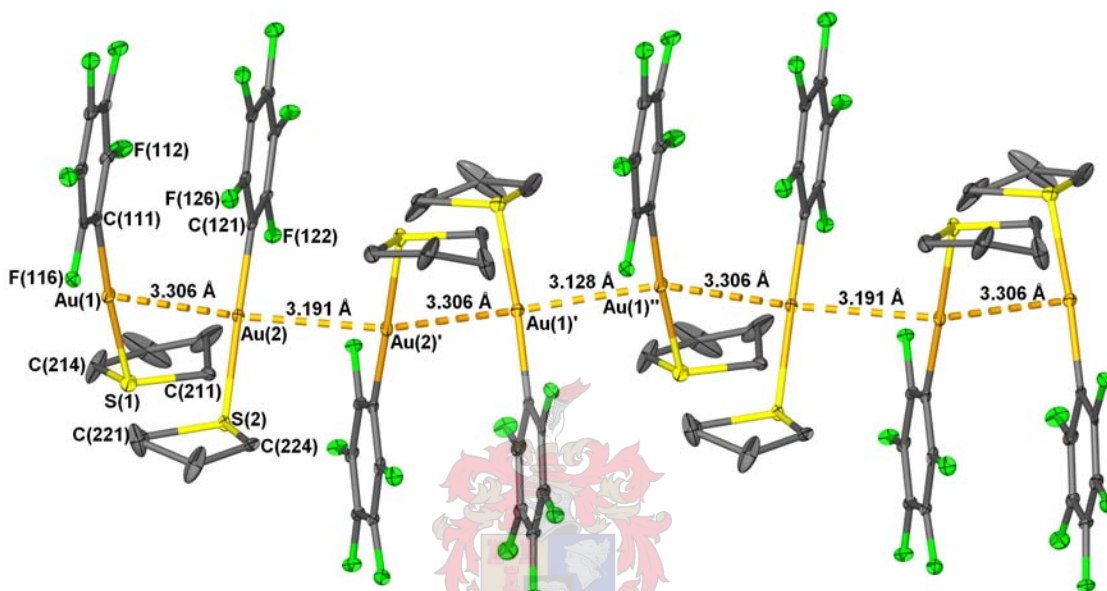


Figure 2.9 Representation showing the organisation of **2** in an infinite chain along the a-axis. Thermal ellipsoids are set at 25% probability. Hydrogen atoms and solvent molecules are omitted for clarity.

Table 2.11 Selected bond lengths (Å) and angles (°) of **1** with estimated standard deviations in parenthesis.

<i>Bond lengths (Å)</i>			
C(111)–Au(1)	2.014(9)	Au(1)···Au(2)	3.306(1)
C(121)–Au(2)	2.03(1)	Au(2)···Au(2)'	3.191(2)
S(1)–Au(1)	2.317(3)	Au(1)'···Au(1)''	3.128(2)
S(2)–Au(2)	2.320(3)		

<i>Bond angles (°)</i>	
C(111)–Au(1)–S(1)	176.3(3)
C(121)–Au(2)–S(2)	178.0(3)

⁵¹ S. Friedrichs, P. G. Jones, *Acta Crystallogr., Sect. C* **2000**, 56, 56-57.

2.3 Conclusion

Herein a series of [Au_x(C₆F₅)_y(tht)_z] gold(I), (II) and (III) compounds were reported. This series included an unprecedented pentafluorophenyl- and tetrahydrothiophene-containing gold(II) complex, that formally forms by radical transfer of a usually inert pfp ligand along with gold–gold bond formation. This compound, which represents the first example of an unbridged unchelated dinuclear gold(II) compound, could also be prepared in a rational manner. In addition, one gold(I) and two gold(III) compounds that contain the same ligands were described. One of the latter products resulted from a novel mononuclear ligand scrambling (metathesis or disproportionation) reaction, proving that such reactions are not only possible for gold(I) complexes but can also occur for gold(III) complexes. In all the complexes (independent of charge) that contained a (C₆F₅)Au(C₆F₅) unit, the Au–C bond lengths decreased in the order Au(II)>Au(III)>Au(I) (ca. 2.11, 2.06 and 2.04 Å). A similar variation was found for the Au–S separation in the tht–Au^{III}–C₆F₅, tht–Au^{III}–tht, tht–Au^{II}–Au^{II} and tht–Au^I–C₆F₅ fragments (ca. 2.36, 2.34; 2.42 and 2.32 Å). Although the differences are small, the results indicated an ionic radius variation with the gold(II) the largest ion and gold(III) larger than gold(I). Theoretical studies involving these compounds are underway.

2.4 Experimental

2.4.1 General procedures and instruments

All reactions were carried out under argon using standard Schlenk- and vacuum-line techniques. Tetrahydrofuran (THF), diethyl ether, *n*-hexane and *n*-pentane were distilled under N₂ from sodium benzophenone ketyl and N,N'-dimethylformamide (DMF) from CaH₂. 5-Bromo-2-thiophene-carbaldehyde, NaN₃, ZnBr₂, benzylbromide, 2-bromo-5-methylthiophene and bromopentafluorophenyl were purchased from Aldrich and tetrahydrothiophene (tht) from Acros. Literature methods were used to prepare [Au(C₆F₅)(tht)] (**1**)⁵² from [HAuCl₄]⁵³ and [Au(C₆F₅)₃(tht)] (**3b**) from [Ti(C₆F₅)₂(Cl)].⁵⁴

⁵² R. Usón, A. Laguna, M. Laguna, *Inorg. Synth.* **1989**, 26, 85-91.

⁵³ A. Haas, J. Helmbrecht, U. Nieman in *Handbuch der Präparativen Anorganischen Chemie*, Vol. 2 (Ed. G. Brauer) 3rd edition, Ferdinand Enke, Stuttgart, **1978**, p1014.

⁵⁴ R. Usón, A. Laguna, *Inorg. Synth.* **1982**, 21, 71-74.

Melting points were determined on a Stuart SMP3 apparatus and are uncorrected. Mass spectra were recorded on an AMD 604 (EI, 70 eV) or a VG 70 SEQ (FAB, 70 eV, recorded in a *m*-nitrobenzylalcohol matrix) instrument. NMR spectra were recorded on a Varian 300/400 FT or INOVA 600 MHz spectrometer (¹H NMR at 300/400/600 MHz, ¹³C NMR at 75/100/150 MHz and ¹⁹F NMR at 376 MHz) with chemical shifts reported relative to an internal solvent resonance or an external reference of CFCl₃ (¹⁹F). Elemental analysis was carried out at the School of Chemistry, University of the Witwatersrand. Prior to elemental analysis, the products were evacuated under high vacuum for 10h.

2.4.2 Preparations and procedures

2.4.2.1 Preparation of 5-bromo-2-(2H-tetrazol-5-yl)thiophene

A solution of 5-bromo-thiophene-2-carbaldehyde (1.19 ml, 1.91 g, 10 mmol) and iodine (2.79 g, 11 mmol) in an ammonia water: THF mixture (90 ml of a 28% solution :10 ml) mixture was stirred for 2h 15 min at room temperature during which the dark solution became colourless. A mixture of NaN₃⁵⁵ (0.78 g, 12 mmol) and ZnBr₂ (3.38 g, 15 mmol) was added to the reaction mixture and then refluxed for 18 h with vigorous stirring. After addition of HCl (100 ml of a 1M solution) and EtOAc (500 ml), the mixture was stirred vigorously until no solid was present and the aqueous layer had a pH of 1. The organic phase was concentrated *in vacuo* and the remaining solid rinsed with EtOAc (2 × 100 ml) to give the title product as a yellow solid (0.66 g, 29%). The product was used without any further purification.

2.4.2.2 Preparation of 2-benzyl-5-(5-bromo-thiophen-2-yl)-2H-tetrazole, I

5-Bromo-2-(1H-tetrazol-5-yl)thiophene (1.155 g, 5 mmol) was added to a mixture of 99% NaH (0.12 g, 5 mmol) and DMF (8.82 ml). After stirring for 30 min, benzylbromide (0.62 ml, 0.86 g, 5 mmol) was added and the mixture stirred at room temperature for 2h. The reaction was quenched with water (60 ml). The precipitate was collected, extracted with ether (50 ml) and concentrated *in vacuo*. The product was isolated by column chromatography with ether / hexane (1:1) as eluent and recrystallised from diethyl ether to obtain the title compound as yellow crystals. (0.98 g, 61%)

⁵⁵ Caution: Due to the release of small amounts of hydrazoic acid, avoid the use of excess amounts of sodium azide.

2.3.2.2 Preparation of tetrakis(pentafluorophenyl)bis(tetrahydrothiophene)-digold(II), 2

Method A: A solution of **I** (0.15 g, 0.47 mmol) in diethyl ether (15 ml) was treated with a solution of freshly prepared [Au(C₆F₅)(tht)] (0.210 g, 0.464 mmol) in diethyl ether (15 ml). The yellow solution was stirred overnight at room temperature, filtered and concentrated *in vacuo*. The concentrated solution was transferred to a crystallisation tube, layered with *n*-hexane and stored under nitrogen at -22 °C. Single crystals of the title complex were obtained after two weeks.

Method B: A solution of [Au(C₆F₅)(tht)] (0.052 g, 0.114 mmol) in diethyl ether (10 ml) was added to a solution of [Au(C₆F₅)₃(tht)] (0.09 g, 0.114 mmol) in diethyl ether (10 ml) while the internal temperature was maintained at -75 °C. The reaction mixture was stirred at this temperature for 2h after which the mixture was slowly brought to room temperature, filtered and concentrated *in vacuo*. A fraction of the concentrated solution was transferred to a crystallisation tube and layered with *n*-hexane. Both solutions were stored under argon at -22 °C. Single crystals of the title complex were obtained after five months as yellow cubes.

2.3.2.3 Preparation of tris(pentafluorophenyl)(tetrahydrothiophene)gold(III), 3a

Method A: Single crystals of the title complex were isolated as colourless needles from the layered crystallisation mixture described in Method A of the procedure for the preparation of **2**.

Method B: A solution of 2-bromo-5-methylthiophene (0.08 ml, 0.08 g, 0.71 mmol) in diethyl ether (15 ml) was treated with a solution of freshly prepared [Au(C₆F₅)(tht)] (0.32 g, 0.71 mmol) in diethyl ether (15 ml). The colourless solution was stirred overnight at room temperature, filtered and concentrated *in vacuo*. The concentrated solution was transferred to a crystallisation tube, layered with *n*-hexane and stored under nitrogen at -22 °C. Single crystals of the title complex were obtained after three weeks as colourless needles.

2.3.2.4 Preparation of tris(pentafluorophenyl)(tetrahydrothiophene)gold(III), 3b

Single crystals of the title complex were isolated as colourless cubes from the layered crystallisation mixture described in Method B of the procedure for the preparation of **2**.

2.3.2.5 Preparation of bis(pentafluorophenyl)bis(tetrahydrothiophene)gold(III)-tetrakis(pentafluorophenyl)gold(III), 4

Single crystals of the title complex were isolated as colourless needles from the layered crystallisation mixture described in Method B of the procedure for the preparation of **2**.

2.4.3 X-ray structure determinations

The crystal data collection and refinement details for ligand **I** and complexes **1**, **2**, **3a**, **3b** and **4** are summarized in Tables 2.12, 2.13 and 2.14. X-ray quality single crystals of the complexes were obtained by crystallisation from concentrated diethyl ether solutions layered with *n*-hexane or *n*-pentane. Data sets for **I**, **1 b**, **2**, **3** and **4** were collected on a Bruker SMART Apex CCD diffractometer with graphite monochromated Mo-K α radiation ($k = 0.71073 \text{ \AA}$).⁵⁶ Data reduction was carried out with standard methods using the software package Bruker SAINT.⁵⁷ SMART data were treated with SADABS.^{58,59} The structures were solved by direct methods (**1**, **3b**, **4**) or interpretation of a Patterson synthesis (**2**, **3a**), which yielded the position of the metal atoms, and conventional difference Fourier methods. All non-hydrogen atoms were refined anisotropically by full-matrix least squares calculations on F^2 using SHELXL-97⁶⁰ within the X-seed environment.^{61,62} The hydrogen atoms were fixed in calculated positions. Figures were generated with X-seed and POV Ray for Windows, with the displacement ellipsoids at 25% probability (**1**, **2**) or 50% probability (**3**, **4**) level. Further information is available from Dr. S. Cronje at the Department of Chemistry and Polymer Science, Stellenbosch University.

⁵⁶ SMART Data Collection Software (version 5.629), Bruker AXS Inc., Madison, WI, **2002**.

⁵⁷ SAINT, Data Reduction Software (version 6.45), Bruker AXS Inc., Madison, WI, **2003**.

⁵⁸ R.H. Blessing, *Acta Crystallogr.* **1995**, *A51*, 33-38.

⁵⁹ SADABS (version 2.05), Bruker AXS Inc., Madison, WI, **2002**.

⁶⁰ G.M. Sheldrick, SHELX-97. Program for Crystal Structure Analysis, University of Göttingen (Germany), **1997**.

⁶¹ L.J. Barbour, *J. Supramol. Chem.* **2001**, *1*, 189-191.

⁶² J.L. Atwood, L.J. Barbour, *Cryst. Growth Des.* **2003**, *3*, 3-8.

Table 2.12 Crystallographic data for compounds **1** and **2**.

	[Au(C ₆ F ₅)(tht)]·0.25(EtO) 1	[Au ₂ (C ₆ F ₅) ₄ (tht) ₂] 2
Empirical formula	[C ₁₀ H ₈ AuF ₅ S ₁] ₁ ·0.25(C ₄ H ₁₀ O ₁)	C ₃₂ H ₁₆ Au ₂ F ₂₀ S ₂
<i>M_r</i>	470.72	1238.50
Temp. (K)	100 (2)	100 (2)
Wavelength (Å)	0.71073	0.71073
Crystal system	Orthorhombic	Tetragonal
Crystal dimensions (mm)	0.20 × 0.15 × 0.10	0.12 × 0.10 × 0.08
Crystal shape and colour	needle, colourless	cubes, yellow
Space group	<i>Pbn</i> b (No. 56)	<i>P4</i> ₁ 2 ₁ 2 (No. 92)
<i>a</i> (Å)	11.851(5)	10.8156(8)
<i>b</i> (Å)	18.664(8)	10.8156(8)
<i>c</i> (Å)	22.576(9)	28.675(4)
α (°)	90.00	90.00
β (°)	90.00	90.00
γ (°)	90.00	90.00
Volume (Å ³)	4994(4)	3354.3(6)
<i>Z</i>	16	4
<i>d</i> _{calcd} (g/cm ³)	2.504	2.452
μ (Mo–Kα) (mm ⁻¹)	11.993	9.000
Absorption correction	Semi-empirical from equivalents (SADABS)	Semi-empirical from equivalents (SADABS)
Absolute structure parameter		0.06(2)
<i>F</i> (000)	3496	2312
θ-range for data collection (°)	1.80 to 28.19	2.36 to 25.68
Index range	-14 ≤ <i>h</i> ≤ 15, -24 ≤ <i>k</i> ≤ 15 -29 ≤ <i>l</i> ≤ 22	-13 ≤ <i>h</i> ≤ 10, -13 ≤ <i>k</i> ≤ 5 -34 ≤ <i>l</i> ≤ 34
No. of reflections collected	29015	12595
No. of unique reflections	5819 (<i>R</i> _{int} = 0.1020)	3102 (<i>R</i> _{int} = 0.0624)
Max. and min. transmission	0.3801 and 0.1137	0.4849 and 0.3646
Refinement parameters / restraints	352 / 0	190 / 24
Goodness of fit on <i>F</i> ²	0.988	1.127
Final <i>R</i> -indices [<i>I</i> > 2σ > (<i>I</i>)]	<i>R</i> ₁ = 0.0512 <i>wR</i> ₂ = 0.0863	<i>R</i> ₁ = 0.0458 <i>wR</i> ₂ = 0.0900
<i>R</i> indices (all data)	<i>R</i> ₁ = 0.1179 <i>wR</i> ₂ = 0.1043	<i>R</i> ₁ = 0.0515 <i>wR</i> ₂ = 0.0920
Largest diff. peak and hole (e.Å ⁻³)	1.477 and -1.605	2.11 and -0.88
Weighing scheme ^a	<i>a</i> = 0.0369 / <i>b</i> = 0	<i>a</i> = 0.0001 / <i>b</i> = 26.3303

^a *wR*₂ = {Σ[w(*F*_o² - *F*_c²)²] / Σ[w(*F*_o²)²]}^{1/2}; *w* = 1/[σ²(*F*_o²) + (*aP*)² + *bP* + *d* + *e*sinθ]; *P* = [f(Max(0 or *F*_o²)) + (1 - *f*) *F*_c²]

Table 2.13 Crystallographic data for polymorphs **3a** and **3b**.

	[Au(C ₆ F ₅) ₃ (tht)] 3a	[Au(C ₆ F ₅) ₃ (tht)] 3b
Empirical formula	C ₂₂ H ₈ AuF ₁₅ S	C ₂₂ H ₈ AuF ₁₅ S
<i>M_r</i>	786.31	786.31
Temp. (K)	100(2)	100(2)
Wavelength (Å)	0.71073	0.71073
Crystal system	Orthorhombic	Monoclinic
Crystal dimensions (mm)	0.18 x 0.07 x 0.04	0.21 × 0.21 × 0.11
Crystal shape and colour	needle, colourless	cube, colourless
Space group	<i>Pbca</i> (No. 61)	<i>P2₁/n</i> (No. 14)
<i>a</i> (Å)	17.913(4)	10.161(1)
<i>b</i> (Å)	10.322(3)	12.635(1)
<i>c</i> (Å)	23.959(6)	17.831(2)
α (°)	90	90.00
β (°)	90	102.726(2)
γ (°)	90	90.00
Volume (Å ³)	4430(2)	2232.9(4)
<i>Z</i>	8	4
<i>d</i> _{calcd} (g/cm ³)	2.358	2.339
Absorption coefficient (μ , mm ⁻¹)	6.874	6.819
Absorption correction	Semi-empirical from equivalents (SADABS)	Semi-empirical from equivalents (SADABS)
F(000)	2960	1480
θ -range for data collection (°)	1.70 to 26.43	1.99 to 26.41
Index range	-22 ≤ <i>h</i> ≤ 22, -12 ≤ <i>k</i> ≤ 12 -21 ≤ <i>l</i> ≤ 29	-12 ≤ <i>h</i> ≤ 12, -15 ≤ <i>k</i> ≤ 15 -22 ≤ <i>l</i> ≤ 16
No. of reflections collected	24193	12755
No. independent reflections	4534 (<i>R</i> _{int} = 0.0484)	4539 (<i>R</i> _{int} = 0.0255)
Max. and min. transmission	0.7629 and 0.5506	0.4740 and 0.2476
Refinement parameters / restraints	352 / 0	352/0
Goodness of fit on <i>F</i> ²	1.118	1.037
Final <i>R</i> -indices [<i>I</i> > 2 σ (<i>I</i>)]	<i>R</i> ₁ = 0.0351 <i>wR</i> ₂ = 0.0717	<i>R</i> ₁ = 0.0218 <i>wR</i> ₂ = 0.0512
<i>R</i> indices (all data)	<i>R</i> ₁ = 0.0436 <i>wR</i> ₂ = 0.0745	<i>R</i> ₁ = 0.0256 <i>wR</i> ₂ = 0.0526
Largest diff. peak and hole (e.Å ⁻³)	1.987 and -1.126	1.101 and -0.464
Weighing scheme ^a	a = 0.0329 / b = 9.0518	a = 0.0288 / b = 0.1630

^a *wR*₂ = { $\sum[w(F_o^2 - F_c^2)^2] / \sum[w(F_o^2)^2]$ }^{1/2}; *w* = 1/[$\sigma^2(F_o^2) + (aP)^2 + bP + d + e \sin \theta$]; *P* = [*f*(Max(0 or *F_o²)) + (1-*f*) *F_c²*]*

Table 2.14 Crystallographic data for compounds **4** and **5**.

	[Au(C ₆ F ₅) ₂ (tht) ₂][Au(C ₆ F ₅) ₄] 4	I
Empirical formula	[C ₄₄ H ₁₆ Au ₂ F ₃₀ S ₂].[C ₅ H ₁₂]	C ₁₂ H ₉ BrN ₄ S
<i>M</i> _r	1644.77	321.20
Temp. (K)	100(2)	100(2)
Wavelength (Å)	0.71073	0.71073
Crystal system	Triclinic	Monoclinic
Crystal size (mm)	0.23 x 0.09 x 0.05	0.30 x 0.30 x 0.30
Crystal shape and colour	needle, colourless	needle, yellow
Space group	<i>P</i> $\bar{1}$ (No. 2)	<i>P</i> 2 ₁ / <i>n</i> (No. 14)
<i>a</i> (Å)	11.541(3)	8.0628(8)
<i>b</i> (Å)	13.675(3)	5.8255(6)
<i>c</i> (Å)	17.772(4)	26.564(3)
α (°)	74.360(4)	90
β (°)	79.626(4)	98.688(2)
γ (°)	66.427(3)	90
Volume (Å ³)	2467.3(9)	1233.4(2)
<i>Z</i>	2	4
<i>d</i> _{calcd} (g/cm ³)	2.214	1.730
Absorption coefficient (μ , mm ⁻¹)	6.176	3.488
Absorption correction	Semi-empirical from equivalents (SADABS)	Semi-empirical from equivalents (SADABS)
<i>F</i> (000)	1564	640
θ -range for data collection (°)	1.67 to 26.47	2.56 to 26.37
Index range	-14 ≤ <i>h</i> ≤ 14, -17 ≤ <i>k</i> ≤ 17, -22 ≤ <i>l</i> ≤ 22	-10 ≤ <i>h</i> ≤ 5, -7 ≤ <i>k</i> ≤ 7, -33 ≤ <i>l</i> ≤ 33
No. of reflections collected	26187	6828
No. independent reflections	10081 (<i>R</i> _{int} = 0.0479)	2509 (<i>R</i> _{int} = 0.0184)
Max. and min. transmission	0.737 and 0.493	0.4209 and 0.3278
Refinement parameters / restraints	747 / 0	163 / 0
Goodness of fit on <i>F</i> ²	1.047	1.064
Final <i>R</i> -indices [<i>I</i> > 2 σ (>(<i>I</i>))]	<i>R</i> ₁ = 0.0432 <i>wR</i> ₂ = 0.0946	<i>R</i> ₁ = 0.0234 <i>wR</i> ₂ = 0.0603
<i>R</i> indices (all data)	<i>R</i> ₁ = 0.0601 <i>wR</i> ₂ = 0.1010	<i>R</i> ₁ = 0.0262 <i>wR</i> ₂ = 0.0619
Largest diff. peak and hole (e.Å ⁻³)	2.449 and -1.759	0.373 and -0.231
Weighing scheme ^a	<i>a</i> = 0.0531 / <i>b</i> = 0	<i>a</i> = 0.0358 / <i>b</i> = 0.4294

^a *wR*₂ = { $\Sigma[w(F_o^2 - F_c^2)^2] / \Sigma[w(F_o^2)^2]$ }^{1/2}; *w* = 1/[$\sigma^2(F_o^2) + (aP)^2 + bP + d + e \sin \theta$]; *P* = [*f*(Max(0 or *F*_o²)) + (1-*f*) *F*_c²]

CHAPTER 3

Utilisation of $[\text{Au}(\text{C}_6\text{F}_5)(\text{tht})]$ in the Preparation of Novel Imidazolin- and Thiazolin-2-ylideneamine Gold(I) Complexes

3.1 Introduction

The coordination chemistry of phosphazenido ligands of the general type $[\text{R}_3\text{P}=\text{N}]^-$ have been studied extensively over the past few decades and this has led to the discovery of a vast amount of structurally diverse main group and transition metal complexes.^{1,2} Although Staudinger and Meyer³ were the first to report the parent trialkyl phosphazene, $\text{R}_3\text{P}=\text{NH}$, in as early as 1919, it was not until many years later, with the discovery of the bis(trialkylphosphine)iminium ligands $[\text{R}_3\text{P}=\text{N}=\text{PR}_3]^+$, that the value of this class of compounds became appreciable. Due to the isoelectronic nature of the $[\text{R}_3\text{P}=\text{N}]^-$ ligand to triorganophosphine oxides, $[\text{O}=\text{PR}_3]$, and triorganosiloxy groups, $[\text{O}=\text{SiR}_3]^-$, similarities in the bonding and structure of metal complexes containing these ligands are often observed.⁴ Furthermore, owing to the ability of these phosphazenido ligands to act as 2σ - as well as 4π -donors, they are also regarded as pseudo-isolobal monodentate analogues of cyclopentadienyl ligands and have been employed as surrogates for these ligands in the preparation of titanium catalysts with enhanced catalytic activity.⁵

In the quest to achieve metal complexes with improved stability and catalytic activity, many research efforts have been devoted to fine-tuning of the coordinated ligands. This has led to the discovery of the imidazolin-2-ylideneamides, related to these $[\text{N}=\text{PR}_3]^-$ ligands. The open coordination-sphere at the imide nitrogen allows these ligands to function as excellent donors capable of stabilising metal centres. The replacement of the PR_3 moiety in phosphazenido ligands by an *N*-heterocyclic carbene (NHC) was an initiative that exploited the striking electronic similarities between the electron rich trialkylphosphines and NHC's.⁶ Furthermore, NHC's are also known to possess σ -donating properties comparable to ligands with P-, N- or O-donor atoms rather than to

¹ K. Denicke, A. Greiner, *Angew. Chem. Int. Ed.* **2003**, *42*, 1340-1354.

² K. Denicke, M. Krieger, W. Massa, *Coord. Chem. Rev.* **1999**, *182*, 19-65.

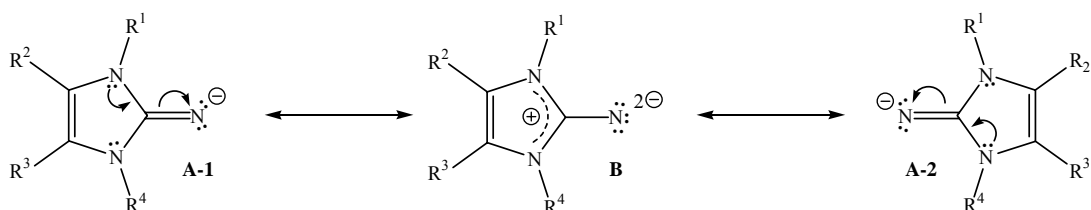
³ H. Staudinger, J. Meyer, *Helv. Chim. Acta.* **1919**, *2*, 635-646.

⁴ K. Denicke, F. Weller, *Coord. Chem. Rev.* **1997**, *158*, 103-169.

⁵ M. Tamm, S. Randoll, E. Erker, B. Reiger, *Dalton Trans.* **2006**, 459-467.

⁶ M. Tamm, S. Randoll, T. Bannenberg, E. Herdtweck, *Chem. Commun.* **2004**, 876-877.

classical Fischer- or Schrock-type carbenes.^{7,8} Transition metal complexes that contain these imidazol-2-ylideneamide ligands, often show amplified catalytic activity and stability. This enhanced performance originates from the innate ability of the heterocyclic ring, with Hückel aromatic character, to increase the electron density on the exocyclic nitrogen atom by stabilizing a positive charge more effectively than a phosphonium group. This phenomenon can be described by two limiting resonance structures **A** and **B** (Scheme 3.1), illustrating the ability of the ring to stabilise the positive charge and as a result increase the basicity of the ligand.⁶



Scheme 3.1 Resonance structures, **A** and **B**, for imidazol-2-ylideneamine ligands showing the enhancement of the electron donating capacity of the ligands by stabilisation of the positive charge.

Kuhn and co-workers^{9,10,11} have made several valuable contributions towards the development of imidazol-2-ylideneamine and imidazol-2-ylideneamide derivatives and their corresponding main group and transition metal complexes. In one of these elegant studies, the donor strength of 2-imido-imidazoline ligands in titanium complexes were compared with those of related ylideneamide ligands. These included alkylideneamides, $[R_2C=N]^-$, and phosphazenido, $[R_3P=N]^-$, ligands. The study indicated the donor strengths of the ligands to decline in the order $Im=N^- \approx Me_3P=N^- > Ph_3P=N^- > Me_2C=N^- \gg R_2C=N^-$, proving that imidazol-2-ylideneamide ligands can be utilised as promising alternatives to other ylideneamide ligands in the preparation of more stable metal complexes.

The most general approach to the preparation of heterocyclic ylideneamide metal complexes was adopted from their phosphazenido ancestors and entails the use of *N*-

⁷ W. A. Herrmann, *Angew. Chem. Int. Ed. Engl.* **2002**, *41*, 1290-1309.

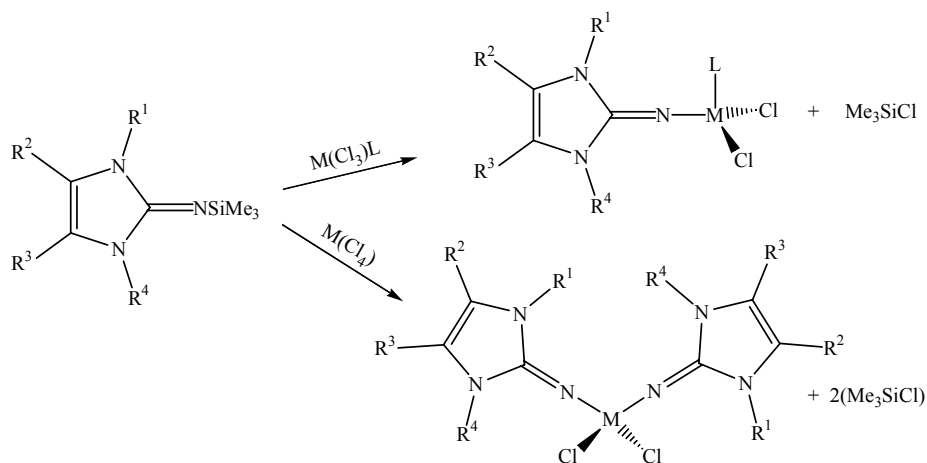
⁸ W. A. Herrmann, V. P. W. Böhm, C. W. K. Gstöttmayr, M. Grosche, C. P. Reisinger, T. Weskamp, *J. Organomet. Chem.* **2001**, *616-618*, 616-628.

⁹ N. Kuhn, R. Fawzi, M. Steimann, J. Wiethoff, D. Bläser, R. Boese, *Z. Naturforsch.* **1995**, *50b*, 1779-1784.

¹⁰ N. Kuhn, R. Fawzi, M. Steimann, J. Wiethoff, *Z. Anorg. Allg. Chem.* **1997**, *623*, 769-774.

¹¹ N. Kuhn, M. Grathwohl, M. Steimann, G. Henkel, *Z. Naturforsch.* **1998**, *53b*, 997-1003.

silylated heterocyclic ylideneamine precursors. Treatment of these *N*-silylated precursor compounds with metalchlorides results in desilylation along with coordination to the metal centre (Scheme 3.2). This affords metal complexes containing one or more ylideneamide ligands, depending on the nature of the metal precursor complex.^{12,6}



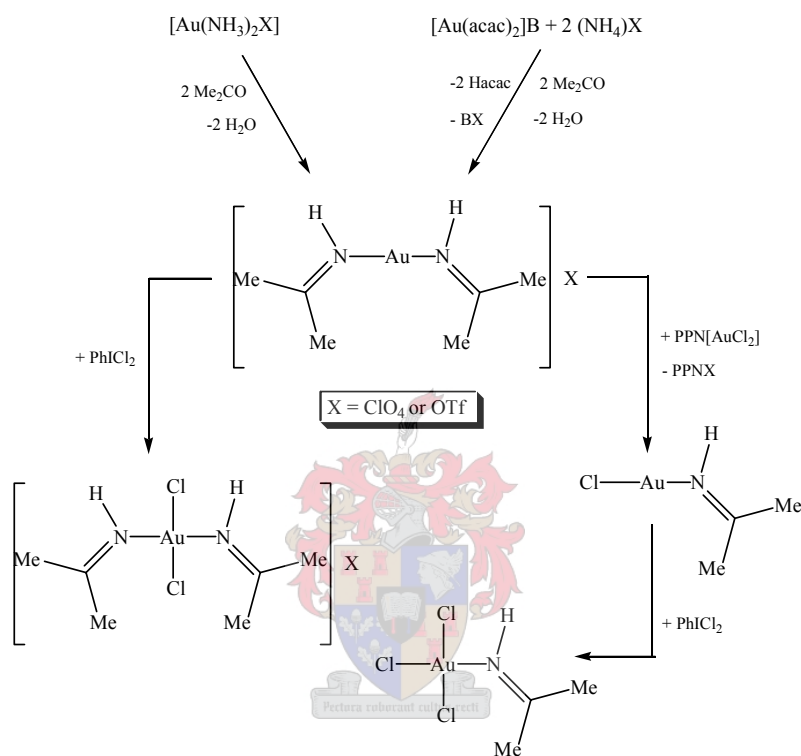
Scheme 3.2 Reaction scheme showing the most general route to the preparation of heterocyclic iminato complexes from *N*-silylated 2-imino-imidazolines and metalchlorides, where M refers to the metal centre and R to hydrogen atoms or alkyl substituents.

Phosphazene [$R_3P=NH$] ligands can readily be prepared by the acid catalysed reactions of *N*-silylated phosphazenes [$Me_3SiN=PR_3$] with *i*-propanol or methanol or by deprotonation of the corresponding aminophosphonium salts [$R_3P=NH_2$]Cl with sodium amide. These ligands are however thermally sensitive and prone to oxidation in the presence of water affording related phosphorane oxides.¹³ In contrast, their imidazol-2-ylideneamine and thiazol-2-ylideneamine analogues are less susceptible to oxidation and may be regarded as superior ligands in terms of stability. Although these 2π -donor ligands are less basic than their 4π -donor imide counterparts, they possess sufficient donor strength to readily replace weaker donor ligands such as halogens or tetrahydrothiophene to form stable metal complexes. The majority of reported ylideneamine metal complexes contain alkylideneamine [$R_2C=NH$], biguanide [$R_2N(C=NH)NH(C=NH)NR_2$] or guanidine [$(R_2N)_2C=NH$] type ligands, coordinated to a hard (class B) metal centre and are prepared by simple ligand substitution reactions. Documented ylideneamine coordinated gold(I) complexes are limited and all reported examples contain one or more of the ligands

¹² N. Kuhn, R. Fawzi, C. Maichle-Mößner, M. Steimann, J. Wiethoff, *Z. Naturforsch.* **1997**, 52b, 1055-1061.

¹³ K. Dehnicke, F. Weller, *Coord. Chem. Rev.* **1997**, 158, 103-169.

[(Me₂N)₂C=NH], [MeN(C=NH)N(CH₂)Me] or [Me₂C=NH]. Furthermore, they are mostly prepared by substitution reactions which involve labile ligands. Vicente and co-workers¹⁴ have however reported alternative routes towards the preparation of isopropylideneamine coordinated metal complexes containing a soft (class A) gold(I) metal centre. These complexes could also be transformed to their gold(III) analogues by means of the oxidative addition of chlorine (Scheme 3.3).



Scheme 3.3 Alternative routes towards the preparation of ketylideneamine complexes containing soft gold(I) and hard gold(III) metal centres, where B = NMe₄ or PPN (PPN = PPh₃N=PPh₃) and PhI₂ refers to (dichloroiodo)benzene.

Although heterocyclic ylideneamine and ylideneamide metal complexes have been described in the literature, they are limited and in particular complexes involving thiazol-2-ylideneamine ligands. In the majority of the known heterocyclic ylideneamine and ylideneamide complexes the nitrogen atoms are coordinated to hard or borderline hard metal centres such as Ti⁴⁺, Sn⁴⁺, Ni²⁺, Fe³⁺ and Al³⁺.^{5,15,16} The only soft metal centres that have been utilised in heterocyclic ylideneamide coordinated complexes are Pd²⁺, Hg²⁺ and

¹⁴ J. Vicente, M. T. Chicote, R. Guerrero, I. M. Saura-Llamas, P. G. Jones, M. C. Ramírez de Arellano, *Chem. Eur. J.* **2001**, *7*, 638-646.

¹⁵ L. V. Baikalova, E. S. Domina, N. N. Chipanina, T. V. Kashika, A. V. Afonin, V. A. Kukhareva, G. A. Gavrilova, *Russ. J. Coord. Chem.* **1998**, *24*, 486-490.

¹⁶ N. Kuhn, M. Grathwohl, C. Nachtigal, M. Steimann, *Z. Naturforsch.* **2001**, *56b*, 704-710.

Cu⁺ whereas Cd²⁺ and Hg²⁺ are the only soft metals present in known heterocyclic ylideneamine complexes.^{17,18}

To the best of our knowledge, there are no reports in the literature describing coordination of a heterocyclic ylideneamine ligand to a gold(I) metal centre. In addition, only one example of an ylideneamine gold(I) complex that contains a pentafluorophenyl (pfp) ancillary ligand has been described in literature, making this a poorly developed area of research that is worth exploring.¹⁹ The goal of this study was therefore to prepare and fully characterise a number of ylideneamine-functionalised heterocyclic ligands and their corresponding gold(I) complexes. These complexes would then represent the first gold complexes to contain ylideneamine-functionalised heterocyclic ligands and would therefore be a vital contribution to this significant class of compounds.

3.2 Results and discussion

3.2.1 Ylideneamine-functionalised heterocyclic ligands and their corresponding (pentafluorophenyl)gold(I) complexes

In section 3.2.1.1 the synthetic value of the gold(I) compound, [Au(C₆F₅)(tht)] is once again emphasized by reporting the utilisation thereof in the preparation of novel heterocyclic ylideneamine gold(I) complexes of the general form [Au(C₆F₅)(L)], where L refers to the ylideneamine ligand. The extensive characterisation, including single crystal X-ray structure analysis, unearthed interesting phenomena, and will be discussed in section 3.2.1.2 and 3.2.3. Additionally, the preparation and characterisation of the free ligands will also be discussed in detail to serve as reference to determine the structural changes thereof upon metal coordination.

3.2.1.1 Preparation of 1,3-dimethyl-1,3-dihydro-benzimidazol-2-ylideneamine, III, 3-methyl-3H-benzothiazol-2-ylideneamine, IV and 3,4-dimethyl-3H-thiazol-2-ylideneamine, V

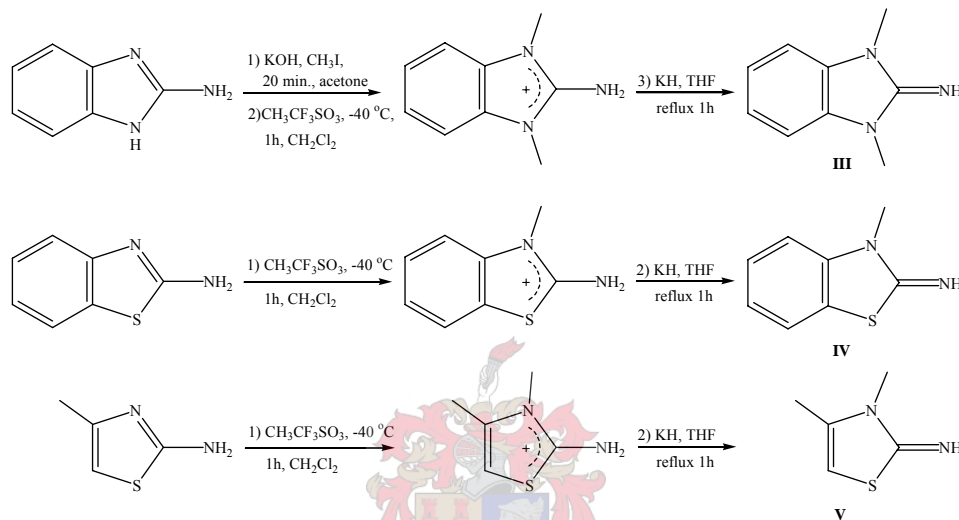
The most general route towards the preparation of ylideneamine-functionalised heterocyclic ligands was developed by Kuhn and co-workers.⁹ This method entails

¹⁷ L. V. Baiklova, E. S. Domina, N. N. Chipanina, L. D. Khamaganova, A. V. Afonin, G. A. Gavrilova, *Russ. J. Coord. Chem.* **1997**, 23, 84-90.

¹⁸ S. Muralidharan, K. S. Nagaraja, M. R. Udupa, *Polyhedron* **1984**, 3, 619-621.

¹⁹ A. Codina, E. J. Fernández, P. G. Jones, A. Laguna, J. M. López-de-Luzuriaga, M. Monge, M. E. Olmos, J. Pérez, M. A. Rodríguez, *J. Am. Chem. Soc.* **2002**, 124, 6781-6786.

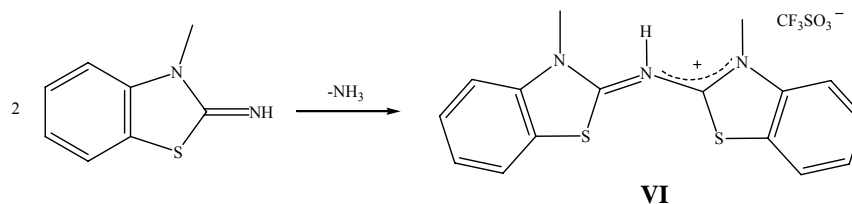
alkylation of the endocyclic nitrogen atom of a 1-methyl-1*H*-imidazol-2-ylamine precursor with MeI to yield a cationic amino compound which can be readily converted to the corresponding ylideneamine compound by subsequent deprotonation with KH. A similar approach was followed in the preparation of ligands **III** - **V**, with the only variation being the choice of alkylating agent. Scheme 3.4 depicts the preparative routes towards deriving the free ligands **III** - **V**, from their corresponding amino precursor compounds.



Scheme 3.4 Reaction scheme for the preparation of the free ylideneamine-functionalized heterocyclic ligand, **III** - **V**, from their corresponding 2-amino precursor compounds.

In the instance of 1,3-dimethyl-1,3-dihydro-benzimidazol-2-ylideneamine, **III**, where multiple alkylations were required, the first alkylation was achieved by first treating a solution of 1*H*-benzimidazol-2-ylamine in acetone with ground KOH. This effected deprotonation of the N¹ position. Electrophilic addition of a methyl group to this site was subsequently achieved by the addition of MeI to the reaction mixture. In all of the ligands **III** - **V**, further alkylation, to yield the cationic species, was achieved by treating a solution of the amino precursor compound in diethyl ether with CH₃SO₃CF₃ while maintaining the internal reaction temperature at -40 °C. Subsequent deprotonation of these cationic species furnished the neutral heterocyclic ylideneamine ligands **III** - **V** in good yields. Deprotonation was readily accomplished by the addition of KH to a solution of the amino precursor in THF followed by a 1h heating period. However, temperature control during the execution of this step proved crucial. Reaction temperatures above 66 °C led to the formation of dimeric byproducts, especially when preparing the thiazole derivatives **IV**

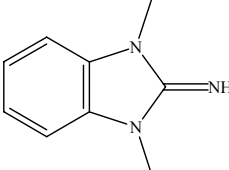
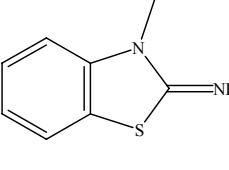
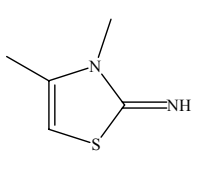
and **V**. A single crystal of the byproduct 3-methyl-2-(3-methyl-3*H*-benzothiazol-2-ylideneamino)benzothiazol-3-ium trifluoromethanesulfonate, **VI**, was isolated from the crystallisation mixture of **IV**. X-ray structure elucidation confirmed the product to be the result of a condensation reaction which entails the loss of ammonia (Scheme 3.5).



Scheme 3.5 Reaction scheme showing the formation of the dimeric byproduct **VI** from compound **IV** with the concomitant loss of ammonia.

Compounds similar to this dimeric byproduct have been prepared by Deligeorgiev and Gadjev²⁰ through reactions of 3-methyl-3*H*-benzothiazol-2-ylideneamine derivatives with HX, where X = CH₃SO₃⁻, ClO₄⁻, Br⁻ or I⁻. During the preparation of ligands **III** and **IV** the formation of these byproducts could be minimized by maintaining the reaction temperature below 65 °C during the reflux period. For ligand **V**, however, the formation of an oily byproduct was observed regardless of strict temperature control. The pure product could be obtained from the crude mixture by sublimation under vacuum (0.1 mmBar at 75 °C). Ligands **III** – **V**, which are highly hygroscopic, are soluble in water and organic solvents such as alcohols, dichloromethane, DMSO, THF, acetone or diethyl ether, but insoluble in alkanes such as *n*-pentane and *n*-hexane. The physical properties and analytical data of ligands **III** - **V** are summarised in Table 3.1.

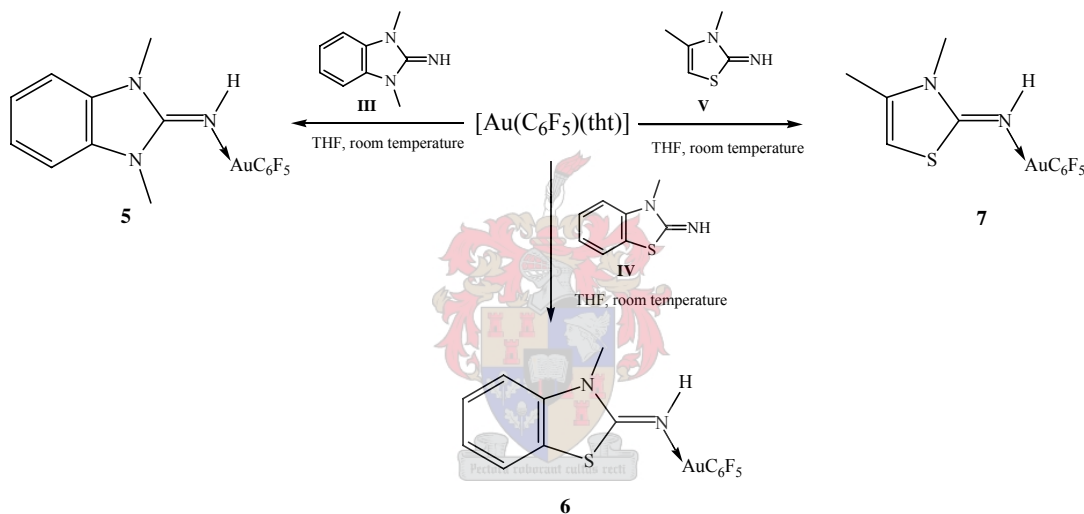
Table 3.1 Physical properties and analytical data of complexes **III**, **IV** and **V**.

Ligand	 III	 IV	 V
m.p. (°C)	59-60	112-114	46-48
Colour	off-white	yellow	colourless
Yield (%)	88	79	62
<i>M_r</i>	161.20	164.23	128.20
<i>M_r</i>	C ₉ H ₁₁ N ₃	C ₈ H ₈ N ₂ S	C ₅ H ₈ N ₂ S

²⁰ T. Deligeorgiev, N. I. Gadjev, *Dyes and Pigments* **1995**, 29, 315-322.

3.2.1.2 Preparation of 1,3-dimethyl-1,3-dihydro-benzimidazol-2-ylideneamine(pentafluorophenyl)gold(I), **5**, 3-methyl-3H-benzothiazol-2-ylideneamine(pentafluorophenyl)gold(I), **6** and 3,4-dimethyl-3H-thiazol-2-ylideneamine(pentafluorophenyl)gold(I), **7**

As discussed in Chapter 2, $[Au(C_6F_5)(tht)]$ functions as a valuable gold(I) precursor complex which freely allows substitution of the tht ligand by other ligands with superior donor abilities. The ylideneamine ligands **III** – **V** are considered to be strong σ - and π -donors and are therefore able to readily replace the tht ligand to form neutral coordination complexes of the general form $[Au(C_6F_5)(L)]$, where L refers to the ylideneamine ligand. The preparation for the neutral ylideneamine coordinated (pentafluorophenyl)gold(I) complexes, **5** – **7**, is depicted in Scheme 3.6.

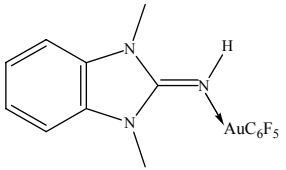
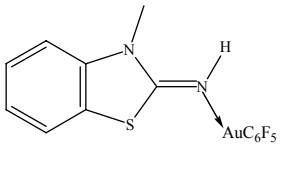
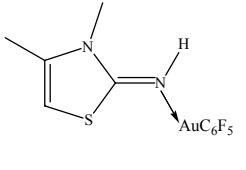


Scheme 3.6 Reaction scheme for the preparation of the ylideneamine coordinated gold(I) complexes, **5** – **7**.

Compounds **5** – **7** were prepared by treating solutions of 1,3-dimethyl-1,3-dihydro-benzimidazol-2-ylideneamine, 3-methyl-3H-benzothiazol-2-ylideneamine and 3,4-dimethyl-3H-thiazol-2-ylideneamine in THF with equimolar amounts of $[Au(C_6F_5)(tht)]$ at room temperature. After a 1 – 3 day stirring period, solid contaminants such as colloidal gold were removed from the reaction mixture by means of a cannula filtration or filtration through an anhydrous salt such as Na_2SO_4 or $MgSO_4$. Removal of the solvent *in vacuo* afforded compounds **5** – **7** as air and moisture sensitive solids in moderate to high yields. Compounds **5** and **6** are soluble in acetone, THF or DMSO whereas compound **7** is soluble in most organic solvents such as short chain alcohols, acetone, diethyl ether, THF, acetonitrile or dichloromethane. All of the complexes are insoluble in alkanes such as

hexane and pentane. Gradual decomposition of compounds **5** and **6** was observed when stored under argon at -22 °C in the solid state, or in solution for prolonged periods of time. Compound **7**, however, showed greater stability and no decomposition was observed under the same conditions. Crystals suitable for X-ray structure determination were either obtained by vapour diffusion of pentane into a solution of the compound in acetone (**5** and **7**) or by allowing slow crystallisation from a concentrated THF solution (**6**). All crystallisation mixtures were stored under argon at -22 °C. Physical and analytical data for compounds **5** – **7** are summarised in Table 3.2.

Table 3.2 Analytical data of complexes **5**, **6** and **7**.

Complex			
	5	6	7
m.p. (°C)	94-100 (decomp.)	128-132 (decomp.)	100-106 (decomp.)
Colour	colourless	colourless	off-white
Yield (%)	70	78	93
<i>M_r</i>	525.23	528.25	492.22
Analysis (%) [*]	C ₁₅ H ₁₁ AuF ₅ N ₃	C ₁₄ H ₈ AuF ₅ N ₂ S	C ₅ H ₈ AuF ₅ N ₂ S
C	34.82 (34.30)	32.03 (31.83)	26.22 (26.84)
H	2.33 (2.11)	1.60 (1.53)	1.38 (1.64)
N	7.65 (8.00)	5.11 (5.30)	5.44 (5.69)

* Required calculated values given in parenthesis. The products were powdered and evacuated for 10h prior to elemental analysis.

3.2.2 Spectroscopic characterisation of compounds **III** – **V** and **5** – **7**

3.2.2.1 Nuclear magnetic resonance spectroscopy

The ¹H, ¹³C and ¹⁵N NMR spectroscopic data of dichloromethane-d₂ solutions of ligands **III** – **IV** are summarised in Table 3.3. The ¹H NMR spectra reveal characteristic NMR resonances for **III** (δ 3.28), **IV** (δ 3.37) and **V** (δ 3.17). In addition, the imine protons are observed as broad singlets at δ 4.16 for **III**, δ 4.95 for **IV** and δ 5.47 for **V**. In the spectrum of **III**, two doublets of doublets are detected in the aromatic region. These resonances occur at δ 6.81 (¹J = 5.6 Hz, ²J = 3.3 Hz), corresponding to the equivalent

protons H^5 and $H^{5'}$, and δ 6.96 ($^1J = 5.7$ Hz, $^2J = 3.4$ Hz), attributable to H^6 and $H^{6'}$ of the phenyl ring. In the 1H NMR spectra of **IV** all aromatic protons are rendered inequivalent by their chemical environment. H^5 and $H^{5'}$ give rise to a doublet of doublets of doublets at δ 7.26 ($^3J = 7.7$ Hz; $^4J = 1.4$ Hz; $^5J = 0.5$ Hz) and a doublet of multiplets at δ 6.86 ($^3J = 8.5$ Hz) respectively. Two triplets of doublets, observed at δ 7.00 ($^3J = 7.8$ Hz; $^4J = 1.3$ Hz) and δ 7.24 ($^3J = 7.8$ Hz; $^4J = 1.4$ Hz), can be assigned to H^6 and $H^{6'}$. In the 1H NMR spectrum of compound **V**, the proton in the 5-position on the thiazole ring, experiences an allylic 4J coupling of 1.4 Hz to the protons of the methyl substituent on the 4-position resulting in a quartet at δ 6.86 (H^4) and a doublet at δ 2.01 (H^6).

Table 3.3 1H , ^{13}C , and ^{15}N NMR spectroscopic data of complexes **III**, **IV** and **V**.

Ligand				
Solvent	Dichloromethane- d_2	Dichloromethane- d_2	Dichloromethane- d_2	
Temperature ($^{\circ}C$)	25	25	25	
Assignment	Chemical shift (ppm)			
1H NMR (300/400 MHz)	$H^5, H^{5'}$	6.81 (dd, 2H, $^1J = 5.6$ Hz, $^2J = 3.3$ Hz)	7.26 (ddd, 1H, $^3J = 7.7$ Hz; $^4J = 1.4$ Hz; $^5J = 0.50$ Hz) / 6.86 (dm, 1H, $^3J = 8.5$ Hz)	5.46 (q, 1H, $^4J = 1.4$ Hz)
	$H^6, H^{6'}$	6.96 (dd, 2H, $^1J = 5.7$ Hz, $^2J = 3.4$ Hz)	7.00 (td, 1H, $^3J = 7.8$ Hz; $^4J = 1.3$ Hz) / 7.24 (td, 1H, $^3J = 7.8$ Hz; $^4J = 1.4$ Hz)	2.01 (d, 3H, $^4J = 1.4$ Hz)
	$H^7, H^{7'}$	3.28 (s, 6H)	3.37 (s, 3H)	3.17 (s, 3H)
	H^8	4.16 (bs, 1H)	4.95 (bs, 1H)	5.47 (bs, 1H)
^{13}C NMR (75/100 MHz)	C^2	156.3 (s)	162.7 (s)	166.6 (s)
	$C^4, C^{4'}$	133.0 (s)	121.9 (s) / 142.0 (s)	136.0 (s)
	$C^5, C^{5'}$	106.2 (s)	126.8 (s) / 109.7 (s)	92.3 (s)
	$C^6, C^{6'}$	120.6 (s)	122.1 (s) / 123.2 (s)	14.9 (s)
	$C^7, C^{7'}$	27.7 (s)	29.4 (s)	30.0 (s)
^{15}N NMR (61 MHz)	N^1, N^3	-278.0		
	N^8	Not observed		

In the ^{13}C NMR spectra of compounds **III** – **V** the weak signal attributable to the highly deshielded C-atom, central to the heteroatoms, appears most downfield at δ 156.3 (**III**), δ 162.7 (**IV**) or δ 166.6 (**V**). Other diagnostic resonance signals include the intense singlets

observed for the NMe carbons at δ 27.7 (**III**), δ 29.4 (**IV**) or δ 30.0 (**V**) and the aromatic carbon signals of compounds **III** and **IV**, detected in the region δ 106-142.

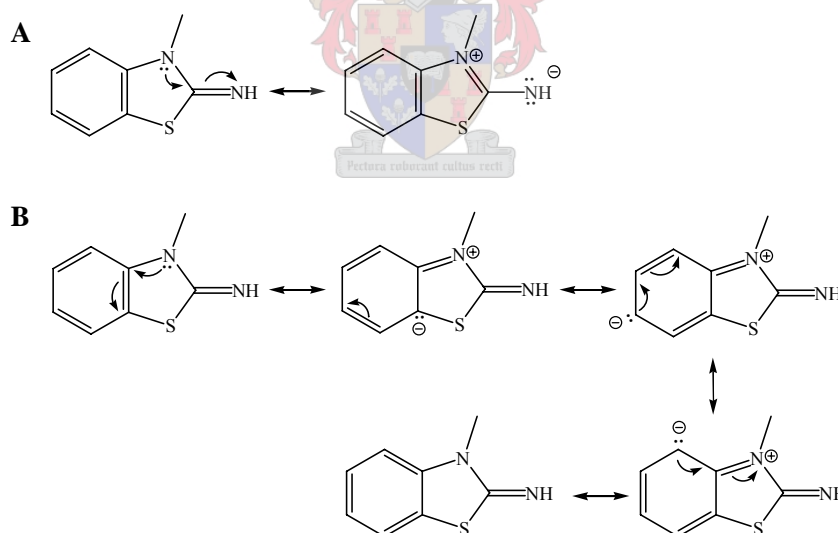
The ¹⁵N NMR spectrum of **III** exhibits only one signal at δ -278.0, that corresponds to both nitrogen atoms within the imidazole ring which are rendered equivalent by their chemical environment. Despite the use of both indirect and direct methods, no resonance signal could be obtained for the exocyclic nitrogen atom.

Table 3.4 summarises the ¹H, ¹³C and ¹⁹F NMR spectroscopic data obtained of a THF-d₈ or acetone-d₆ solution of complexes **5** – **7**. In both the ¹H and ¹³C NMR spectra of **5** – **7**, tetrahydrothiophene resonances were clearly absent confirming the substitution thereof by the ylideneamine ligands. From the ¹H NMR spectra of complexes **5** – **7** it is evident that coordination of the ligand to the metal centre results in a pronounced downfield shift of the NH proton resonances. This effect is most prominent in complex **5** and declines in the order $\Delta\delta$ 4.27 (**5**) > $\Delta\delta$ 2.77 (**6**) > $\Delta\delta$ 1.48 (**7**) as delocalisation of the system decreases. All remaining proton resonances also experience significant downfield shifts upon coordination compared to the resonances associated with the protons of the free ligands. The distinctive allylic ⁴J coupling observed for ligand **V**, is less pronounced in the corresponding gold(I) complex **7** with the H⁵ resonance observed as a singlet and the H⁶ resonance as a doublet with a reduced coupling constant of 1.3 Hz. The singlet observed for H⁵ is however very broad, providing further evidence for the presence of weak coupling. This subdued allylic coupling might be the consequence of a reduced electron density on the ring system following coordination to the Au(C₆F₅) unit, effecting decreased aromatic character and electron delocalisation.

Resonances observed for the NMe groups in the ¹³C NMR spectra of complexes **5** and **6**, as well as the ligand ring carbons in compounds **5** and **7** all have chemical shifts slightly downfield from those of the free ligands. No noteworthy change is observed in the chemical shift of C² in complex **5**. However, in the spectrum of complex **7**, the C² resonance experiences a large downfield shift of $\Delta\delta$ 95. The presence of the Au(C₆F₅) entity in **5**, **6** and **7**, is confirmed by the complex C–F coupling patterns observed in the region δ 118-151, characteristic of the C₆F₅ ligand. The coupling patterns are similar to those observed in the gold(I) precursor compound, **1**, as was previously described in

section 2.2.2.1 of Chapter 1. For compound **7**, the C-F coupling pattern of the C₆F₅ *ipso*-carbon is not observed due to the low intensity of the signal.

Further evidence, with regard to the formation of ylideneamine coordinated gold(I) complexes, is provided by an interesting observation in the ¹³C NMR spectra of **6**. It is noticeable that the downfield shifts of the carbon ring atoms C⁴, C^{5'} and C⁶ (see Table 3.4 for numbering scheme) are more pronounced than those observed for C^{4'}, C⁵ and C^{6'}. In fact, a discrete upfield shift is observed for the resonance signals of C^{4'} and C^{6'}. This phenomenon can be described in terms of the contributing resonance structures. In the free ligand two possibilities for competitive electron delocalisation exist (Scheme 3.7) with **B**, resulting in five resonance structures, being the principal possibility. However, upon coordination, the strong electron release of the imine N-atom towards the gold centre makes the resonance structures in **A** more important. This results in a decrease in electron delocalisation through possibility **B** and subsequently a reduction in the electron density on the carbons in *ortho* and *para* positions to the C^{4'} carbon atom. These carbons are therefore rendered more deshielded than prior to metal coordination.



Scheme 3.7 The two competitive electron delocalisation routes, **A** and **B**, possible for ligand **IV** leading to a total of seven resonance structures.

For each of the complexes **5** – **7**, three sets of diagnostic F–F coupling resonances in the ¹⁹F NMR spectra also confirm the presence of the C₆F₅ ligand. The coupling patterns are comparable to those of the parent gold(I) compound with resonances appearing at chemical shifts slightly downfield to those observed for compound **1**.

Table 3.4 1H , ^{13}C , ^{19}F and ^{15}N NMR spectroscopic data of complexes **5**, **6** and **7**.

Complex				
Solvent Temperature (°C)	Tetrahydrofuran- d_8 25	Tetrahydrofuran- d_8 25	Acetone- d_6 25	
Assignment	Chemical shift (ppm)			
1H NMR δ (ppm) (400/600 MHz)	H^4 $H^{5'}$, $H^{5''}$ $H^{6'}$, $H^{6''}$ $H^{7'}$, $H^{7''}$ H^8	7.32 (dd, 2H, $^1J = 5.9$ Hz, $^2J = 3.4$ Hz) 7.47 (dd, 2H, $^1J = 5.9$ Hz, $^2J = 3.4$ Hz) 3.73 (s, 6H) 8.43 (bs, 1H)	7.56 (dm, 1H, $^3J = 7.8$ Hz) / 7.23 (d, 1H, $^3J = 8.0$ Hz) 7.17 (td, 1H, $^3J = 7.7$ Hz, $^4J = 1.0$ Hz) / 7.36 (td, 1H, $^3J = 8.4$ Hz, $^4J = 1.1$ Hz) 3.55 (s, 3H) 7.72 (bs, 1H)	6.12 (bs, 1H) 2.24 (d, 3H, $^4J = 1.2$ Hz) 3.47 (s, 3H) 6.92 (bs, 1H)
^{13}C NMR δ (ppm) (100/150 MHz)	C^2 C^4 , $C^{4'}$ C^5 , $C^{5'}$ C^6 , $C^{6'}$ C^7 , $C^{7'}$ $C_6F_5-C^{ipso}$ $C_6F_5-C^{ortho}$ $C_6F_5-C^{meta}$ $C_6F_5-C^{para}$	156.4 (s) 131.4 (s) 110.5 (s) 124.4 (s) 39.2 (s) 126.1 (tm, $^2J = 57.3$ Hz) 148.6 (ddm, $^1J = 228.3$ Hz, $^2J = 26.9$ Hz) 137.3 (dm, $^1J = 226.5$ Hz) 138.5 (dm, $^1J = 248.5$ Hz)	173.1 (s) 124.4(s) / 141.8 (s) 127.6 (s) / 111.6 (s) 123.0 (s) / 122.6 (s) 30.1 (s) 118.4 (tm, $^2J = 57.6$ Hz) 150.1 (ddm, $^1J = 226.3$ Hz, $^2J = 23.9$ Hz) 137.4 (dm, $^1J = 247.7$ Hz) 138.7 (dm, $^1J = 244.0$ Hz)	176.1 (s) 139.2 (s) 97.5 (s) 15.8 (s) 27.1 (s) not observed 150.7 (ddm, $^1J = 226.8$ Hz, $^2J = 24.5$ Hz) 139.3 (dm, $^1J = 248.7$ Hz) 138.0 (dm, $^1J = 243.1$ Hz)
^{19}F NMR δ (ppm) (376 MHz)	F^{ortho} F^{meta} F^{para}	-116.6 (m) -161.1 (t, $^3J = 19.6$ Hz) -164.3 (m)	-116.5 (m) -163.1 (tt, $^3J = 5.3$ Hz, $^4J = 0.5$ Hz) -165.3 (m)	-121.2 (m) -167.7 (t, $^3J = 19.6$ Hz) -169.8 (m)

3.2.2.2 Mass spectrometry

The EI-MS and FAB-MS spectrometric data for ligands **III** – **V** are summarised in Table 3.5. From the FAB-MS spectra of compounds **III** and **IV** it is evident that very little fragmentation takes place with this mild ionization technique. The only diagnostic peaks present in the spectrum of **III** appear at m/z 162, assigned to the molecular ion, and m/z 147 corresponding to the loss of a methyl group. A similar fragmentation pattern is observed for compound **IV**, with peaks of the mentioned fragments emerging at m/z 165

and m/z 150. A higher degree of fragmentation is evident from the EI-MS spectrum of **V**. The strong peak detected at m/z 128 can be assigned to the molecular ion peak. Other peaks at m/z 113 (M^+-CH_3), m/z 100 (M^+-NCH_3), m/z 86 (M^+-CH_3-NH) and m/z 56 ($CH_3NC=NH$, base peak) confirm the proposed structure of compound **V**.

Table 3.5 Mass spectrometric data of ligands **III**, **IV** and **V**.

Fragment	m/z (I in %)		
	III	IV	V
$\{[M]\}^+$	162 (100)	165 (100)	128 (90)
$\{[M]-CH_3\}^+$	147 (17)	150 (6)	113 (15)
$\{[M]-NCH_3\}^+$			100 (27)
$\{[M]-CH_3-NH\}^+$			86 (25)
$\{CH_3NC=NH\}^+$			56 (100)

The characteristic fragmentation peaks attained by FAB-MS analysis for complexes **5** and **6**, are listed in Table 3.6. Although FAB-MS analysis was executed for **7**, this technique, despite the soft nature thereof, proved unsuccessful for this complex and the acquired spectra failed to deliver any diagnostic peaks. No fragmentation data is therefore listed for this compound. Even though no molecular ion peak is noticed in the FAB-MS spectrum of compound **5**, other diagnostic signals corresponding to the loss of a CH_3 group (m/z 511), and further loss of the $Au(C_6F_5)$ moiety (m/z 147) are present. Other indicative fragmentation peaks include m/z 355 ($M^+-C_6F_5$) and m/z 162 [$M^+-Au(C_6F_5)$]. Complex **6** shows a weak molecular ion peak at m/z 528 and other significant fragmentation patterns comprise of the loss of a CH_3 , C_6F_5 or an $Au(C_6F_5)$ unit (m/z 514, m/z 361 and m/z 165 respectively).

Table 3.6 Mass spectrometric data of complexes **5**, **6** and **7**.

Fragment	m/z (I in %)		
	5	6	7
$\{[M]\}^+$	—	528 (8)	
$\{[M]-CH_3\}^+$	511 (11)	514 (3)	
$\{[M]-C_6F_5\}^+$	355 (28)	361 (4)	No diagnostic peaks observed
$\{[M]-Au(C_6F_5)\}^+$	162 (89)	165 (73)	
$\{[M]-Au(C_6F_5)-CH_3\}^+$	147 (46)	—	

3.2.2.3 *Infrared spectroscopy*

Solid state ATR (attenuated total reflectance) FT-IR spectra of compounds **III** – **V** were determined and the results are summarised in Table 3.7. The FT-IR spectrum of the free ligand **III** exhibits a broad intense absorption band at 3235 cm^{-1} attributable to the stretching vibrations of the =N–H group. Other bands observed in this region ($3500\text{--}2800\text{ cm}^{-1}$) include two weak bands at 3058 cm^{-1} and 2931 cm^{-1} due to stretching vibrations of the aromatic sp^2 and aliphatic sp^3 C–H bonds respectively. Strong bands observed in the region $1625\text{--}1608\text{ cm}^{-1}$ can be assigned to the C=N stretching vibrations while the weak band detected at 1326 cm^{-1} belongs to vibrations of the C–N single bonds. Furthermore, strong bands observed in the region $1500\text{--}1392\text{ cm}^{-1}$ and at 724 cm^{-1} correspond to the stretching and out of plane bending vibrations (δ_{oop}^b) of the aromatic C=C bonds respectively.

In the FT-IR spectrum of **IV** the diagnostic, intense broad absorption band of the $\nu(=N-H)$, appears at 3243.8 cm^{-1} and is shifted to a slightly higher wavenumber with respect to the corresponding band observed in the spectra of the free ligand **III**. The absorption band, generated by the stretching vibrations of the sp^3 C–H bonds, emerges at the same wavenumber as was observed for the free ligand **III**. Absorption bands for the $\nu(C=N)$ occur in the region $1596\text{--}1574\text{ cm}^{-1}$, whereas the $\nu(C-N)$ results in a band of medium intensity at 1330 cm^{-1} . In addition, bands attributed to aromatic $\nu(C-H)$, $\nu(C=C)$ and $\delta_{\text{oop}}^b(C=C)$ are identified at 3047 cm^{-1} , $1474\text{--}1417\text{ cm}^{-1}$ and 736 cm^{-1} respectively.

Table 3.7 Infrared spectroscopic data of ligands **III**, **IV** and **V**.

Functional group	Wavenumber (cm^{-1})		
	III	IV	V
$\nu(=N-H)$	3235 (st)	3243 (st)	3239 (w)
Ar $\nu(C-H)$	3058 (w)	3047 (w)	3062 (w)
sp^3 $\nu(C-H)$	2931 (w)	2931 (w)	2916 (w)
$\nu(C=N)$	1625-1608 (st)	1596-1574 (st)	1606-1564 (st)
Ar $\nu(C=C)$	1500-1392 (st)	1474-1417 (st)	1418-1364 (st)
$\nu(C-N)$	1326 (w)	1330 (m)	
Ar $\delta_{\text{oop}}^b(C=C)$	724 (st)	736 (st)	

Characteristic absorption bands in the FT-IR spectrum of **V**, attributable to stretching vibration of the =N–H, sp^3 C–H and C=N moieties, are prominent at 3239 cm^{-1} , 2916 cm^{-1}

and in the region 1606-1564 cm⁻¹ respectively. Additionally, characteristic aromatic $\nu(\text{C-H})$ and $\nu(\text{C=C})$ bands are observed at 3062 cm⁻¹ and in the region 1418-1364 cm⁻¹.

FT-IR spectroscopic data determined for compounds **5** – **7** are summarised in Table 3.8. In the compounds, **5** – **7**, the $\nu(\text{=N-H})$ absorption bands are shifted significantly towards higher frequencies with respect to those of the free ligands, suggesting coordination to gold(I) by their imine nitrogen atoms. This observation is further substantiated by the appearance of four new intense absorption bands in the spectrum of each complex, attributable to the Au(C₆F₅) entities, in the regions 1501-1498 cm⁻¹, 1058-1060 cm⁻¹, 946-949 cm⁻¹ and 199-801 cm⁻¹. In compound **5**, an increase of 110 cm⁻¹ is observed in the wavenumber of the $\nu(\text{C-N})$ absorption band. The same trend is observed for compound **6** with an increase in wavenumber of 108 cm⁻¹. However, in the spectrum of complex **7**, the $\nu(\text{C-N})$ absorption band is obscured by the $\nu(\text{C=C})$ absorption bands and is therefore not observed.

Table 3.8 Infrared spectroscopic data of ligands **5**, **6** and **7**.

Functional group	Wavenumber (cm ⁻¹)		
	5	6	7
$\nu(\text{=N-H})$	3399 (st)	3375 (m)	3379 (st)
$\nu(\text{C}_6\text{F}_5)$ and $\delta^b(\text{C}_6\text{F}_5)$	1498 (st)	1501 (st)	1499 (st)
	1058 (m)	1058 (m)	1060 (m)
	946 (st)	950 (st)	949 (st)
	799 (st)	801 (st)	800 (st)
	$\text{sp}^2 \nu(\text{C-H})$	3174 (w)	2960 (w)
$\nu(\text{C=N})$	1624	1569 (st)	1554 (st)
Ar $\nu(\text{C=C})$	1498-1450 (st)	1477-1453 (st)	1499-1437 (st)
$\nu(\text{C-N})$	1436 (m)	1438 (m)	

3.2.2 Structure determinations of compounds **III** – **V** and **5** – **7**

The crystal and molecular structures of compounds **III** – **V** and **5** – **7** were determined by single crystal X-ray diffraction and are, to the best of our knowledge, now reported for the first time. For compounds **5** – **7** this represents the first reported examples of gold complexes containing 2-ylideneamine-functionalised heterocycles as ligands. In view of the fact that very few crystal structure determinations of ylideneamine-functionalised heterocyclic ligands have been reported in the literature, a discussion of the free ligand structures are included to serve as reference for discussion of their coordination complex derivatives.

3.2.3.1 Crystal and molecular structure of compound **III**

Compound **III** co-crystallises with three molecules of water from a dichloromethane water mixture as colourless rectangles in the monoclinic space group $P2_1/c$ with $Z = 4$ molecules in the unit cell. Figure 3.1 depicts the molecular structure of **III**, showing the numbering scheme. Selected bond lengths and angles are summarised in Table 3.9.

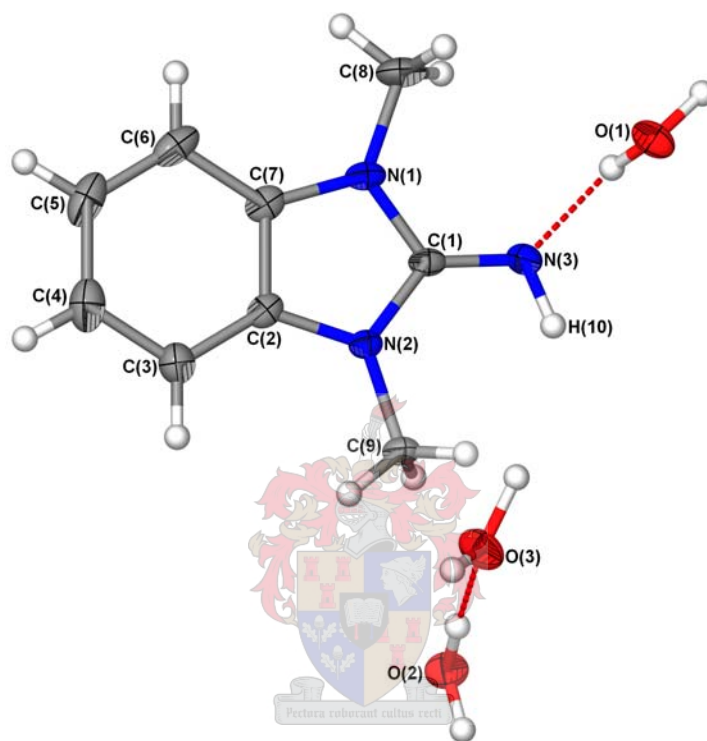


Figure 3.1 Molecular structure of **III** together with three water molecules showing the numbering scheme. Hydrogen bonds are shown as red fractioned lines.

The geometry of **III** is planar with only the methyl H-atoms protruding from the plane. The C(1)=N(3) bond length of 1.295(3) Å is in close agreement with the C=N distance of 1.296(2) Å, reported for 1,3-dimethyl-1,3-dihydro-imidazol-2-ylideneamine.⁹ Additionally, the C–N bond lengths [1.376(3) / 1.374(2) Å] are also comparable to those of the latter compound [1.375(2) / 1.371(2) Å]. These double C=N and single C(sp²)–N(sp²) bonds do not differ substantially from the standard values for such bonds [1.27 and 1.41 Å, respectively]²¹, proving delocalisation over these bonds to be negligible and the 2-ylideneamine form to be predominant. The only bond in compound **III** that appears to be influenced by the presence of the phenyl ring is C(2)–C(7) [1.395(3) Å], which is

²¹ A. Marchi, L. Marvelli, M. Cattabriga, R. Rossi, M. Neves, V. Bertolasi, V. Ferretti, *J. Chem. Soc., Dalton Trans.* **1999**, 1937-1943.

appreciably longer than the analogous bond in 1,3-dimethyl-1,3-dihydro-imidazol-2-ylideneamine [1.330(2) Å] – all other bond lengths do not deviate significantly from the literature values. Furthermore, the two exocyclic N=C=N bonding angles of 123.5 (2)° and 130.3(2)° are, as can be expected, much greater than the endocyclic N-C-N angle of 106.3(2)°. No noteworthy discrepancies from literature values are observed for the bonding angles of **III**.

The solid state packing of **III** is largely governed by a complex network of hydrogen bonds involving the imine nitrogen atoms and water molecules. In addition to these associations, some weak π -stacking interactions are observed which in combination with the hydrogen-bonding network, render the crystal lattice organisation very efficient. The molecules assemble in pairs, with the imidazole ring of each molecule within a pair weakly associated with the phenyl ring of the other *via* an offset face to face π -interaction of 3.44 Å. When the crystal lattice packing is viewed along the a-axis, these pairs of molecules form two distinct layers, which alternate along the b-axis [Figure 3.2 (a)]. In Figure 3.2 (b) a view of the molecular packing along the diagonal of the ac-plane is shown, revealing the neat zig-zag arrangement of the molecular assemblies, interlinked by hydrogen bonds.

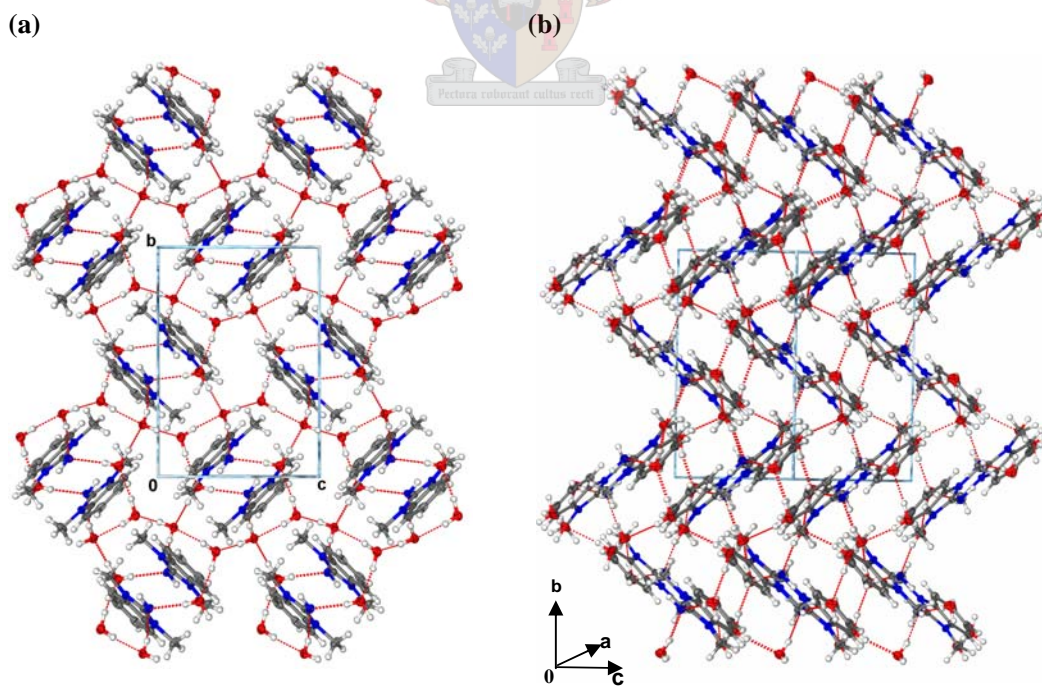


Figure 3.2 a) Solid state packing of **III** viewed along the a-axis, showing the hydrogen-bonding network (red bonds) involving water molecules b) Molecular packing viewed along the diagonal of the ac plane.

Table 3.9 Selected bond lengths (Å) and angles (°) of **III** with estimated standard deviations in parenthesis.

<i>Bond lengths (Å)</i>			
N(3)–C(1)	1.295(3)	N(2)–C(9)	1.451(2)
N(1)–C(1)	1.376(3)	N(1)–C(7)	1.388(3)
N(1)–C(8)	1.450(3)	N(2)–C(2)	1.374(2)
N(2)–C(1)	1.374(2)	C(2)–C(7)	1.395(3)
<i>Bond angles (°)</i>			
H(10)–N(3)–C(1)	111(2)	C(1)–N(1)–C(7)	110.0 (2)
N(3)–C(1)–N(1)	123.5(2)	C(1)–N(2)–C(2)	110(2)
N(3)–C(1)–N(2)	130.3(2)	N(1)–C(7)–C(2)	106.9(2)
C(1)–N(1)–C(8)	124.0(2)	N(2)–C(2)–C(7)	106.9(2)
C(1)–N(2)–C(9)	123.8(2)	C(2)–N(2)–C(9)	126.2(2)
N(1)–C(1)–N(2)	106.3(2)	C(7)–N(1)–C(8)	125.9(2)

3.2.3.2 Crystal and molecular structure of compound VI

The byproduct **VI**, crystallised from a dichloromethane solution of compound **IV** as yellow needles in the monoclinic space group $P2_1/c$, with two unique molecules of **VI** and one dichloromethane molecule present in the asymmetric unit. The unit cell contains $Z = 20$ molecules. Figure 3.3 depicts the molecular structure, indicating the numbering scheme, and Table 3.10 summarises selected bond lengths and angles of only one of the symmetrically unique molecules of **VI** as the bond lengths and angles in the two molecules do not differ significantly. All atoms are shown as spheres since the poor quality of the data set does not allow for anisotropic refinement. The C(1)–N(1) and C(1)–N(2) separations are intermediate between the ranges of double C=N and single C–N bond lengths, suggesting charge stabilisation by extensive delocalisation of the π -electron density over these bonds. The C(9)–N(2) and C(9)–N(3) bonds, on the other hand, display separations in closer agreement with typical double C=N and single C–N bond distances respectively proving delocalisation over these bonds to be negligible. Observed C–S distances range between 1.75(1) Å and 1.79(1) Å and the C–S–C angles are 90.6(5)° and 91.0(6)°. It is noteworthy that the N(2)–C(1)–S(1) angle of 129.3(8)° is significantly larger than the N(2)–C(9)–S(2) angle of 109.2(8)°, probably due to the differences in the bond character of the involved C–N bonds. The C(2)–C(7) and C(15)–C(10) separations, 1.40(2) Å and 1.38(2) Å, are comparable to the C(2)–C(7) separation of 1.395(3) Å in compound **III**. Hydrogen-bonding is observed between N(2) and the methyl protons H(13)

Table 3.10 Selected bond lengths (Å) and angles (°) of **VI** with estimated standard deviations in parenthesis.

<i>Bond lengths (Å)</i>			
N(2)–C(1)	1.32(1)	N(3)–C(16)	1.43(1)
N(2)–C(9)	1.30(1)	S(1)–C(1)	1.75(1)
N(1)–C(1)	1.35(1)	S(2)–C(9)	1.79(1)
N(3)–C(9)	1.36(1)	S(1)–C(2)	1.75(1)
N(1)–C(7)	1.40(1)	S(2)–C(10)	1.76(1)
N(3)–C(15)	1.38(1)	C(2)–C(7)	1.40(2)
N(1)–C(8)	1.48(2)	C(15)–C(10)	1.38(2)
<i>Bond angles (°)</i>			
H(8)–N(2)–C(1)	117.0	C(1)–N(1)–C(7)	115.9(9)
H(8)–N(2)–C(9)	116.9	C(9)–N(3)–C(15)	115.6(9)
C(1)–N(2)–C(9)	126(1)	C(1)–S(1)–C(2)	90.6(5)
N(1)–C(1)–N(2)	119.7(9)	C(9)–S(2)–C(10)	91.0(6)
N(3)–C(9)–N(2)	123(1)	N(1)–C(7)–C(2)	111(1)
N(2)–C(1)–S(1)	129.3(8)	N(3)–C(15)–C(10)	114(1)
N(2)–C(9)–S(2)	109.2(8)	S(1)–C(2)–C(7)	111.5(9)
N(1)–C(1)–S(1)	110.9(8)	S(2)–C(10)–C(15)	109.8(9)
N(3)–C(9)–S(2)	109.2(8)		

3.2.3.3 Crystal and molecular structure of compound **V**

Compound **V** crystallises from dichloromethane as colourless needles in the triclinic space group $P\bar{1}$, with four unique molecules in the asymmetric unit and $Z = 8$ molecules in the unit cell. Figure 3.5 depicts the molecular structure of **V**, indicating the numbering scheme. Selected bond lengths and angles are summarised in Table 3.11. The bond lengths and angles of the four unique molecules do not differ significantly from each other. The $C(sp^2)=N(sp^2)$ and $C(sp^3)-N(sp^2)$ bond lengths are comparable to those observed for **III** and related literature examples with no noteworthy differences.^{22,23} An average bonding distance of 1.776(3) Å is observed for the bond between the sulphur atom and the carbon atom central to the heteroatoms and is comparable to those observed in compound **VI**. In addition, a slight decrease in the S–C–C and N–C–C angles is also observed ($\Delta\angle$ ca. 6°). It is noteworthy that the endocyclic C–C bond lengths are considerably shorter than those of ligands **III** and **VI**, marking the increased double bond character in the absence of an aromatic ring. Similar to compound **III**, the individual angles about the C(1), C(6), C(16) and C(11) atoms deviate significantly from the ideal trigonal planar arrangement with the

²² L. Forlani, P. De Maria, E. Foresti, G. Pradella, *J. Org. Chem.* **1981**, *46*, 3178-3181.

²³ V. A. Mamedov, A. A. Kalinin, A. T. Gubaidullin, I. Z. Nurkhametova, I. A. Litvinov, Y. A. Levin, *Chem. Heterocycl. Compd.* **2000**, *35*, 1459-1473.

observed exocyclic N=C–S and N=C–N angles much greater than the endocyclic N–C–S angles.

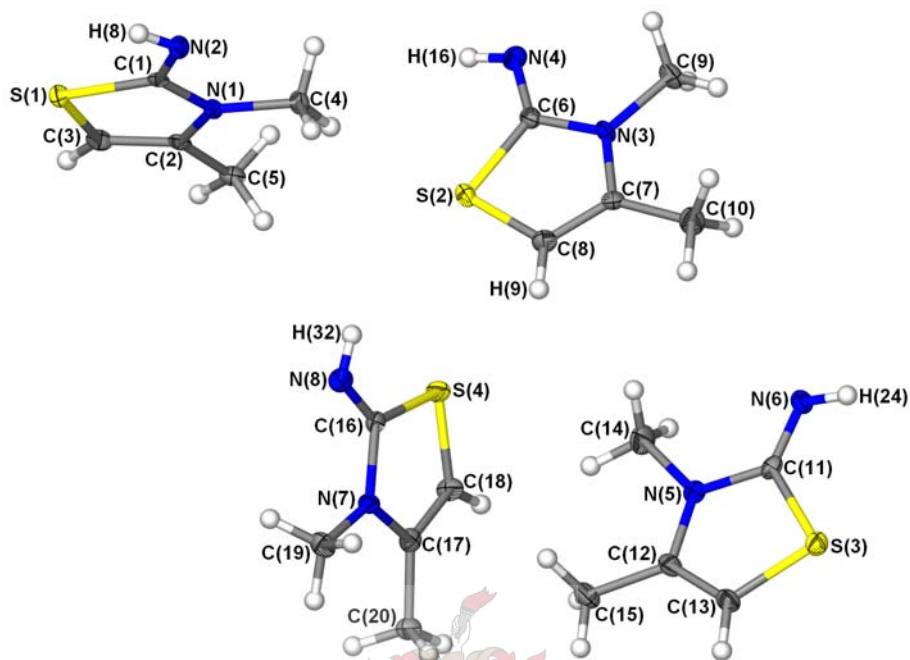


Figure 3.5 Molecular structure of **V** showing the numbering scheme of the four unique molecules in the asymmetric unit.

From a view of the solid state packing of **V** along the a-axis, it is evident that the molecules assemble in two distinct layers (A and B) which alternate along the b-axis (Figure 3.6).

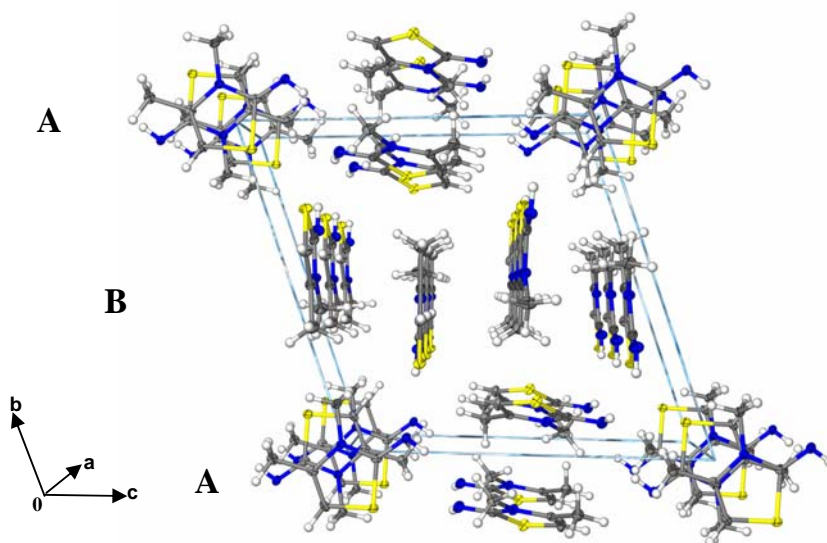


Figure 3.6 Perspective view along the a-axis of the unit cell packing of **V** showing the two alternating discrete layers A and B.

In layer A the molecules assemble in pairs which repeat along the a-axis. These pairs display two different orientations, with each of the molecules within a pair related to the other *via* an inversion centre. No molecular pairing is however observed in layer B. The crystal lattice does not display any significant intermolecular forces and in both layers, the ligand rings are not aligned, which prohibits any π - π interactions between neighbouring molecules.

Table 3.11 Selected bond lengths (Å) and angles (°) of **V** with estimated standard deviations in parenthesis.

<i>Bond lengths (Å)</i>			
H(8)–N(2)	0.81(3)	N(1)–C(1)	1.372(4)
H(16)–N(4)	0.82(3)	N(3)–C(6)	1.372(4)
H(24)–N(6)	0.82(3)	N(5)–C(11)	1.378(3)
H(32)–N(8)	0.80(3)	N(7)–C(16)	1.377(4)
N(2)–C(1)	1.280(3)	N(1)–C(4)	1.455(3)
N(4)–C(6)	1.271(4)	N(3)–C(9)	1.464(3)
N(6)–C(11)	1.268(4)	N(5)–C(14)	1.458(4)
N(8)–C(16)	1.279(4)	N(7)–C(19)	1.459(3)
S(1)–C(1)	1.781(3)	N(1)–C(2)	1.401(3)
S(2)–C(6)	1.775(3)	N(3)–C(7)	1.398(4)
S(3)–C(11)	1.784(3)	N(5)–C(12)	1.399(4)
S(4)–C(16)	1.764(3)	N(7)–C(17)	1.393(4)
S(1)–C(3)	1.742(3)	C(2)–C(3)	1.329(4)
S(2)–C(8)	1.747(3)	C(7)–C(8)	1.328(4)
S(3)–C(13)	1.748(3)	C(12)–C(13)	1.336(4)
S(4)–C(18)	1.747(3)	C(17)–C(18)	1.332(4)
<i>Bond angles (°)</i>			
H(8)–N(2)–C(1)	110(2)	C(11)–S(3)–C(13)	91.5(2)
H(16)–N(4)–C(6)	115(2)	C(16)–S(4)–C(18)	91.6(1)
H(24)–N(6)–C(11)	111(2)	C(1)–N(1)–C(2)	115.5(2)
H(32)–N(8)–C(16)	108(2)	C(6)–N(3)–C(7)	115.9(2)
N(2)–C(1)–N(1)	123.5(3)	C(11)–N(5)–C(12)	116.2(2)
N(4)–C(6)–N(3)	123.1(3)	C(16)–N(7)–C(17)	115.7(2)
N(6)–C(11)–N(5)	123.7(3)	C(1)–N(1)–C(4)	118.9(2)
N(7)–C(16)–N(8)	122.8(3)	C(6)–N(3)–C(9)	119.1(2)
N(2)–C(1)–S(1)	128.5(2)	C(11)–N(5)–C(14)	119.2(2)
N(4)–C(6)–S(2)	129.4(2)	C(16)–N(7)–C(19)	119.1(2)
N(6)–C(11)–S(3)	128.9(2)	S(1)–C(3)–C(2)	112.4(2)
N(8)–C(16)–S(4)	129.3(2)	S(2)–C(8)–C(7)	111.5(2)
S(1)–C(1)–N(1)	108.0(2)	S(3)–C(13)–C(12)	112.0(2)
S(2)–C(6)–N(3)	107.5(2)	S(4)–C(18)–C(17)	111.6(2)
S(3)–C(11)–N(5)	107.3(2)	N(1)–C(2)–C(3)	113.0(3)
S(4)–C(16)–N(7)	107.9(2)	N(3)–C(7)–C(8)	113.4(3)
C(1)–S(1)–C(3)	91.0 (1)	N(5)–C(12)–C(13)	113.0(3)
C(6)–S(2)–C(8)	91.7(1)	N(7)–C(17)–C(18)	113.3(3)

3.2.3.4 Crystal and molecular structure of compound 5

Compound **5** crystallises from THF as colourless needles in the monoclinic space group $P2_1/c$ with two symmetrically unique molecules in the asymmetric unit and $Z = 8$ molecules in the unit cell. Figure 3.7 depicts the molecular structure and numbering scheme of the unique molecules present in the asymmetric unit. Selected bond lengths and angles are summarised in Table 3.12. No significant differences exist between the bond lengths or angles of the two molecules in the asymmetric unit. The molecular structure consists of a $Au(C_6F_5)_2$ unit coordinated to the imine nitrogen of the neutral ligand **III**.

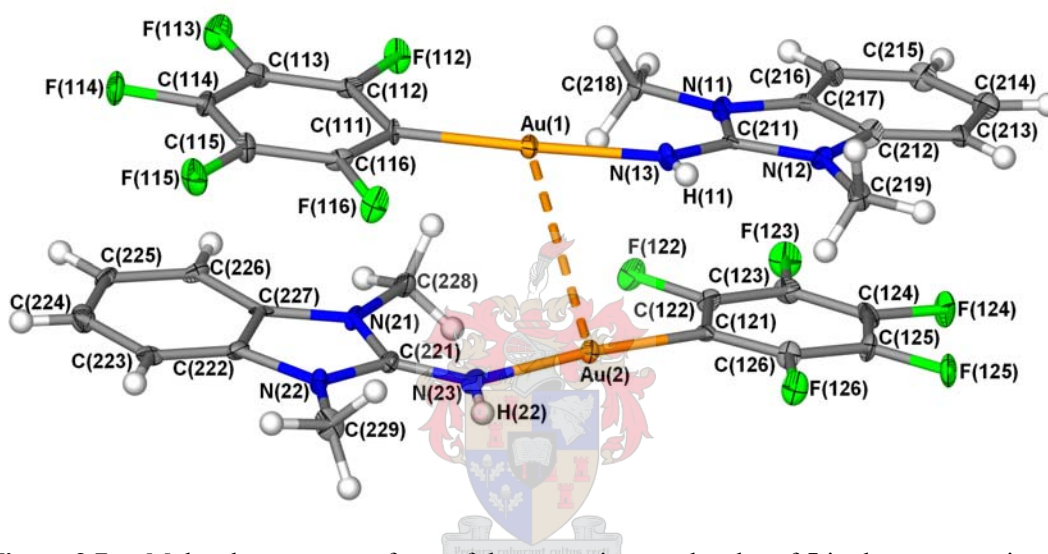


Figure 3.7 Molecular structure of one of the two unique molecules of **5** in the asymmetric unit, showing the numbering scheme.

The geometry about both gold(I) centers is close to linear [$176.4(3)^\circ / 175.5(3)^\circ$] with the planes of the pfp and 1,3-dimethyl-1,3-dihydro-benzimidazol-2-ylideneamine substituents approaching co-planarity [interplanar angle of 8.4°]. Furthermore, the gold centres of the unique molecules are associated *via* a very weak aurophilic interaction of $3.5824(6)$ Å, which is comparable to the interaction distance of $3.5884(7)$ Å reported for the literature example $[Au(C_6F_5)_2\{N(H)=CPh_2\}]$.¹⁹ The latter represents the only other documented example of a gold(I) compound containing an ylideneamine group coordinated to a $Au(C_6F_5)_2$ moiety. All bond lengths and angles of the coordinated ligand remain virtually unchanged with respect to those of the free ligand. In addition, the Au–C separations of the ylideneamine coordinated complex [$2.009(7) / 2.013(7)$ Å] also do not deviate significantly from those of the gold(I) precursor complex [$2.014(9) / 2.03(1)$ Å] (see Chapter 2, section 2.2.3) suggesting that substitution of a tht ligand for an ylideneamine-

functionalised heterocycle does not alter the bond lengths and angles substantially. The Au–N bonding distances, 2.042(6) Å and 2.062(6) Å, are in close agreement with the (C₆F₅)Au–N separations observed for the mentioned literature example, [Au(C₆F₅){N(H)=CPh₂}] [2.044(8) Å], as well as examples where the gold centre is coordinated to an endocyclic N-atom.^{24,25,26} In addition, the C=N–Au angles of 133.5(5)° and 131.7(5)° are also comparable to the angle of 132.0(6)° reported for [Au(C₆F₅){N(H)=CPh₂}].

In the solid state, molecules of **5** assemble in pairs, with the molecules within a pair linked by aurophilic interactions along the b-axis. In addition to these interactions, face to face π – π interactions (carbon to centroid distance 3.426 Å) between the adjacent pfp and benzimidazole rings also participate in directing the molecular packing. This leads to the π -stacking of neighbouring molecules in a head to tail fashion along the a-axis (Figure 3.8). A view along this axis reveals two discrete layers in the bc-plane.

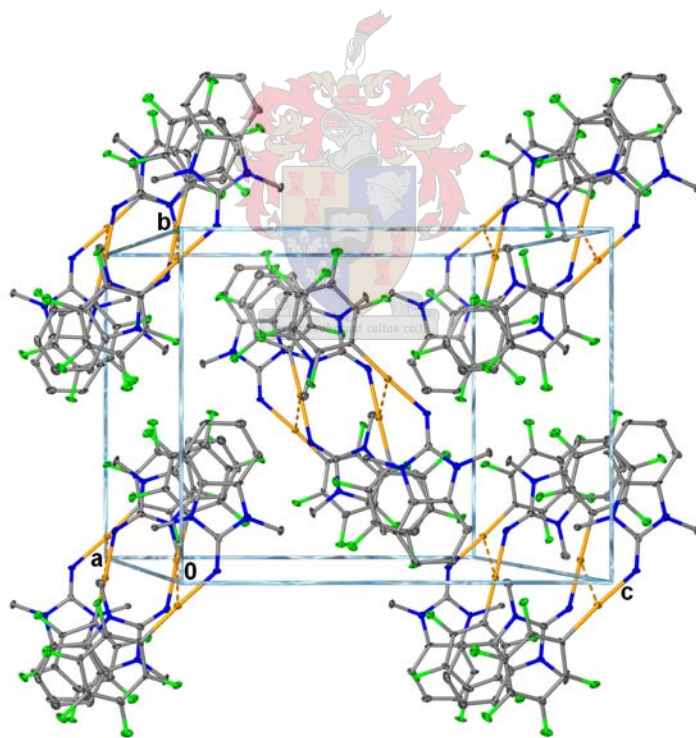


Figure 3.8 A perspective view of the molecular packing of **5** in the solid state (skewed view along the a-axis) revealing the π -stacking of molecules along the a-axis. Hydrogen atoms are omitted for clarity.

²⁴ J. E. Aquado, M. J. Calhorda, M. Concepción Gimeno, A. Laguna, *Chem. Comm.* **2005**, 3355-3356.

²⁵ S. Cronje, H. G. Raubenheimer, H. S. C. Spies, C. Esterhuysen, H. Schmidbaur, A. Schier, G. J. Kruger, *Dalton Trans.* **2003**, 14, 2859-2866, and references cited therein.

²⁶ W. F. Gabrielli, *PhD Dissertation* **2005**, University of Stellenbosch, Chapter 3.

Table 3.12 Selected bond lengths (Å) and angles (°) of **5** with estimated standard deviations in parenthesis.

<i>Bond lengths (Å)</i>			
Au(1)···Au(2)	3.5824(6)	N(11)–C(217)	1.385(9)
Au(1)–C(111)	2.009(7)	N(21)–C(227)	1.384(9)
Au(2)–C(121)	2.013(7)	N(12)–C(212)	1.387(9)
Au(1)–N(13)	2.042(6)	N(22)–C(222)	1.400(9)
Au(2)–N(23)	2.062(6)	N(11)–C(218)	1.466(8)
N(13)–C(211)	1.303(8)	N(21)–C(228)	1.463(9)
N(23)–C(221)	1.295(9)	N(12)–C(219)	1.458(8)
N(11)–C(211)	1.373(8)	N(22)–C(229)	1.455(9)
N(21)–C(221)	1.360(9)	C(212)–C(217)	1.41(1)
N(12)–C(211)	1.373(9)	C(222)–C(227)	1.40(1)
N(22)–C(221)	1.381(9)		
<i>Bond angles (°)</i>			
N(13)–Au(1)–Au(2)	73.4(2)	N(21)–C(221)–N(22)	107.6(6)
N(23)–Au(1)–Au(2)	73.9(2)	C(211)–N(11)–C(217)	109.9(6)
C(111)–Au(1)–Au(2)	109.9(2)	C(221)–N(21)–C(227)	109.4(6)
C(121)–Au(1)–Au(2)	110.1(2)	C(211)–N(12)–C(212)	109.4(6)
N(13)–Au(1)–C(111)	176.4(3)	C(221)–N(22)–C(222)	109.2(6)
N(23)–Au(2)–C(121)	175.5(3)	C(211)–N(11)–C(218)	125.7(6)
C(211)–N(13)–Au(1)	133.5(5)	C(221)–N(21)–C(228)	125.9(6)
C(221)–N(23)–Au(2)	131.7(5)	C(211)–N(12)–C(219)	123.7(6)
N(11)–C(211)–N(13)	126.4(6)	C(221)–N(22)–C(229)	124.4(6)
N(21)–C(221)–N(23)	127.7(6)	N(11)–C(217)–C(212)	106.4(6)
N(12)–C(211)–N(13)	126.4(6)	N(21)–C(227)–C(222)	107.8(6)
N(22)–C(221)–N(23)	124.7(6)	N(12)–C(212)–C(217)	107.1(6)
N(11)–C(211)–N(12)	107.2(6)	N(22)–C(222)–C(227)	105.9(6)

3.2.3.5 Crystal and molecular structure of compound **6**

Compound **6** crystallises, from THF as colourless cubes in the triclinic space group $P\bar{1}$. The asymmetric unit consist of one unique molecule of **6** and one molecule of THF with $Z = 2$ molecules in the unit cell. The molecular structure and numbering scheme are depicted in Figure 3.9 and selected bond lengths and angles are summarised in Table 3.13. Unlike in compound **5**, the pfp and 3-methyl-3*H*-benzothiazol-2-ylideneamine ligand planes are perfectly aligned, making the overall molecular geometry of **6** planar with only the hydrogen atoms of the Me groups protruding from the plane. The N–Au–C unit is best described as linear with an angle of 177.6(2)°. Contradictory to the in solution NMR observations, the C(211)–N(2) and C(211)–N(1) bond lengths [1.283(7) Å and 1.356(7) Å, respectively] are within the range of standard values reported for double C=N and single C–N bonds [1.27 Å and 1.41 Å, respectively] and do not testify to substantial electron

delocalisation over these bonds in the solid state. As was observed for compound **5**, the Au–C separation remains unaffected by coordination to the imine nitrogen and displays a distance of 2.013(5) Å following coordination to the ylideneamine ligand. The Au–N bond length of 2.041(5) Å agrees well with that of compound **5** [2.042(6) Å] as well as previously-mentioned literature examples.^{19,24,25,26} Apart from the slightly smaller C–N–Au angle [127.3(4)°], all other angles in **6** compare favourably to literature values.

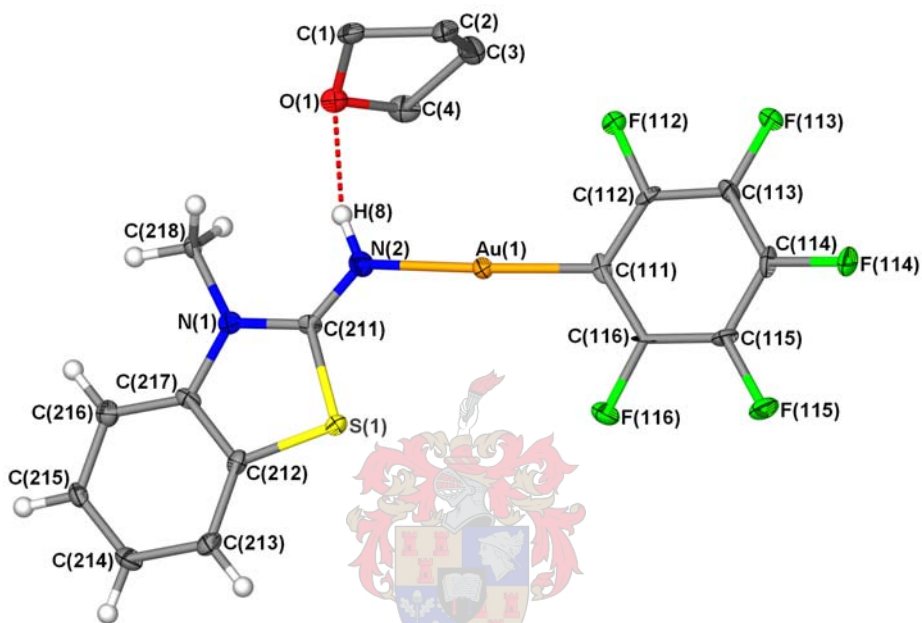


Figure 3.9 Molecular structure of **6** showing the numbering scheme. Hydrogen atoms of the THF molecule are omitted for clarity.

Although molecules of **6** are perfectly planar, no significant intermolecular forces other than the hydrogen bonding, involving the THF oxygen atoms and the imine protons, are present in the crystal lattice. Auophilic interactions between neighbouring molecules are most likely prohibited by the steric demands of the included THF molecules which prevent molecular separations smaller than 4.047 Å. This favouring of hydrogen bond formation over auophilic associations may also be an enthalpy effect. Although the energy of an auophilic interaction [29–33 kJ.mol⁻¹] has been estimated by NMR experiments to be in the same order of magnitude as a typical hydrogen bond [20–30 kJ.mol⁻¹],²⁷ the hydrogen bond per molecule ratio in the crystal lattice is 2:2 whereas the auophilic bond per molecule ratio would be 1:2. The formation of twice as many hydrogen bonds therefore results in a much greater energy gain, compared to association

²⁷ H. Schmidbaur, W. Graf, W. Müller, G. Müller, *Angew. Chem. Int. Ed. Engl.* **1988**, *27*, 417419.

via aurophilic bonds. This observation is in agreement with a recent report by Laguna and co-workers, who have concluded that hydrogen-bonding can compete with aurophilic interactions.¹⁹ The molecules assemble in pairs along the a-axis with each molecule within a pair related to the other *via* an inversion centre (Figure 3.10). When viewed along the a-axis, the solid state packing of **6** reveals only one discrete layer, which repeats in the bc-plane.

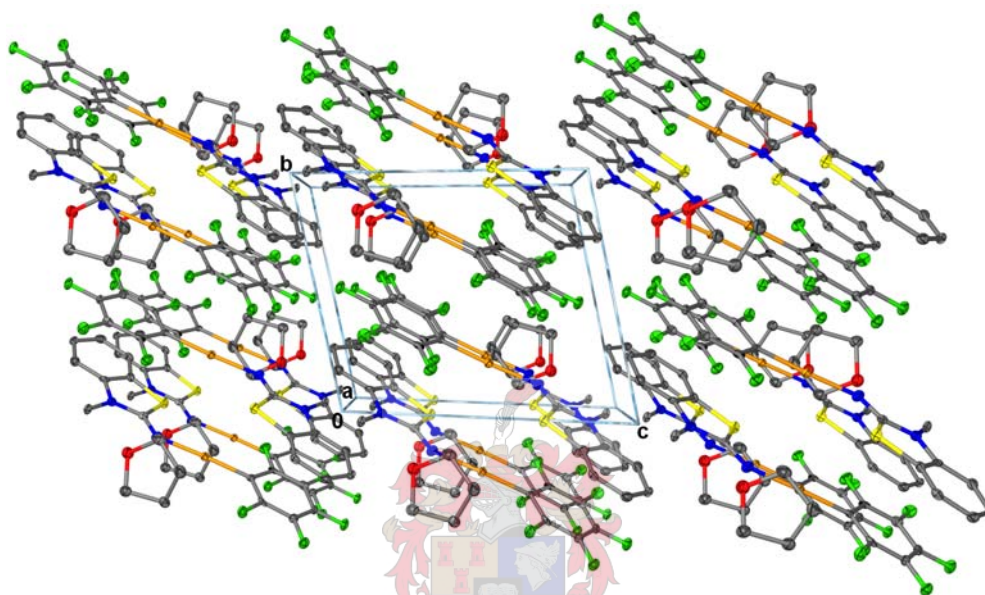


Figure 3.10 Perspective drawing of the molecular packing of **6** viewed along the a-axis. Hydrogen atoms are omitted for clarity.

Table 3.13 Selected bond lengths (Å) and angles (°) of **6** with estimated standard deviations in parenthesis.

<i>Bond lengths (Å)</i>			
Au(1)–C(111)	2.013(5)	N(1)–C(217)	1.393(6)
Au(1)–N(2)	2.041(5)	S(1)–C(212)	1.767(5)
N(2)–C(211)	1.283(7)	N(1)–C(218)	1.437(7)
N(1)–C(211)	1.356(7)	C(212)–C(217)	1.390(8)
S(1)–C(211)	1.757(5)		
<i>Bond angles (°)</i>			
N(2)–Au(1)–C(111)	177.6(2)	C(211)–N(1)–C(217)	116.0(4)
C(211)–N(2)–Au(1)	127.3(4)	C(211)–S(1)–C(212)	90.8(2)
N(1)–C(211)–N(2)	127.6(5)	C(211)–N(1)–C(218)	120.9(4)
S(1)–C(211)–N(2)	122.1(4)	N(1)–C(217)–C(212)	112.0(5)
N(1)–C(211)–S(1)	110.3(4)	S(1)–C(212)–C(217)	110.8(4)

3.2.3.6 Crystal and molecular structure compound 7

Compound **7** crystallises from acetone as colourless needles in the monoclinic space group $P2_1/n$. The asymmetric unit consist of one distinct molecule of **7** and one acetone molecule, with $Z = 2$ molecules in the unit cell. Figure 3.11 depicts the molecular structure showing the numbering scheme. Selected bond lengths and angles are summarised in Table 3.14.

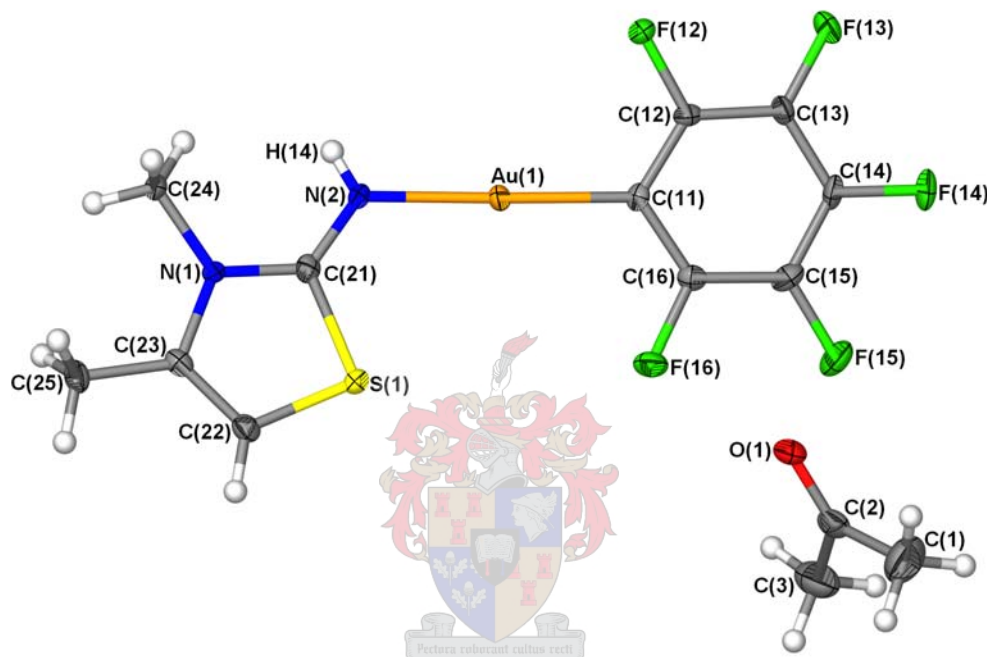


Figure 3.11 Molecular structure of **7** showing the numbering scheme.

The geometry about the gold(I) centre is essentially linear [$178.9(2)^\circ$] with the Au–C bonding distance in good agreement with those observed for complexes **1**, **5** and **6**. The Au–N separation [$2.028(4) \text{ \AA}$] is, in contrast, slightly shorter than those of compounds **5** and **6**, indicating the formation of a somewhat stronger bond between the gold(I) centre and the imine N-atom of ligand **V**. Due to the rather high standard deviations of these bond lengths, some uncertainty as to the significance of this result exists. This observation is however consistent with the former discussion on the noted stabilities of these compounds (Section 3.2.1.2). In addition, the C–N–Au angle of $125.7(4)^\circ$ is significantly smaller than those observed for compounds **5** and **6**. As in complex **5**, the pfp and 3,4-dimethyl-3*H*-thiazol-2-ylideneamine ligand planes approach co-planarity with an interplanar angle of 7.3 \AA . The C(21)=N(2) and C(21)–N(1) bond lengths [$1.292(6)$ and $1.358(6) \text{ \AA}$] differ significantly and are longer and shorter, than the average separation

observed respectively for the corresponding bonds in the free ligand. This again explains the greater relative importance of the contributing structures in possibility A of Scheme 3.7. Furthermore, the N(1)–C(21)–N(2) and N(1)–C(21)–S(1) angles [128.4(5)° and 121.6(4)°], are significantly greater and smaller respectively than the corresponding angles in the free ligand structure, further testimony of a greater degree of delocalisation over the N–C–N bonds.

Despite the apparent simplicity of compound **7**, no intermolecular aurophilic interactions are observed in the crystal lattice. The formation of such interactions appears to be overruled by the weak π - π interaction between the pfp and thiazole rings of neighbouring molecules along the a-axis (Figure 3.12). The non-existence of aurophilic interactions may also be due to the inclusion of acetone molecules in the crystal lattice which prohibit the formation of molecular arrangements that would allow for such interactions. Since the gold atoms of the molecules are located on either side of the π -stacked units, close gold-gold contacts are prohibited. Furthermore, no hydrogen-bonding is observed between the oxygen atoms of the acetone molecules and the imine hydrogen atoms and the molecular packing is therefore solely directed by π -stacking of the ligand rings. Two discrete layers exist with each layer consisting of molecules linked by weak π - π interactions to form an infinite chain along the c-axis.

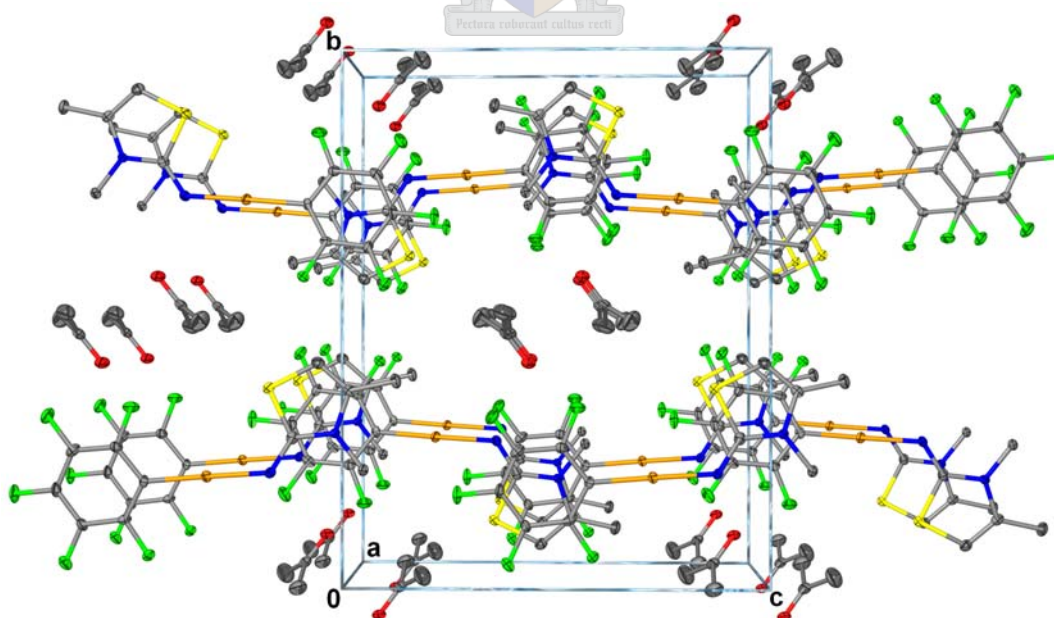


Figure 3.12 Perspective drawing of the unit cell packing of **7** viewed along the a-axis showing the π -stacking interactions between the ligand rings of neighbouring molecules.

Table 3.14 Selected bond lengths (Å) and angles (°) of **7** with estimated standard deviations in parenthesis.

<i>Bond lengths (Å)</i>			
Au(1)–C(11)	2.003(5)	N(1)–C(23)	1.405(6)
Au(1)–N(2)	2.028(4)	S(1)–C(22)	1.745(5)
N(2)–H(14)	0.75(5)	N(1)–C(24)	1.465(6)
N(2)–C(21)	1.292(6)	C(22)–C(23)	1.335(7)
N(1)–C(21)	1.358(6)	C(23)–C(25)	1.492(7)
S(1)–C(21)	1.748(5)		
<i>Bond angles (°)</i>			
N(2)–Au(1)–C(11)	178.9(2)	C(21)–N(1)–C(24)	121.7(4)
C(21)–N(2)–Au(1)	125.7(4)	C(21)–S(1)–C(22)	90.7(2)
N(1)–C(21)–N(2)	128.4(5)	C(21)–N(1)–C(23)	114.5(4)
S(1)–C(21)–N(2)	121.6(4)	N(1)–C(23)–C(22)	112.7(4)
N(1)–C(21)–S(1)	110.0(4)	S(1)–C(22)–C(23)	112.1(4)

3.3 Conclusions

Herein the successful synthesis and complete characterisation of a series of novel gold(I) complexes derived from benzimidazol- and thiazol-2-ylideneamine ligands have been described. These complexes represent the first gold(I) complexes to contain ylideneamine-functionalised heterocyclic ligands. The present work has shown that despite the fact that ylideneamine ligands are regarded as hard to borderline ligands, they are able to readily coordinate to soft gold(I) centres to form complexes of ample stability. Thiazol-2-ylideneamine(pfp)gold(I) complexes display greater stability than their benzimidazol-2-ylideneamine(pfp)gold(I) analogues, with the observed stabilities of the complexes decreasing in the order **7** > **6** ≥ **5**.

NMR studies show a decrease in electron delocalisation over the ligand system in conjunction with a reduction in aromatic character following coordination to a gold(I) centre. Furthermore coordination results in a pronounced downfield shift of the =NH proton resonances. The effect is most prominent in complex **5** and decreased for compounds **5** – **7** in the order **5** > **6** > **7**.

From FT-IR spectroscopy it is clear that $\nu(=NH)$ absorption bands shift significantly towards higher frequencies upon coordination of ligands **III** – **V** to a gold(I) centre. This trend is also applicable to the (C–N) absorption bands.

X-ray crystallographic investigation revealed that the geometry about the gold(I) centre in all complexes is essentially linear with Au–N separations in good agreement with literature values reported for related compounds. Coordination of the free ligands **III** and **IV** to a metal centre did not alter the ligand bond lengths and angles substantially. In complexes **5** and **6**, the measured C–N and C=N bonding distances were within the range of standard values for such bonds and did not testify to significant electron delocalisation over the N–C–N skeleton. In compound **7**, however, coordination of ligand **V** to an Au(C₆F₅) unit did result in an increased electron delocalisation over the N–C–N bonds. Furthermore, it could be established that substitution of a tht ligand for a ylideneamine does not significantly affect the Au–C bond length. Finally, crystal structure determinations revealed that hydrogen-bonding and π - π interactions play fundamental roles in the solid state packing of ligands **III** – **V** and complexes **5** – **7**. In addition, weak aurophilic interactions between neighbouring gold(I) centres in complex **6**, direct the packing of the molecular assemblies.

3.4 Experimental

3.4.1 General procedures and instruments

Reactions were carried out under argon using standard Schlenk and vacuum-line techniques. Tetrahydrofuran (THF), *n*-hexane, *n*-pentane and diethyl ether were distilled under N₂ from sodium benzophenone ketyl, acetone from 3 Å molecular sieves, and dichloromethane from CaH₂. Methyl iodide, CF₃SO₃CH₃, 4-methyl-thiazol-2-ylamine and benzothiazol-2-ylamine were purchased from Aldrich. 1*H*-benzimidazol-2-ylamine and KH were purchased from Fluka. Literature methods were used to prepare [Au(C₆F₅)(tht)]²⁸ from [Au(Cl)(tht)].²⁹

Melting points were determined on a Stuart SMP3 apparatus and are uncorrected. Mass spectra were recorded on an AMD 604 (EI, 70 eV), VG Quattro (ESI, 70 eV methanol, acetonitrile) or VG 70 SEQ (FAB, 70 eV) instrument. In the case of EI-MS and FAB-MS the isotopic distribution patterns were checked against the theoretical distribution. NMR spectra were recorded on a Varian 300/400 FT or INOVA 600 MHz spectrometer (¹H

²⁸ R. Usón, A. Laguna, M. Laguna, *Inorg. Synth.* **1989**, 26, 85-91.

²⁹ R. Usón and A. Laguna in: *Organometallic Synthesis, Vol. 3* (Eds. R. B. Lang, J. J. Eisch) Elsevier, Amsterdam, **1986**, p325.

NMR at 300/400/600 MHz, ¹³C NMR at 75/100/150 MHz, ¹⁵N NMR at 60.8 MHz and ¹⁹F NMR at 376 MHz) with the chemical shifts reported relative to the solvent resonance or an external reference, NH₃NO₂ (¹⁵N) or CFCl₃ (¹⁹F). Infrared spectra were recorded on a Thermo Nicolet Avatar 330FT-IR with a Smart OMNI ATR (attenuated total reflectance) sampler. Elemental analysis was carried out at the School of Chemistry, University of the Witwatersrand. Prior to elemental analysis, products were evacuated under high vacuum for 10h.

3.4.2 Preparations and procedures

3.4.2.1 Preparation of 1,3-dimethyl-1,3-dihydro-benzimidazol-2-ylideneamine, III

Powdered KOH (0.37 g, 6.50 mmol) was added to a stirring solution of 1*H*-benzimidazol-2-ylamine (0.43 g, 3.25 mmol) in acetone (13 ml). A thick colourless precipitate was visible after 10 min. After the addition of CH₃I (0.20 ml, 0.46 g, 2.25 mmol) the reaction mixture was stirred vigorously for 10 min. after which the brown solution (with only the excess KOH still suspended) was transferred to a separating funnel containing benzene (120 ml). The organic layer was washed with water (1 × 20 ml) and a saturated NaCl solution (20 ml) and subsequently dried over anhydrous MgSO₄. The solvent was removed *in vacuo* and the remaining off-white solid was redissolved in CH₂Cl₂ (30 ml). After cooling the solution to -40 °C, CF₃SO₃CH₃ (0.37 ml, 0.53 g, 3.25 mmol) was added to the solution and the reaction mixture stirred at this temperature for 1 h. The mixture was allowed to reach room temperature, whereafter the volatiles were removed *in vacuo*. The remaining colourless residue was washed with diethyl ether (2 × 20 ml), dried *in vacuo* and resuspended in THF (30 ml). KH (0.13 g, 3.25 mmol) in THF (5 ml) was added to the stirring suspension. Gas evolution was evident after addition of the KH. The mixture was refluxed for 1h during which the colourless suspension cleared up to yield a yellow solution. The solution was stripped of solvent and the solid residue was extracted with CH₂Cl₂. The CH₂Cl₂ extract was filtered through anhydrous MgSO₄, and reduced to dryness to yield the pure product as a colourless microcrystalline solid (0.46 g, 88 %). Colourless crystals of **III** were obtained by slow evaporation of a concentrated solution of the compound in CH₂Cl₂.

3.4.2.2 Preparation of 3-methyl-3H-benzothiazol-2-ylideneamine, IV

The alkylating agent, CF₃SO₃CH₃ (0.68 ml, 1.0 g, 6.0 mmol), was added dropwise to a solution of benzothiazol-2-ylamine (0.91 g, 6.0 mmol) in ether (20ml) at -40°C. Upon addition of the CF₃SO₃CH₃, a thick colourless precipitate formed. The reaction mixture was allowed to stir at this temperature for 1 h and then to slowly reach room temperature. The solvents and other volatiles were removed *in vacuo* and the resulting colourless solid was washed with ether (2 × 40 ml), dried *in vacuo*, and resuspended in THF (20 ml). A suspension of KH (0.24 g, 6.03 mmol) in THF (5 ml) was added to the stirring mixture. Hydrogen gas liberation, in the form of heavy bubble formation, could be observed. The mixture was refluxed for 1h during which the colourless suspension cleared up to yield a yellow solution. The solution was reduced to dryness and the solid residue was extracted with CH₂Cl₂. The CH₂Cl₂ extract was subsequently filtered through anhydrous MgSO₄. After removal of the solvent by evaporation under vacuum the pure product was obtained as a yellow solid³⁰ (0.79 g, 79 %).

3.4.2.3 Preparation of 3,4-dimethyl-3H-thiazol-2-ylideneamine, V

The alkylating agent, CF₃SO₃CH₃ (1.13 ml, 1.64 g, 10.0 mmol), was added dropwise to a solution of 4-methyl-thiazol-2-ylamine (1.14 g, 10.0 mmol) in ether (30ml) at -40°C. Upon addition of the CF₃SO₃CH₃, a thick colourless precipitate formed. The reaction mixture was allowed to stir at this temperature for 1 h whereafter it was warmed to room temperature and reduced to dryness *in vacuo*. The remaining colourless solid was washed with ether (2 × 20 ml), dried *in vacuo*, and resuspended in THF (30 ml). A suspension of KH (0.40 g, 10 mmol) in THF (10 ml) was added to the stirring mixture. Gas liberation could be observed in the form of bubbles. The mixture was refluxed for 1h during which the colourless suspension cleared up to afford a light yellow solution. The solution was stripped of solvent and the solid residue was extracted with CH₂Cl₂ and the extract subsequently filtered through anhydrous MgSO₄. After removal of the solvent by evaporation under vacuum, the crude product was sublimed under vacuum (0.1 mBar) at 75 °C to achieve the pure product as a colourless crystalline solid (0.79 g, 62 %). Colourless crystals of **V** were obtained by slow evaporation of a concentrated solution of the compound in CH₂Cl₂.

³⁰ Caution: 3-methyl-3H-benzothiazol-2-ylideneamine may irritate respiratory tracts when inhaled.

3.4.2.4 Preparation of 1,3-dimethyl-1,3-dihydro-benzimidazol-2-ylideneamine(pentafluorophenyl)gold(I), 5

A solution of [Au(C₆F₅)(tht)] (0.32 g, 0.70 mmol) in THF (10 ml) was transferred to a Schlenk tube containing **III** (0.11 g, 0.70 mmol) dissolved in THF (20 ml). The reaction mixture was allowed to stir for three days at room temperature, during which a little decomposition occurred. The resulting yellow solution was filtered (cannula filtration) and reduced to dryness *in vacuo*. The remaining residue was washed with ether (2 × 30ml) and dried to yield the pure product as a colourless solid (0.26 g, 70%). Colourless crystals of **5** were obtained, by slow diffusion of pentane into a THF solution of the compound at -22 °C.

3.4.2.5 Preparation of 3-methyl-3H-benzothiazol-2-ylideneamine(pentafluorophenyl)gold(I), 6

A solution of freshly prepared [Au(C₆F₅)(tht)] (0.22 g, 0.48 mmol) in THF (10 ml) was transferred to a Schlenk tube containing **IV** (0.08 g, 0.49 mmol) dissolved in THF (20 ml). Mild decomposition occurred after the addition and the solution was therefore filtered (canula filtration), to remove colloidal gold, and transferred to a clean reaction vessel. The reaction mixture was allowed to stir for three days at room temperature. Further decomposition occurred during this stirring period and the resulting solution was filtered through anhydrous MgSO₄ and reduced to dryness *in vacuo* to yield the title compound as a colourless solid. (0.20 g, 78%). Colourless crystals of **6** were obtained by slow crystallisation from a concentrated THF solution of the compound in a crystallisation tube at -22 °C.

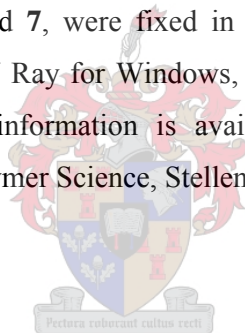
3.4.2.6 Preparation of 3,4-dimethyl-3H-thiazol-2-ylideneamine(pentafluorophenyl)-gold(I), 7

A solution of freshly prepared [Au(C₆F₅)(tht)] (0.30 g, 0.67 mmol) in THF (10 ml) was transferred to a Schlenk tube containing **V** (0.09 g, 0.79 mmol) dissolved in THF (30 ml). The reaction mixture was allowed to stir for four days at room temperature. Slight decomposition occurred during this stirring period and the reaction mixture was filtered through anhydrous Na₂SO₄ and reduced to dryness *in vacuo*. The crude product was washed with diethyl ether (2 × 20 ml) and dried under vacuum to yield the title compound

as an off-white solid (0.31 g, 93 %). Colourless crystals of **7** were obtained, from slow diffusion of pentane into an acetone solution of the compound at -22 °C.

3.4.3 X-ray structure determinations

Crystal data collection and refinement details of compounds **III**, **IV**, **VI**, **5**, **6** and **7** are summarised in Tables 3.14 - 3.16. Data sets were collected on a Bruker SMART Apex CCD diffractometer with graphite monochromated MoK α radiation ($\lambda = 0.71073 \text{ \AA}$).³¹ Data reduction was performed according to standard methods using the software package Bruker SAINT and data were treated with SADABS.^{32,33,34} All the structures were solved using direct methods or interpretation of a Patterson synthesis, which yielded the position of the metal atoms, and conventional difference Fourier methods. All non-hydrogen atoms were refined anisotropically by full-matrix least squares calculations on F² using SHELX-97³⁵ within an X-seed environment.^{36,37} All hydrogen atoms, except the imine hydrogen atoms of ligand **V** and compound **7**, were fixed in calculated positions. Figures were generated with X-seed³⁶ and POV Ray for Windows, with the displacement ellipsoids at 50% probability level. Further information is available from Dr. S. Cronje at the Department of Chemistry and Polymer Science, Stellenbosch University.



³¹ SMART Data Collection Software (version 5.629), Bruker AXS Inc. (Madison), WI, **2003**.

³² SAINT, Data Reduction Software (version 6.45), Bruker AXS Inc. (Madison), WI, **2003**.

³³ R. H. Blessing, *Acta Crystallogr., Sect. A*, **1995**, *51*, 33-38.

³⁴ SADABS (version 2.05), Bruker AXS Inc. (Madison), WI, **2002**.

³⁵ G. M. Shelrick, SHELX-97. Program for Crystal Structure Analysis, University of Göttingen (Germany), **1997**.

³⁶ L. J. Barbour, *J. Supramol. Chem.* **2003**, *1*, 189-191.

³⁷ J. L. Atwood, L. J. Barbour, *Cryst. Growth Des.* **2003**, *3*, 3-8.

Table 3.15 Crystallographic data of compounds **III** and **VI**.

	III	VI
Empirical formula	$C_9H_{17}N_3O_3$	$[C_{17}H_{15}F_3N_3O_3S_3] \cdot [CH_2Cl_2]$
M_r	215.26	547.44
Temp. (K)	100 (2)	100 (2)
Wavelength (Å)	0.71073	0.71073
Crystal system	Monoclinic	Monoclinic
Crystal dimensions (mm)	$0.23 \times 0.20 \times 0.08$	$0.21 \times 0.05 \times 0.03$
Crystal shape and colour	rectangles, colourless	needles, yellow
Space group	$P2_1/c$ (No. 14)	$P2_1/c$ (No. 14)
a (Å)	11.348(3)	14.385(2)
b (Å)	12.090(4)	13.759(2)
c (Å)	8.619(3)	20.626(3)
α (°)	90.00	90
β (°)	98.098(5)	98.288(2)
γ (°)	90.00	90
Volume (Å ³)	1170.7(6)	4040(1)
Z	4	20
d_{calcd} (g/cm ³)	1.221	1.661
μ (Mo-K α) (mm ⁻¹)	0.092	0.554
Absorption correction	Semi-empirical from equivalents (SADABS)	Semi-empirical from equivalents (SADABS)
F(000)	464	2064
θ -range for data collection (°)	1.81 to 26.42	1.78 to 25.74
Index range	$-12 \leq h \leq 14, -9 \leq k \leq 15$ $-10 \leq l \leq 10$	$-14 \leq h \leq 17, -16 \leq k \leq 16,$ $-24 \leq l \leq 25$
No. of reflections collected	6351	21059
No. of unique reflections	2400 ($R_{\text{int}} = 0.0307$)	7622 ($R_{\text{int}} = 0.0740$)
Max. and min. transmission	0.993 and 0.979	0.9836 and 0.8926
Refinement parameters / restraints	166 / 0	551 / 0
Goodness of fit on F^2	1.113	0.844
Final R-indices [$I > 2\sigma(I)$]	$R_1 = 0.0609$ $wR_2 = 0.1311$	$R_1 = 0.1578$ $wR_2 = 0.3124$
R indices (all data)	$R_1 = 0.0723$ $wR_2 = 0.1370$	$R_1 = 0.1992$ $wR_2 = 0.3413$
Largest diff. peak and hole (e.Å ⁻³)	0.278 and -0.224	3.042 and -2.695
Weighing scheme ^a	$a = 0.0529 / b = 0.6793$	$a = 0.0741 / b = 292.904$

^a $wR_2 = \{\sum[w(F_o^2 - F_c^2)^2] / \sum[w(F_o^2)^2]\}^{1/2}$; $w = 1/[\sigma^2(F_o^2) + (aP)^2 + bP + d \sin\theta]$; $P = [f(\text{Max}(0 \text{ or } F_o^2)) + (1-f) F_c^2]$

Table 3.16 Crystallographic data of compounds **V** and **5**.

	V	5
Empirical formula	C ₅ H ₈ N ₂ S	C ₁₅ H ₁₁ AuF ₅ N ₃
<i>M_r</i>	128.19	525.23
Temp. (K)	100 (2)	100 (2)
Wavelength (Å)	0.71073	0.71073
Crystal system	Triclinic	Monoclinic
Crystal dimensions (mm)	0.30 × 0.10 × 0.05	0.21 × 0.08 × 0.07
Crystal shape and colour	needle, colourless	needle, colourless
Space group	<i>P</i> $\bar{1}$ (No. 2)	<i>P</i> 2 ₁ / <i>c</i> (No.14)
<i>a</i> (Å)	6.949(1)	13.684(2)
<i>b</i> (Å)	13.498(3)	13.522(2)
<i>c</i> (Å)	14.301(3)	16.365(2)
α (°)	108.286(3)	90.00
β (°)	101.346(3)	107.753(2)
γ (°)	91.652(3)	90.00
Volume (Å ³)	1242.9(4)	2883.9(7)
<i>Z</i>	8	8
<i>d</i> _{calcd} (g/cm ³)	1.370	2.419
μ (Mo–K α) (mm ⁻¹)	0.408	10.263
Absorption correction	Semi-empirical from equivalents (SADABS)	Semi-empirical from equivalents (SADABS)
F(000)	544	1968
θ -range for data collection (°)	1.60 to 25.69	1.99 to 26.47
Index range	-8 ≤ <i>h</i> ≤ 8, -16 ≤ <i>k</i> ≤ 16, -17 ≤ <i>l</i> ≤ 7	-17 ≤ <i>h</i> ≤ 16, -12 ≤ <i>k</i> ≤ 16, -18 ≤ <i>l</i> ≤ 20
No. of reflections collected	6852	15458
No. of unique reflections	4625 (<i>R</i> _{int} = 0.0467)	5767 (<i>R</i> _{int} = 0.0520)
Max. and min. transmission	0.980 and 0.884	0.4856 and 0.2123
Refinement parameters / restraints	313 / 0	437 / 0
Goodness of fit on <i>F</i> ²	0.880	1.067
Final <i>R</i> -indices [<i>I</i> > 2 σ (>(<i>I</i>))]	<i>R</i> ₁ = 0.0456 <i>wR</i> ₂ = 0.0800	<i>R</i> ₁ = 0.0373 <i>wR</i> ₂ = 0.0751
<i>R</i> indices (all data)	<i>R</i> ₁ = 0.0772 <i>wR</i> ₂ = 0.0879	<i>R</i> ₁ = 0.0506 <i>wR</i> ₂ = 0.0818
Largest diff. peak and hole (e.Å ⁻³)	0.428 and -0.271	2.009 and -1.267
Weighing scheme ^a	<i>a</i> = 0.0260 / <i>b</i> = 0	<i>a</i> = 0.0256 / <i>b</i> = 6.0957

^a $wR_2 = \{\sum[w(F_o^2 - F_c^2)^2] / \sum[w(F_o^2)^2]\}^{1/2}$; $w = 1/[\sigma^2(F_o^2) + (aP)^2 + bP + d + e \sin \theta]$; $P = [f(\text{Max}(0 \text{ or } F_o^2)) + (1-f) F_c^2]$

Table 3.17 Crystallographic data of compounds **6** and **7**.

	6	7
Empirical formula	C ₁₈ H ₁₆ AuF ₅ N ₂ OS	C ₂₈ H ₂₈ Au ₂ F ₁₀ N ₄ O ₂ S ₂
<i>M_r</i>	600.35	1100.60
Temp. (K)	100 (2)	100 (2)
Wavelength (Å)	0.71073	0.71073
Crystal system	Triclinic	Monoclinic
Crystal dimensions (mm)	0.12 × 0.12 × 0.09	0.21 × 0.05 × 0.03
Crystal shape and colour	cube, colourless	needle, colourless
Space group	<i>P</i> $\bar{1}$ (No. 2)	P21/n (No. 14)
<i>a</i> (Å)	9.314(2)	6.776(1)
<i>b</i> (Å)	9.359(2)	17.691(3)
<i>c</i> (Å)	11.778(3)	14.043(2)
α (°)	99.081(3)	90.00
β (°)	112.814(3)	91.856(3)
γ (°)	96.172(3)	90.00
Volume (Å ³)	918.2(4)	1682.6(4)
<i>Z</i>	2	2
<i>d</i> _{calcd} (g/cm ³)	2.171	2.172
μ (Mo–K α) (mm ⁻¹)	8.185	8.922
Absorption correction	Semi-empirical from equivalents (SADABS)	Semi-empirical from equivalents (SADABS)
F(000)	572	1040
θ -range for data collection (°)	1.92 to 25.77	1.85 to 25.72
Index range	-11 ≤ <i>h</i> ≤ 11, -11 ≤ <i>k</i> ≤ 11, -14 ≤ <i>l</i> ≤ 14	-8 ≤ <i>h</i> ≤ 6, -21 ≤ <i>k</i> ≤ 21, -14 ≤ <i>l</i> ≤ 17
No. of reflections collected	8867	9242
No. of unique reflections	3385 (<i>R</i> _{int} = 0.0261)	3191 (<i>R</i> _{int} = 0.0340)
Max. and min. transmission	0.4788 and 0.3645	0.765 and 0.593
Refinement parameters / restraints	254 / 0	225 / 0
Goodness of fit on <i>F</i> ²	1.061	1.006
Final <i>R</i> -indices [<i>I</i> > 2 σ > (<i>I</i>)]	<i>R</i> ₁ = 0.0289 <i>wR</i> ₂ = 0.0692	<i>R</i> ₁ = 0.0278 <i>wR</i> ₂ = 0.0569
<i>R</i> indices (all data)	<i>R</i> ₁ = 0.0327 <i>wR</i> ₂ = 0.0709	<i>R</i> ₁ = 0.0371 <i>wR</i> ₂ = 0.0601
Largest diff. peak and hole (e.Å ⁻³)	3.065 and -1.085	1.344 and -0.549
Weighing scheme ^a	<i>a</i> = 0.0473 / <i>b</i> = 0.2027	<i>a</i> = 0.0297 / <i>b</i> = 0

^a $wR_2 = \{\sum[w(F_o^2 - F_c^2)^2] / \sum[w(F_o^2)^2]\}^{1/2}$; $w = 1/[\sigma^2(F_o^2) + (aP)^2 + bP + d + e \sin \theta]$; $P = [f(\text{Max}(0 \text{ or } F_o^2)) + (1-f) F_c^2]$

CHAPTER 4

Preparation and Characterisation of Novel Ylideneamine Gold(I) Complexes with Phosphine or Carbene (NHC) Ancillary Ligands

4.1 Introduction

Ylideneamine ligands, especially biguanides, and their transition metal complexes have attracted a considerable amount of interest over the years owing to their biological activity. Metformin (1,1-dimethylbiguanide) [Figure 4.1 (a)] and derivatives thereof, in particular, are well known for their medicinal value. This class of compounds shows significant versatility in their biological activity and have been employed as therapeutic agents for the treatment of pain, anxiety, memory disorders, diabetes and malaria.^{1,2,3,4} Apart from these functions, they are also recognised for their fungicidal and antimicrobial properties.^{5,6} Furthermore, recent studies have shown that bis(*N,N'*-dialkylbiguanidato)-oxovanadium(IV) [Figure 4.1 (b)] complexes can be employed in the treatment of hypertension, obesity, hypercholesterolemia and hyperglyceridemia while ^{99m}Techneium complexes of biguanide show potential as renal imaging agents (Figure 4.1).^{7,8}

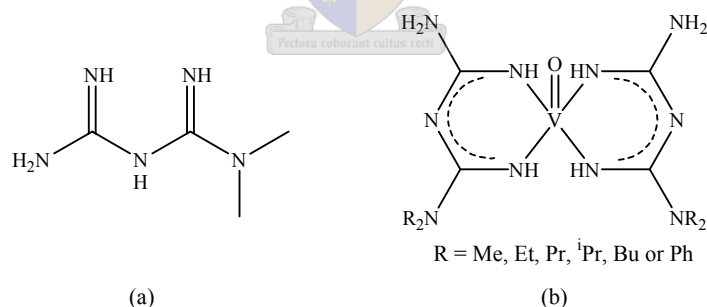


Figure 4.1 (a) 1,1-Dimethylbiguanide (metformin) and (b) bis(*N,N'*-dialkylbiguanidato)-oxovanadium(IV).

¹ P. Morain, C. Abrahams, B. Portevin, G. De Nanteuil, *Mol. Pharmacol.* **1994**, *46*, 732-742.

² C. R. Sirtori, C. Pasik, *Pharmacol. Res.* **1994**, *30*, 187.

³ A. J. J. Wood, C. J. Bailey, R. C. Turner, *New England J. Med.* **2003**, *334*, 574-228.

⁴ P. Pingnard, *Ann. Biol. Clin.* **1962**, *20*, 352.

⁵ M. Rosin, A. Welk, O. Bernhardt, M. Ruhnau, F. A. Pitten, T. Kramer, A. Kramer, *J. Clin. Periodontol.* **2001**, *28*, 1121-1126.

⁶ V. Badea, T. Negreanu-Pirjol, *Archives of the Medical Union* **2005**, *40*, 12-18.

⁷ Y. Le, L. Xu, *Faming Zhuanli Shenqing Gongkai Shuomingshu* **2003**, 10pp.

⁸ M. Neves, I. Dormehl, E. Kilian, W. Louw, K. Lalaoui, J. J. Perdroso de Lima, *Nucl. Med. Biol.* **2000**, *26*, 593-597.

Benzimidazol-2-ylamine and benzimidazol-2-ylideneamine derivatives are also of great biological relevance and have been utilised in the formulation of treatments for severe illnesses such as Parkinson's disease, multiple sclerosis, neurological disorders and strokes.^{9,10,11} These derivatives and all other ylideneamine type ligands contain an N–H functionality which play a fundamental role in biological activity by participating in the formation of hydrogen bonds to biomolecules. In addition, structure-function studies have shown this functionality to be essential for anti-cancer activity.¹² Although the biological activity of ylideneamine derivatives and certain metal complexes thereof has been studied extensively, literature provides very little information regarding their anti-tumour activity.

In contrast, gold(I) phosphine complexes are renowned for showing potential as anti-tumour agents.¹³ These include compounds such as $[\text{Au}(\text{Cl})(\text{PEt}_3)]$, $[\text{Au}(\text{dppe})_2]\text{Cl}$ [where dppe = 1,2-bis(diphenylphosphino)ethane] and Auranofin (Figure 4.2), the latter is, however, more valued for its role in the treatment of rheumatoid arthritis.¹⁴

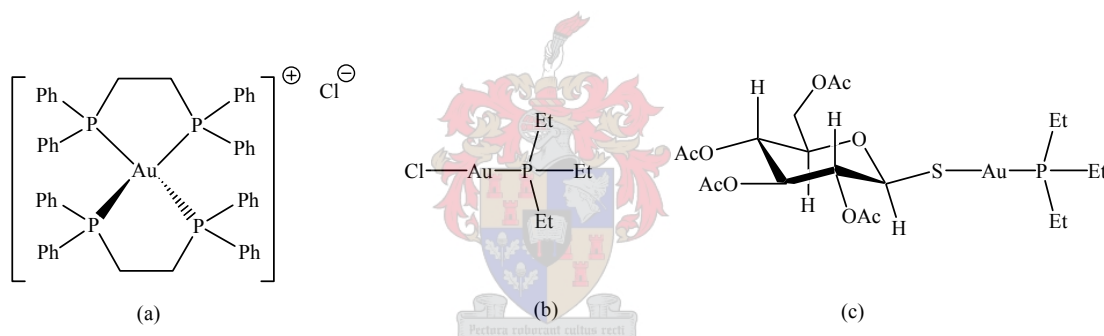


Figure 4.2 Gold(I) phosphine complexes with anti-tumour activity: (a) $[\text{Au}(\text{dppe})_2]\text{Cl}$ (b) $[\text{Au}(\text{Cl})(\text{PEt}_3)]$ (c) Auranofin.

In two coordinate linear gold(I) phosphine complexes, the anti-tumour activity and cytotoxicity are not only modulated by the phosphine substituents but also by the nature of the *trans* ligand. Complexes with good leaving groups as *trans* ligands display reduced anti-tumour activity. This arises from the reactivity of these compounds towards thiols. The -SH functional groups present in biomolecules can readily replace labile *trans* ligands

⁹ A. Boireau, M. C. Dubroecq, A. Imperato, P. Jimonet, S. Mignani, J. Randle, *PCT Int. Appl.* **1997**, 13pp.

¹⁰ J. Sterling, L. Hayardeny, E. Falb, Y. Herzig, D. Lerner, *U.S. Pat. Appl. Publ.* **2004**, 25pp.

¹¹ J. Ramnauth, N. Bhardwaj, R. Suman, S. Maddaford, *PCT Int. Appl.* **2004**, 74pp.

¹² D. Fan, C. T. Yang, J. D. Randford, J. J. Vittal, *Dalton Trans.* **2003**, 4749-4753.

¹³ E. R. T. Tiekink, *Gold Bull.* **2003**, *36*, 117-124.

¹⁴ M. V. Baker, P. J. Barnard, S. Berners-Price, S. K. Brayshaw, J. L. Hickey, B. W. Skelton, A. H. White, *J. Organomet. Chem.* **2005**, *690*, 5625-5635.

to form strong protein–Au(PR₃) bonds, and subsequently prevent gold(I) phosphines from reaching their intracellular targets.¹⁵

Important factors to take into consideration when evaluating metal complexes for potential medicinal use are their solubility and stability in biological media. In addition, an imperative characteristic that must be inherent to a potential anti-tumour agent is the ability to selectively target fast proliferating carcinoma cells over healthy cells. McKeage and co-workers¹⁶ have shown that the selectivity of complexes can be fine-tuned by adjusting the hydrophilic/hydrophobic balance of the coordinated ligands. This can be achieved through the introduction of appropriate functional groups. Furthermore, Baker *et al.*¹⁷ established that cationic compounds with intermediate lipophilicity display the greatest selectivity. Their superior selectivity arises from their ability to permeate the mitochondria of carcinoma cells. This is due to the fact that carcinoma cells exhibit elevated plasma and membrane potentials, with respect to normal cells. This negative membrane potential allows lipophilic cationic complexes to rapidly cross the membrane barrier and accumulate in the mitochondrial plasma. Since the mitochondria play a fundamental role in the regulation of programmed cell death (apoptosis), this holds the key to triggering selective cell death.¹⁷

In order to gain insight into the role of phosphine ligands in the mechanism of action, Baker and co-workers¹⁸ developed a series of dinuclear gold(I) complexes with bridging *N*-heterocyclic carbene (NHC) ligands (Figure 4.3). Their choice of surrogates for the replacement of the phosphine ligands was based on the electronic similarities between NHC and trialkylphosphine ligands together with their facile preparation. The study revealed that this class of compounds is remarkably stable. Furthermore, preliminary studies showed that several of these complexes induce membrane permeabilisation in rat liver mitochondria, indicating that NHC gold(I) complexes are promising alternatives to consider in the development of chemotherapeutic agents.

¹⁵ S. Berners-Price, P. J. Sadler in: *Bioinorganic Chemistry* (Eds. M. J. Clarke, J. B. Goodenough, J. A. Ibers, C. K. Jørgensen, D. M. P. Mingos, J. B. Neilands, G. A. Palmer, D. Reinen, P. J. Sadler, R. Weiss, R. J. P. Williams) Springer-Verlag, Germany, **1988**, p38-69.

¹⁶ M. J. McKeage, S. Berners-Price, P. Galettis, R. J. Bowen, W. Brouwer, L. Ding, L. Zhuang, B. C. Baguley, *Cancer Chemother. Pharmacol.* **2000**, *46*, 343-350.

¹⁷ M. V. Baker, P. J. Barnard, S. Berners-Price, S.K. Brayshaw, J. L. Hickey, B. W. Skelton, A. H. White, *Dalton Trans.* **2006**, 3708-3715.

¹⁸ P. J. Barnard, M. V. Baker, S. J. Berners-Price, B. W. Skelton, A. H. White, *Dalton Trans.* **2004**, 1038-1047.

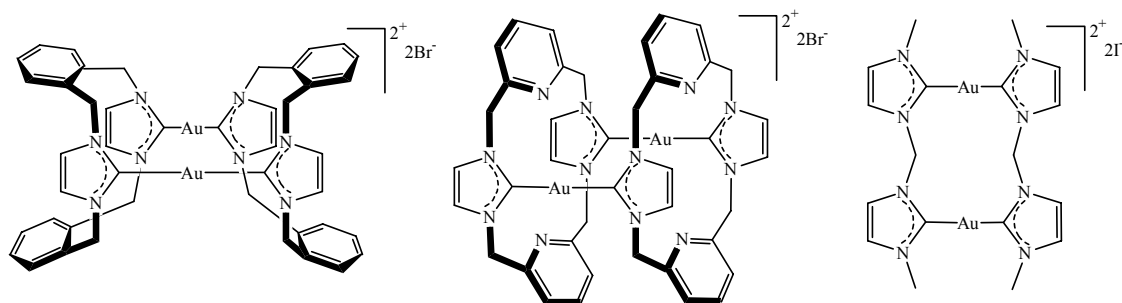
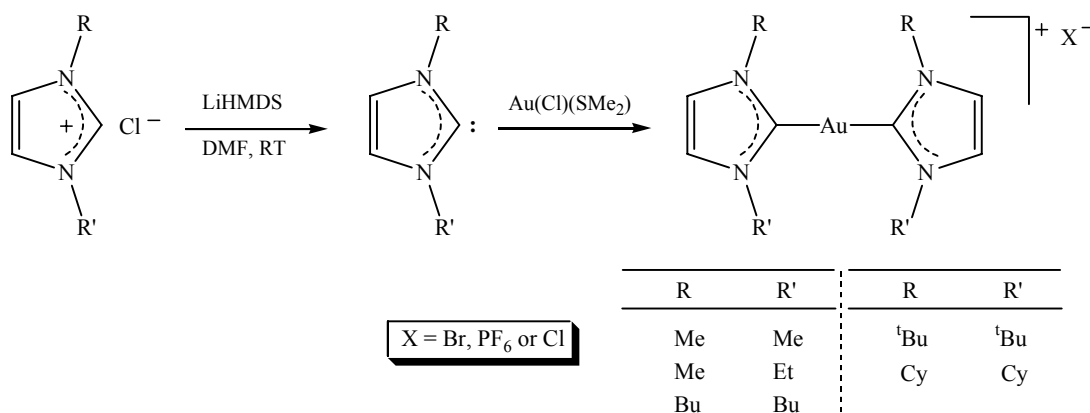


Figure 4.3 Selected examples of gold(I) complexes with bridging NHC ligands.

Another advantage in the use of NHC ligands as surrogates for phosphines is the ease with which the lipophilicity of such ligands can be adjusted. In a study to determine the ideal lipophilic/hydrophilic balance for NHC complexes of gold(I), Baker and co-workers¹⁷ prepared a series of cationic complexes of the general form $[\text{Au}(\text{ImR}_2)]^+$ (where Im = Imidazole, Scheme 4.1). In their study the lipophilicity of the complexes were adjusted by systematically varying the substituents on the imidazole rings. In addition, the effects of the different complexes on mitochondrial membrane permeabilization were assessed and correlated to their lipophilicity. In this series, a direct correlation exists between the time taken for complexes to induce mitochondrial swelling and the lipophilicity of the complexes. Complexes that contain methyl (Me) and ethyl (Et) substituents do not lead to significant mitochondrial swelling while swelling proceeds rapidly when mitochondria are exposed to complexes with bulky tertiary butyl (^tBu) and cyclohexyl (Cy) substituents.



Scheme 4.1 The synthetic route to $[\text{Au}(\text{ImR}_2)]\text{X}$ complexes with varied lipophilicity.

Although gold(I) NHC carbene complexes are well documented, such complexes with ylideneamine ancillary ligands have not been reported to date. Furthermore, reports of

phosphine gold(I) complexes with ylideneamine ancillary ligands are limited and all known compounds contain ketimine- or guanidine-type ligands.¹⁹

The work presented in this chapter was inspired by the biological activity displayed by ylideneamine metal complexes together with the known anti-cancer potential of (phosphine)gold(I) compounds. Further encouragement came from recent findings in our laboratory which showed that gold(I) phosphines with nitrogen coordinated purine ligands possess remarkable activity against HeLa cells (Human adenocarcinoma of the cervix) as well as significant tumour selectivity. The present study was aimed at the preparation and extensive characterisation of a series of lipophilic cationic gold(I) phosphine or NHC complexes which contained ylideneamine-functionalised heterocyclic ancillary ligands. The ultimate goal was to determine whether a possible synergism exists between these important functionalities by assessment of their potential as anti-cancer agents. In addition, we aimed at exploring whether deprotonation of these neutral ligands prior to or after coordination was feasible in order to generate their corresponding neutral gold(I) complexes.

4.2 Results and discussion

4.2.1 Cationic ylideneamine coordinated (triphenylphosphine)gold(I) complexes

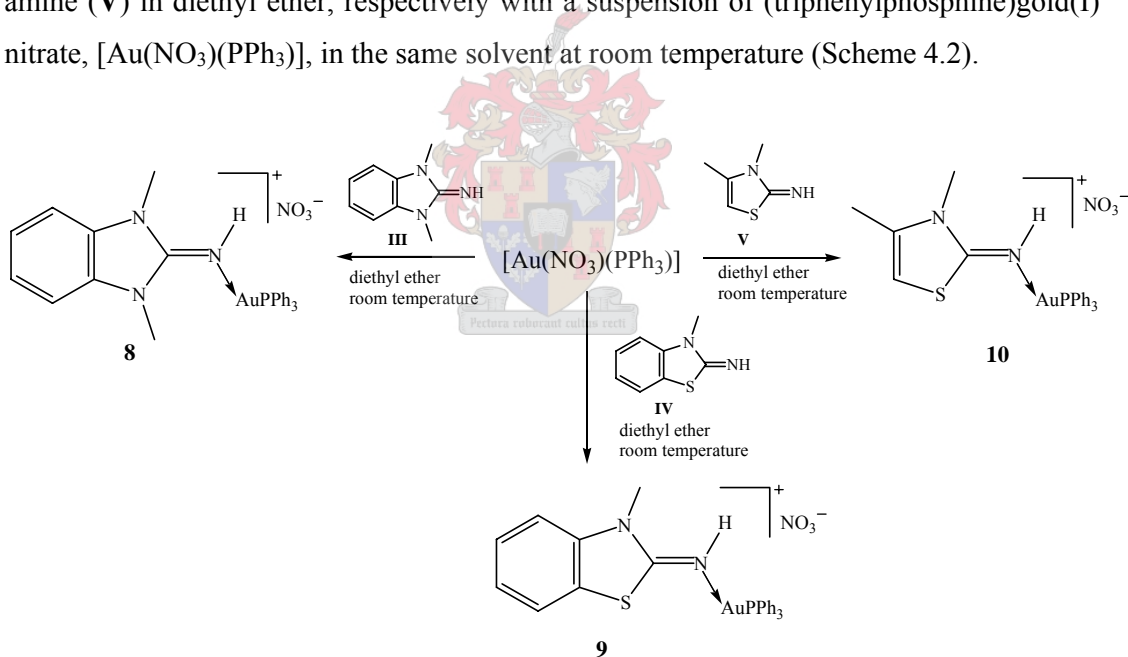
This chapter expands the series of novel gold(I) complexes with ylideneamine-functionalised heterocyclic ligands described in Chapter 3. The preparation of the cationic ylideneamine coordinated gold(I) phosphine or gold(I) NHC complexes is described in sections 4.2.1.1 and 4.2.1.2, while sections 4.2.2.1 – 4.2.2.3 are devoted to interesting phenomena unearthed by NMR, FT-IR and FAB-MS analysis of these compounds. Insight into their molecular and crystal structures could be gained from single crystal X-ray structure determinations and is discussed in section 4.2.2. In addition, the *in vitro* anti-tumour activities of selected compounds were assessed using HeLa cells as the target cell line as discussed in section 4.2.4. Furthermore, several attempts at the deprotonation of ligands before and after complexation were made during this study and a brief discussion on the results obtained from these attempts is included as section 4.2.5. NMR, FT-IR and FAB-MS data determined for compounds prepared during these attempts are discussed in

¹⁹ W. Schneider, A. Bauer, A. Schier, H. Schmidbaur, *Chem. Ber./Recueil* **1997**, *130*, 1417-1422.

section 4.2.6. Two crystal and molecular structures were determined as part of the deprotonation study and are described in section 4.2.7.

4.2.1.1 Preparation of 1,3-dimethyl-1,3-dihydro-benzimidazol-2-ylideneamine(triphenylphosphine)gold(I) nitrate, 8, 3-methyl-3H-benzothiazol-2-ylideneamine(triphenylphosphine)gold(I) nitrate, 9 and 3,4-dimethyl-3H-thiazol-2-ylideneamine(triphenylphosphine)gold(I) nitrate, 10

Schmidbaur and co-workers¹⁹ have established that one equivalent of (triphenylphosphine)gold(I) triflate, $[\text{Au}(\text{CF}_3\text{SO}_3)(\text{PPh}_3)]$, or (triphenylphosphine)gold(I) tetrafluoroborate, $[\text{Au}(\text{BF}_4)(\text{PPh}_3)]$, can quantitatively convert tetramethylguanidine or benzhydrylideneamine into the corresponding monoaurated ylideneamine complexes. The novel compounds **8** – **10** were now prepared, following a similar substitution approach, by treating solutions of 1,3-dimethyl-1,3-dihydro-benzimidazol-2-ylideneamine (**III**), 3-methyl-3H-benzothiazol-2-ylideneamine (**IV**) and 3,4-dimethyl-3H-thiazol-2-ylideneamine (**V**) in diethyl ether, respectively with a suspension of (triphenylphosphine)gold(I) nitrate, $[\text{Au}(\text{NO}_3)(\text{PPh}_3)]$, in the same solvent at room temperature (Scheme 4.2).

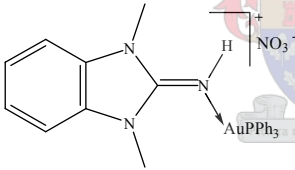
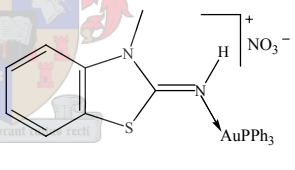
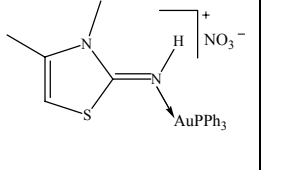


Scheme 4.2 Reaction scheme for the preparation of the cationic ylideneamine coordinated gold(I) complexes, **8** – **10**.

Given that the solubility of compounds **8** – **10** are comparable to that of $[\text{Au}(\text{NO}_3)(\text{PPh}_3)]$, the ylideneamine ligands were used in a small excess to ensure complete conversion of the $[\text{Au}(\text{NO}_3)(\text{PPh}_3)]$ to the ylideneamine coordinated gold(I) complexes. During the three day stirring period, formation of the ylideneamine coordination complexes was accompanied by the formation of new suspensions with notably different textures. After the three day

stirring period, the yellow solutions had turned colourless, marking the consumption of most of the free ligand, while the new products accumulated in the form of creamy precipitates on the walls of the reaction vessel. Since complexes **8** – **10** were insoluble in diethyl ether, the remaining free ligand could be removed by washing the crude product with this solvent. Subsequent drying of the remaining solid *in vacuo* afforded the pure products as colourless solids in high yields. Despite the fact that ‘hard’ to ‘borderline-hard’ nitrogen donor atoms are regarded to be incompatible with soft metal centres, compounds **8** – **10** are remarkably air and moisture stable. These cationic complexes are soluble in organic solvents such as short chain alcohols, acetone, dichloromethane, THF or DMSO. Their stability and good solubility makes them even more appealing candidates for biological screening, since the stability of the compounds in solution are a vital consideration for biological evaluation. All of the complexes are insoluble in water and alkanes such as hexane or pentane. Crystals suitable for X-ray crystal structure determinations were obtained by vapour diffusion of pentane into solutions of the compounds in acetone (**8**) or dichloromethane (**9**) under argon at -22 °C. The physical and analytical data of compounds **8** – **10** are summarised in Table 4.1.

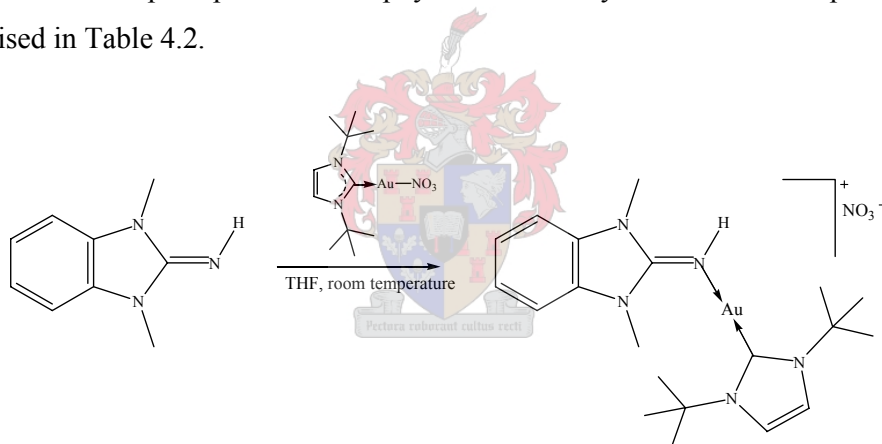
Table 4.1 Analytical data of complexes **8**, **9** and **10**.

Complex			
	8	9	10
m.p. (°C)	126 - 128 (decomp.)	130-135	95–100
Colour	colourless	colourless	colourless
Yield (%)	88	89	84
M_r	682.46	685.49	649.45
Analysis (%)*	$C_{27}H_{26}AuN_4O_3P$	$C_{26}H_{23}AuN_3O_3PS$	$C_{23}H_{23}AuN_3O_3PS$
C	47.33 (47.52)	45.88 (45.56)	42.37 (42.54)
H	3.91 (3.84)	3.45 (3.38)	3.45 (3.57)
N	8.42 (8.21)	6.22 (6.13)	6.58 (6.47)

* Required calculated values given in parenthesis. Products were powdered and evacuated for 10h prior to elemental analysis

4.2.1.2 Preparation of 1,3-dimethyl-1,3-dihydro-benzimidazol-2-ylideneamine(1,3-di-*tert*-butylimidazol-2-ylidene)gold(I) nitrate, **11**

Baker and co-workers²⁰ have reported an elegant route towards the preparation of (1,3-di-*tert*-butylimidazol-2-ylidene)gold(I) nitrate, [Au(NO₃)(1,3-^tBuIm-2-ylidene)]. In the present study, this compound was utilised to prepare the unprecedented complex **11**, which represents the first example of an ylideneamine gold(I) complex that contains an NHC ancillary ligand. By treating a solution of ligand **III** in THF, with an equimolar amount of [Au(NO₃)(1,3-^tBuIm-2-ylidene)] at ambient temperature, the cationic complex **11** could be obtained in a 96% yield (Scheme 4.3). Complex **11** had limited solubility in THF and upon formation precipitated partially from solution. The solvent was, therefore, after an overnight reaction period, removed *in vacuo* and the crude product extracted with dichloromethane to affect a brownish solution. Solid contaminants were removed by filtration through anhydrous MgSO₄ and the resulting solution was stripped of solvent *in vacuo* to affect the pure product. The physical and analytical data of compound **11** are summarised in Table 4.2.

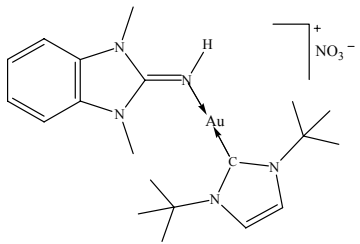


Scheme 4.3 Reaction scheme for the preparation of the cationic ylideneamine coordinated gold(I) complex, **11**, that contains an NHC ancillary ligand.

Compound **11** is a fairly air and moisture stable, off-white solid, soluble in organic solvents such as short chain alcohols, dichloromethane or DMSO but insoluble in water, hexane or pentane. Crystals suitable for X-ray structure determination were obtained by vapour diffusion of pentane into a solution of the compound in dichloromethane under argon at -22 °C.

²⁰ M. V. Baker, P. J. Barnard, S.K. Brayshaw, J. L. Hickey, B. W. Skelton, *Dalton. Trans.* **2005**, 37-43.

Table 4.2 Physical and analytical data of complex **11**.

Complex	 <p style="text-align: center;">11</p>
m.p. (°C)	127-132 (decomp.)
Colour	off-white
Yield (%)	96
M_r	600.47
Analysis (%)*	C ₂₀ H ₃₁ AuN ₆ O ₃
C	40.22 (40.00)
H	5.36 (5.20)
N	13.87 (14.00)

* Required calculated values given in parenthesis. The product was powdered and evacuated for 10h prior to elemental analysis.

4.2.2 Spectroscopic characterisation of compounds **8** – **11**

4.2.2.1 Nuclear magnetic resonance spectroscopy

The ¹H, ¹³C, ³¹P and ¹⁵N NMR spectroscopic data obtained for dichloromethane-d₂ solutions of complexes **8** – **10** are summarised in Table 4.3. In the ¹H NMR spectra of the cationic ylideneamine coordinated gold(I) compounds **8** – **10**, characteristic NMe resonances are observed at δ 3.85 (**8**), δ 3.85 (**9**) and δ 3.85 (**10**). These resonances are all shifted slightly downfield with respect to the NMe resonances of the free ligands **III** – **V** (Δδ 0.3-0.4). In all spectra, the presence of the cationic Au(PPh₃)⁺ moiety is confirmed by the detection of additional resonances in the form of an unresolved multiplet in the region δ 7.47-7.61. Although the aromatic proton resonances of complexes **8** and **9** all appear at chemical shifts significantly downfield from those of the free ligands **III** and **IV**, no noteworthy changes in the coupling constants are observed. For compound **8**, as was observed for **III**, the protons H⁵ and H^{5'} as well as H⁶ and H^{6'} are rendered equivalent by their chemical environment and give rise to two doublets of doublets at δ 7.12 (³J = 5.8 Hz, ⁴J = 3.1 Hz) and 7.20 (³J = 5.8 Hz, ⁴J = 3.1 Hz) respectively. Unlike compound **8**, all aromatic protons in compound **9** are inequivalent resulting in four sets of resonances in the

aromatic region of the ^1H NMR spectrum. H^5 and $\text{H}^{5'}$ give rise to a triplet at δ 7.47 ($^3J = 7.78$ Hz) and a doublet at δ 7.14 ($^3J = 8.0$ Hz) respectively. It is noteworthy that long range coupling of the aromatic protons is less pronounced in the coordinated compound than in the free ligand. Furthermore, a triplet observed at δ 7.23 ($^3J = 7.8$ Hz) and a triplet of doublets observed at δ 7.42 ($^3J = 8.5$ Hz; $^4J = 1.1$ Hz), can be assigned to H^6 and $\text{H}^{6'}$, respectively. In the ^1H NMR spectrum of compound **10**, the resonances detected for H^5 (δ 5.84) and the Me group in the 4 position of the thiazole ring (δ 2.14), display reduced mutual allylic coupling with respect to coupling observed in the free ligand. The same observation was made for compound **7**, and was ascribed to a reduction in electron density of the pseudo-aromatic ring system upon coordination to the gold(I) centre. This reduction in electron density affects decreased electron delocalisation and suppressed long range coupling.

Additional insight, concerning the degree of charge stabilisation within the different ring systems after coordination, could be gained by comparing the imine proton chemical shifts in the ^1H NMR spectra of the metal coordinated complexes to the NH shifts observed for the free ligands. Although difference in concentration are known to have an influence on the NH chemical shifts, it is noted that coordination to a gold(I) centre has a more pronounced effect on the NH chemical shifts of the 2-imino-thiazoline derivatives than on their 2-imino-imidazoline counterparts. NH resonances of complexes **9** (δ 9.15) and **10** (δ 8.34) are detected at chemical shifts considerably downfield to those of the free ligands **IV** (δ 4.95) and **V** (δ 5.47) (Chapter 3, section 3.2.2.1), marking the deshielding effect of electron density discharge towards the metal centre. However, in contrast to this observation, the NH resonance (δ 1.82) in the spectrum of **8** emerges at a chemical shift significantly upfield from the corresponding signal in free ligand spectrum (δ 4.16). This dissimilar behaviour is brought about by two contributing factors. The first factor involves the phenomenon of magnetic anisotropy. Functional groups that possess π -electrons are known to generate secondary anisotropic fields when placed in a magnetic field.²¹ In the free ligand **III**, the C=N group generates such a field resulting in shielding and deshielding regions. Figure 4.4 depicts these regions with shielding areas indicated by a + sign and deshielding areas by a – sign. Protons falling within the conical area are shielded while protons outside this region are deshielded.

²¹ D. L. Pavia, G. M. Lampman, G. S. Krutz, *Introduction to Spectroscopy*, 3rd Edition, Brooks/Cole, Washington, **2001**, p124-127.

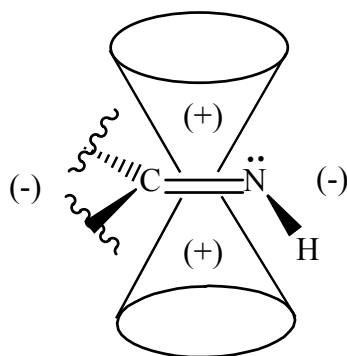


Figure 4.4 The anisotropic effect of the π -electrons in the double bond of the ylidenamine functional group. Atoms falling within the conical areas are shielded (indicated with +) whilst atoms outside these areas are deshielded (indicated with -).

The imine proton falls outside the conical areas and is therefore deshielded. However, after coordination to the gold(I) centre the extent of delocalisation over the nitrogen-carbon bonds increases in order to stabilise the positive charge on the complex. This enhanced delocalisation causes the exocyclic C=N bond to obtain more single-bond character reducing the anisotropic effect of the π -electrons. Furthermore, the change in bond character also affects the hybridisation resulting in a nitrogen atom with more sp^3 character. The reduced s-character renders the atom less electronegative and consequently less deshielding. The combination of these two factors causes the imine proton resonance in **8** to undergo a significant upfield shift. Since the nature of the thiazoline rings does not allow such effective delocalisation, these factors are overruled by the deshielding effect of the metal centre.

From the ^{13}C NMR spectra of compounds **8** – **10**, it is evident that coordination to gold(I) does not alter the chemical shifts of the NMe carbons significantly. All ligand ring carbon atom signals are however shifted to values slightly more downfield from those observed for the free ligand. In the ^{13}C spectrum of compound **8** the resonance of the highly deshielded C^2 atom remains unchanged, and is observed as a singlet of low intensity at δ 156.3. On the other hand, the corresponding resonances in the spectra of **9** and **10** did experience significant downfield shifts and are detected at δ 172.4 ($\Delta\delta$ 9.7) and δ 174.5 ($\Delta\delta$ 7.9) respectively. Four additional sets of doublets are detected in the region δ 128-135 of each spectrum and correspond to the characteristic C–P coupling of the phenyl ring carbons of the $\text{Au}(\text{PPh}_3)^+$ moiety. The doublet at δ 128.3-128.7 can be assigned to the C–P coupled *ipso*-carbon atom, whilst the doublet at δ 129.7 is attributable to the C–P coupled

meta-carbon atom. Resonances of the *ortho*- and *para*-carbon atoms are observed as doublets in the regions δ 134.4-134.5 and δ 132.4-132.6, respectively.

In the ^{31}P NMR spectra of compounds **8** – **10**, only one intense singlet at δ 32.0 for **8**, δ 27.7 for **9** and δ 31.0 for **10** is observed. These resonances display an insignificant downfield shift of $\Delta\delta \pm 3.0$, relative to the precursor compound, $[\text{Au}(\text{NO}_3)(\text{PPh}_3)]$.

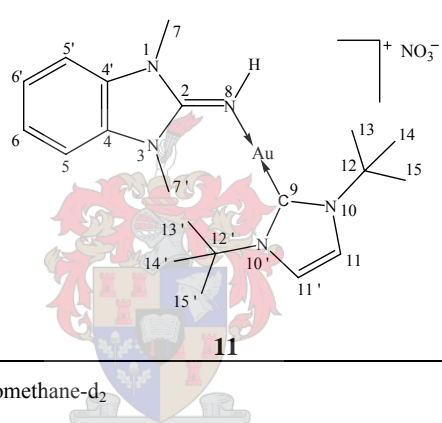
Table 4.3 ^1H , ^{13}C , ^{15}N and ^{31}P NMR spectroscopic data of complexes **8**, **9** and **10**.

Complex				
Solvent	Dichloromethane-d ₂	Dichloromethane-d ₂	Dichloromethane-d ₂	
Temperature (°C)	25	25	25	
Assignment	Chemical shift (ppm)			
^1H NMR (300/400 MHz)	H ⁵ , H ^{5'}	7.12 (dd, 2H, $^3J = 5.7$ Hz, $^4J = 3.1$ Hz)	7.47 (d, 1H, $^3J = 7.8$ Hz) / 7.14 (d, 1H, $^3J = 8.0$ Hz)	5.84 (bs, 1H)
	H ⁶ , H ^{6'}	7.20 (dd, 2H, $^3J = 5.8$ Hz, $^4J = 3.1$ Hz)	7.23 (t, 1H, $^3J = 7.8$ Hz) / 7.42 (td, 1H, $^3J = 8.5$ Hz, $^4J = 1.1$ Hz)	2.14 (d, 3H, $^4J = 1.0$ Hz)
	H ⁷ , H ^{7'}	3.76 (s, 6H)	3.69 (s, 3H)	3.48 (s, 3H)
	H ⁸	1.82 (bs, 1H)	9.15 (bs, 1H)	8.34 (bs, 1H)
	PPh	7.52-7.61 (m, 15H)	7.52-7.60 (m, 15H)	7.47-7.59 (m, 15H)
^{13}C NMR (75/100 MHz)	C ²	156.3 (s)	172.4 (s)	174.5 (s)
	C ⁴ , C ^{4'}	131.2 (s)	122.4(s) , 141.1 (s)	137.6 (s)
	C ⁵ , C ^{5'}	108.7 (s)	127.7 (s) , 111.8 (s)	96.3 (s)
	C ⁶ , C ^{6'}	122.9 (s)	122.4 (s) , 124.6 (s)	14.9 (s)
	C ⁷ , C ^{7'}	30.0 (s)	31.2 (s)	31.8 (s)
	PPh-C ^{ipso}	128.7 (d, $^1J = 63.1$ Hz)	128.3 (d, $^1J = 63.6$ Hz)	128.3 (d, $^1J = 64.0$ Hz)
	PPh-C ^{ortho}	134.4 (d, $^2J = 13.7$ Hz)	134.5 (d, $^2J = 13.3$ Hz)	134.4 (d, $^2J = 13.7$ Hz)
	PPh-C ^{meta}	129.7 (d, $^3J = 12.0$ Hz)	129.7 (d, $^3J = 12.0$ Hz)	129.7 (d, $^3J = 12.0$ Hz)
PPh-C ^{para}	132.4 (d, $^4J = 2.6$ Hz)	132.6 (d, $^4J = 2.6$ Hz)	132.5 (d, $^4J = 2.6$ Hz)	
^{31}P NMR (121/161MHz)	P	32.0 (s)	27.7 (s)	31.0 (s)
^{15}N NMR (61 MHz)	N ¹ , N ³	-270.7		
	N ⁸	not observed		

A slight downfield shift ($\Delta\delta$ 8.7) is observed for the resonance of the equivalent N¹ and N³ in the ¹⁵N NMR spectrum of **8** compared to that of **III**. All attempts to detect the N⁸ resonance for complex **8** failed. These attempts included a two dimensional ¹H, ¹⁵N gHMQC (gradient heteronuclear multiple quantum coherence) experiment.

Table 4.4 summarises the ¹H and ¹³C NMR spectroscopic data obtained for a dichloromethane-d₂ solution of complex **11**. The chemical shifts of all ylideneamine ligand resonances in the ¹H as well as ¹³C NMR spectra are in close agreement with those observed for compound **8**, marking the striking electronic similarities between the triphenylphosphine and NHC ligands.

Table 4.4 ¹H and ¹³C NMR spectroscopic data of complex **11**.

Complex		
Solvent	Dichloromethane-d ₂	
Temperature (°C)	25	
Assignment	Chemical shift (ppm)	
¹ H NMR (400 MHz)	H ⁵ , H ^{5'}	7.11 (dd, 2H, ³ J = 5.9 Hz, ⁴ J = 3.2 Hz)
	H ⁶ , H ^{6'}	7.20 (dd, 2H, ³ J = 5.8 Hz, ⁴ J = 3.2 Hz)
	H ⁷ , H ^{7'}	3.79 (s, 6H)
	H ⁸	2.18 (bs, 1H)
	H ¹¹ , H ^{11'}	7.21 (s, 2H)
H ¹³ , H ^{13'} , H ¹⁴ , H ^{14'} , H ¹⁵ , H ^{15'}	1.89 (s, 18H)	
¹³ C NMR (100 MHz)	C ²	156.2 (s)
	C ⁴ , C ^{4'}	131.3 (s)
	C ⁵ , C ^{5'}	108.5 (s)
	C ⁶ , C ^{6'}	122.8 (s)
	C ⁷ , C ^{7'}	29.7 (s)
	C ⁹	165.6 (s)
	C ¹¹ , C ^{11'}	117.4 (s)
	C ¹² , C ^{12'}	59.3 (s)
C ¹³ , C ^{13'} , C ¹⁴ , C ^{14'} , C ¹⁵ , C ^{15'}	31.9 (s)	

In the ^1H NMR spectrum of **11**, the NH resonance follows the same trend observed for complex **8**, with the signal emerging significantly upfield (δ 2.18) from the corresponding signal in free ligand spectrum (δ 4.16). All other ligand resonances, however, experience a downfield shift following coordination verifying that coordination had indeed taken place. Further evidence is present in the form of two additional resonances observed at δ 7.21 and δ 1.81, indicating the presence of the NHC ligand. The intense signal at δ 1.81 is attributable to the methyl groups of the ^tBu unit, which are rendered equivalent by free rotation about the C–N bond, while the signal at δ 7.21 corresponds to the ring protons H^{11} and $\text{H}^{11'}$.

In the ^{13}C NMR spectrum of compound **11**, the chemical shifts of resonances corresponding to the ring carbon atoms of the ylideneamine ligand are comparable to those observed in the ^{13}C spectrum of compound **8**. A significant downfield shift of $\Delta\delta$ 10, is observed for the resonance of the characteristic carbene carbon atom (δ 165.6), compared to that of the precursor compound, (1,3-di-*tert*-butylimidazol-2-ylidene)gold(I) nitrate (δ 155.6). The quaternary carbon atoms of the ^tBu groups give rise to a signal at δ 59.3, while the methyl groups of the ^tBu units resonate as an intense singlet at δ 31.9. Furthermore, the resonance detected at δ 117.4 is attributable to the equivalent C^{11} and $\text{C}^{11'}$ carbons and appears unaffected by substitution of the nitrate anion with the ylideneamine ligand.

4.2.2.2 Mass spectrometry

Table 4.5 summarises the FAB-MS spectrometric data obtained of compounds **8** – **10**. In the FAB-MS spectra of complexes **8** – **10**, peaks that correspond to the cation of the molecules are observed at m/z 620, m/z 623 and m/z 587, respectively. In all spectra peaks attributable to the $\text{Au}(\text{PPh}_3)^+$ unit (m/z 459) and the characteristic homoleptic rearrangement product, $[\text{Au}(\text{PPh}_3)_2]^+$, are observed (m/z 720). Other diagnostic signals in the spectrum of compound **8** include signals that correspond to the cations of the molecules after the elimination of a Me group (m/z 606), a phenyl group (m/z 543) and an $\text{Au}(\text{PPh}_3)^+$ moiety (m/z 162). In the spectrum of **9** the only other meaningful peak is observed at m/z 164 and corresponds to the loss of an $\text{Au}(\text{PPh}_3)^+$ moiety. No other characteristic fragmentation peaks, apart from those already mentioned, were detected in the spectrum of **10**.

Table 4.5 Mass spectrometric data of complexes **8**, **9** and **10**.

Fragment	<i>m/z</i> (I in %)		
	8	9	10
{[M]-NO ₃ } ⁺	620 (87)	623 (100)	587 (71)
{[M]-NO ₃ -CH ₃ } ⁺	606 (5)	—	—
{[M]-NO ₃ -Ph} ⁺	543 (4)	—	—
{[M]-NO ₃ -Au(PPh ₃)} ⁺	162 (95)	164 (34)	—
{Au(PPh ₃)} ⁺	459 (25)	459 (6)	459 (82)
{Au(PPh ₃) ₂ } ⁺	720 (12)	720 (9)	720 (18)

The FAB-MS spectrometric data of compound **11** is listed in Table 4.6. The spectrum reveals a peak at *m/z* 538 corresponding to the cation of the molecule, which fragments with the loss of a Me group to deliver a signal at *m/z* 524. In addition to these fragmentation patterns, a biscarbene rearrangement complex, [Au(C₁₁H₂₀N₂)₂]⁺, is observable as a peak at *m/z* 557.

Table 4.6 Mass spectrometric data of complex **11**.

Fragment	<i>m/z</i> (I in %)
	11
{[M]-NO ₃ } ⁺	538 (22)
{[M]-NO ₃ -CH ₃ } ⁺	524 (5)
{Au(^t Bu ₂ Im) ₂ } ⁺	557 (69)
{[Au(^t Bu ₂ Im) ₂]- ^t Bu} ⁺	377 (15)

4.2.2.3 Infrared spectroscopy

Table 4.7 summarises the solid state ATR FT-IR spectroscopic data obtained for compounds **8** – **11**. The FT-IR spectrum of complex **8** exhibits a very weak broad absorption band at 3249 cm⁻¹ and a strong band at 1605 cm⁻¹ attributable to the stretching vibrations of the N–H and C=N groups respectively. The N–H vibration is shifted to a slightly higher wavenumber with respect to the corresponding band observed in the spectra of the free ligand **III** (3235 cm⁻¹). Other diagnostic bands in the spectrum of **8** are observed in the region 1496-1435 cm⁻¹ and at 743 cm⁻¹, attributable to the stretching and out of plane (oop) bending vibrations of the aromatic C=C bonds respectively.

In the FT-IR spectrum of **9**, absorption bands, characteristic of the N–H, sp² C–H and C=N moieties, are prominent but of lower intensity than those of the free ligand **III**. They

occur at 3165 cm^{-1} , 3059 cm^{-1} and in the region 1598-1577 cm^{-1} . Similar bands at 3186 cm^{-1} and in the region 1478-1434 cm^{-1} are also observed in the spectrum of **10** and can be assigned to the N–H and C=N stretching vibrations. Additional indicative bands in the spectra of **9** are those of the aromatic $\nu(\text{C–H})$ and $\nu(\text{C=C})$ which are observed at 3059 cm^{-1} and in the region 1477-1434 cm^{-1} . No aromatic $\nu(\text{C–H})$ absorption band is observed in the spectrum of **10**, $\nu(\text{C=C})$ bands are however present in the same region as was observed for compound **9**.

The FT-IR spectrum of compound **11** also shows bands associated with the N–H and C=N stretching vibrations at 3193 cm^{-1} and 1628 cm^{-1} . These bands occur at lower frequencies than those of the free ligand **III**. Other diagnostic absorption bands include those attributable to the stretching sp^2 C–H and C=C vibrations, observed at 2966 cm^{-1} and 1499 cm^{-1} respectively and the out of plane sp^2 C=C bending vibrations observed at 733 cm^{-1} .

Table 4.7 Infrared spectroscopic data of ligands **8**, **9**, **10** and **11**.

Functional group	Wavenumber (cm^{-1})			
	8	9	10	11
$\nu(\text{N–H})$	3249 (w)	3165 (w)	3186 (w)	3193 (w)
$\text{sp}^2 \nu(\text{C–H})$	3048 (w)	3059 (w)	n.o.	2966 (m)
$\nu(\text{C=N})$	1605 (st)	1598-1577 (st)	1545 (st)	1628 (st)
$\text{sp}^2 \nu(\text{C=C})$	1496-1435 (m)	1477-1434 (m)	1478-1434 (m)	1499 (m)
$\text{sp}^2 \delta_{\text{oop}}^{\text{b}}(\text{C=C})$	743 (m)	746 (m)	750 (m)	733 (m)

It is noteworthy that the N–H absorption bands of complexes **9**, **10** and **11** are detected at lower wavenumbers than in the free ligands **III** (3235 cm^{-1}), **IV** (3243 cm^{-1}), and **V** (3239 cm^{-1}), suggesting electron delocalisation over the carbon-nitrogen bonds to be more pronounced in the coordinated ligands. The reduced electron density on the exocyclic nitrogen atom, as a consequence of coordination to the gold(I) centre, may also contribute to the lowering of vibrational frequencies. Furthermore, an interesting observation was made when the FT-IR spectra of compounds **5** – **7** were compared to those of compounds **8** – **11**. From this comparison it was evident that coordination of ligands **III** – **V** to a neutral $\text{Au}(\text{C}_6\text{F}_5)$ moiety, has a more pronounced effect on the N–H and C=N stretching vibrations [$\nu(\text{N–H})$ 3375-3399 cm^{-1} and $\nu(\text{C=N})$ 1624-1554 cm^{-1}] than coordination to a positively charged $\text{Au}(\text{PPh}_3)^+$ or $\text{Au}(\text{NHC})^+$ entity. This phenomenon is the result of positive charge stabilisation through electron delocalisation over the nitrogen-carbon

bonds in compounds **8** – **11**. The more significant delocalisation reduces the double-bond character and hence the bond strength of the C=N unit which, owing to a lowering in the force constant of the bond, leads to lower energy absorption.

4.2.3 Structure determinations of compounds **8a** – **11**

The crystal and molecular structures of the novel compounds **8a**, **9** and **11** were determined by single crystal X-ray diffraction, expanding the series of novel gold(I) complexes containing 2-ylideneamine-functionalised heterocyclic ligands reported in Chapter 3. Note that structure **8a** represents one of two structures obtained for compound **8**. Structure **8b** will be discussed in section 4.2.7. Furthermore, these structures represent the first examples of (triphenylphosphine)gold(I) complexes containing 2-ylideneamine-functionalised heterocycles as ancillary ligands.

4.2.3.1 *Crystal and molecular structure of compound 8a*

The benzimidazol-2-ylideneamine coordinated (triphenylphosphine)gold(I) compound **8a** crystallises together with two solvent molecules from an acetone solution as colourless cubes in the triclinic space group $P\bar{1}$ with $Z = 2$ molecules in the unit cell. Figure 4.5 depicts the molecular structure of **8a**, showing the numbering scheme, and selected bond lengths and angles are listed in Table 4.8. The molecular structure consists of a neutral ylideneamine ligand coordinated to a $\text{Au}(\text{PPh}_3)^+$ unit, affording a charged complex neutralised by a nitrate counterion hydrogen bonded to the imine proton. The geometry about the gold centre approaches linearity with an observed N–Au–P angle of $176.9(3)^\circ$. In addition, the plane of the benzimidazole entity is slightly tilted with respect to the plane formed by the imine hydrogen, gold and phosphorus atoms (torsion angle of 13.8°). The Au–N bond length of $2.03(1) \text{ \AA}$ is within the range of Au–N separations observed for compound **5** and the literature examples, tetramethylguanidine(triphenylphosphine)gold(I) triflate and benzophenoneimine(triphenylphosphine)gold(I) tetrafluoroborate [$2.044(9) \text{ \AA}$ and $2.036(7) \text{ \AA}$, respectively].¹⁹ These literature examples represent the only other known crystal structures of gold(I) complexes that contain a $\text{Au}(\text{PPh}_3)^+$ unit coordinated to an exocyclic =NH functional group. All bond lengths and angles in the coordinated ligand remain virtually unchanged compared to those of the free ligand. Although a comparison of the solid state FT-IR spectroscopic data of compounds **5** and **8** suggest that coordination of ligand **III** to a $\text{Au}(\text{C}_6\text{F}_5)$ unit has a more pronounced effect on the

stretching vibrations of the C=N moiety than coordination to a $\text{Au}(\text{PPh}_3)^+$ entity, no appreciable difference between the C=N bond lengths in complexes **5** and **8** is observed. The C=N distance of 1.30(2) Å also does not differ substantially from that of the mentioned literature examples [1.27(1) Å and 1.30(1) Å] or free ligand **III** [1.295(3) Å]. Furthermore, the C–N bond lengths [1.38(1) Å and 1.35(1) Å] remain unaltered by metal coordination and fall within the range of standard bond lengths observed for single $\text{C}(\text{sp}^2)\text{--N}(\text{sp}^2)$ bonds indicating that, in contrast to NMR observations in solution, no appreciable delocalisation occurs in the solid state. Substitution of the weakly coordinated nitrate ligand in $[\text{Au}(\text{NO}_3)(\text{PPh}_3)]^{22}$ with ligand **III** results in a significant elongation of the Au–P bond length (from 2.208(3) Å to 2.226(3) Å), implying a labilising *trans* influence by the ylideneamine ligand. The Au–P distance is in good agreement with those of the mentioned literature examples [2.229(2) Å and 2.234(2) Å].¹⁹

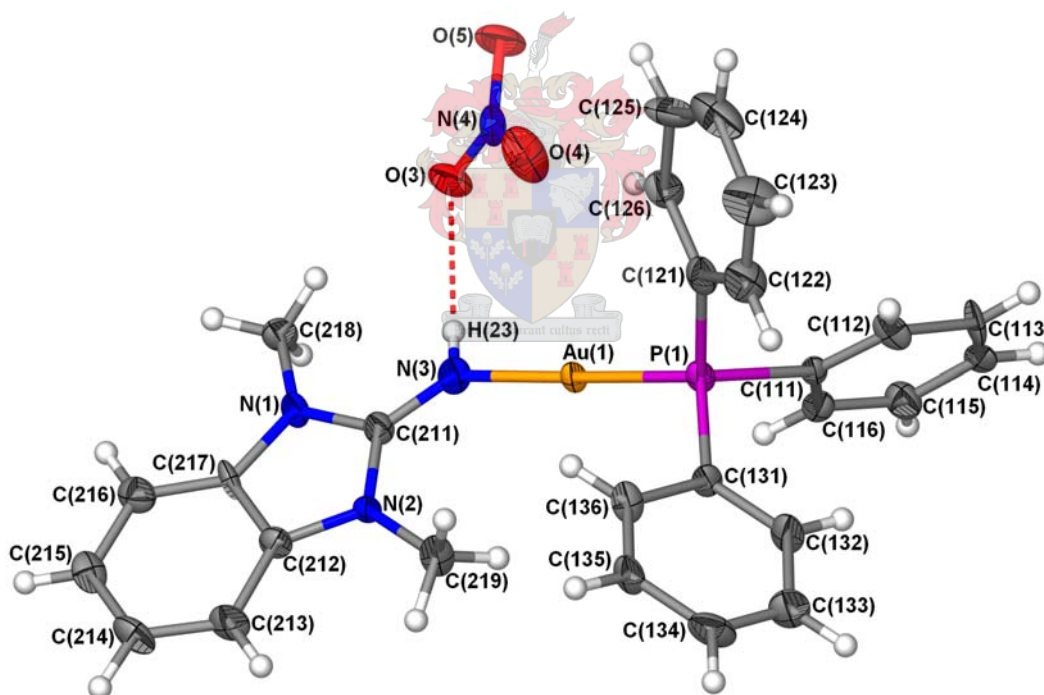


Figure 4.5 Molecular structure of **8a** showing the numbering scheme. Thermal ellipsoids are set at 50% probability and solvent molecules are omitted for clarity.

²² J. C. Wang, M. N. I. Khan, J. P. Fackler Jr., *Acta Crystallogr. Sect. C* **1989**, 45, 1008-1010.

An advantage for the formation of close gold-gold contacts in the crystal lattice is the absence of sterically bulky substituents on the phosphine ligand as well as the ancillary ligand.²³ Therefore, due to the bulky nature of the phenyl rings together with the presence of the nitrate anions and included acetone molecules, none of the complexes **8** – **10** display aurophilic interactions in their solid state packing. Figure 4.6 depicts the molecular packing of compound **8**, with like ligands aligned along the a-axis. Apart from the hydrogen bonding between the imine hydrogen atoms and the oxygen atoms of the nitrate counterions ($\text{N-H} \cdots \text{O}$, 2.25 Å), weak π -stacking of neighbouring benzimidazole rings (centroid to centroid distance, 2.16 Å) are the only other feature worth mentioning. The smallest gold-gold separations observed in the crystal lattice are 7.114 Å and do not qualify as aurophilic interactions.

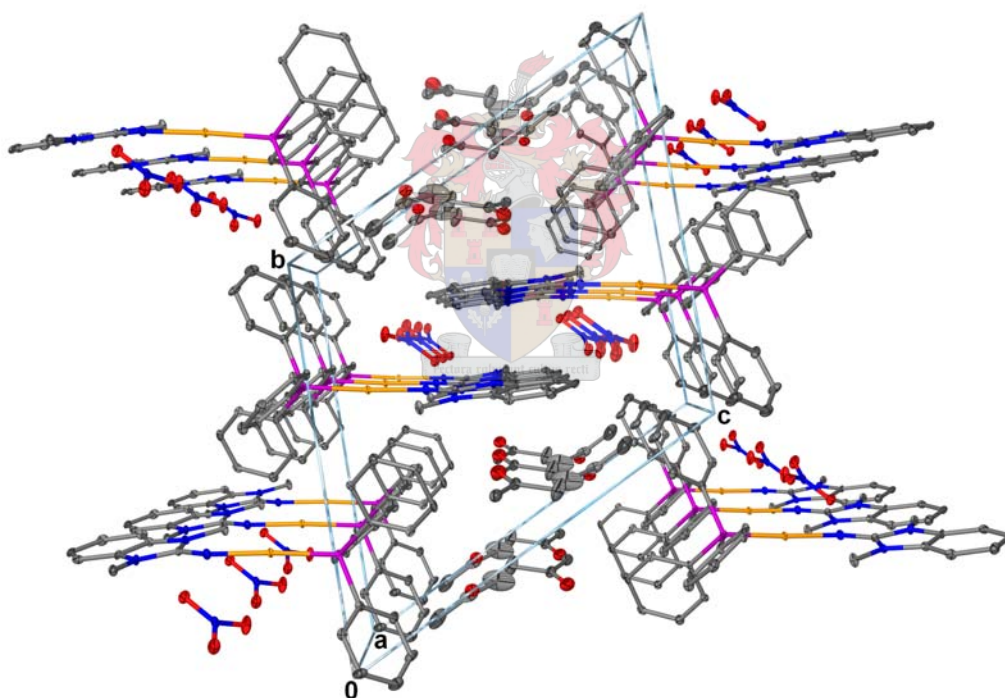


Figure 4.6 Perspective drawing of the molecular packing of **8a** viewed along the a-axis; thermal ellipsoids are set at 20% probability for clarity.

²³ M. C. Gimeno, A. Laguna in: *Comprehensive Coordination Chemistry II, Vol 6* (Eds. J. A. McCleverty, T. J. Meyer), Elsevier Pergamon, Oxford **2004**, p1043.

Table 4.8 Selected bond lengths (Å) and angles (°) of **8** with estimated standard deviations in parenthesis.

<i>Bond lengths (Å)</i>			
Au(1)–P(1)	2.23(3)	N(1)–C(218)	1.44(1)
Au(1)–N(3)	2.03(1)	N(2)–C(219)	1.46(1)
N(1)–C(211)	1.38(1)	C(212)–C(217)	1.39(2)
N(2)–C(211)	1.35(1)	P(1)–C(111)	1.84(1)
N(3)–C(211)	1.30(2)	P(1)–C(121)	1.81(1)
N(1)–C(217)	1.40(1)	P(1)–C(131)	1.81(1)
N(2)–C(212)	1.39 (1)		
<i>Bond angles (°)</i>			
N(3)–Au(1)–P(1)	176.9(3)	N(1)–C(217)–C(212)	106.6(9)
C(211)–N(3)–Au(1)	131.3(8)	N(2)–C(212)–C(217)	107.2(9)
N(1)–C(211)–N(2)	107(1)	C(111)–P(1)–Au(1)	115.1(4)
N(1)–C(211)–N(3)	126(1)	C(121)–P(1)–Au(1)	112.5(4)
N(2)–C(211)–N(3)	127(1)	C(131)–P(1)–Au(1)	112.7(4)
C(211)–N(1)–C(217)	109.1(9)	C(111)–P(1)–C(121)	104.7(5)
C(211)–N(2)–C(212)	109.8(9)	C(111)–P(1)–C(131)	105.9(5)
C(211)–N(1)–C(218)	125(1)	C(121)–P(1)–C(131)	105.2(6)
C(211)–N(2)–C(219)	127(1)		

4.2.3.2 Crystal and molecular structure of compound **9**

The benzothiazol-2-ylideneamine coordinated (triphenylphosphine)gold(I) **9** crystallises from dichloromethane as colourless needles in the triclinic space group $P\bar{1}$ with $Z = 4$ molecules in the unit cell. Figure 4.7 depicts the molecular structure of **9**, showing the numbering scheme, and selected bond lengths and angles are summarised in Table 4.9. The N–Au–P angle [178.4(2) Å] exhibits the standard linear geometry innate to gold(I) complexes with the phenyl rings of the phosphine ligand arranged in the typical propeller-like fashion. Furthermore, the bond lengths and angles of the coordinated ligand show no anomalies compared to those observed for the Au(C₆F₅) coordinated ligand in compound **6**. From an evaluation of the Au–N bond lengths of compounds **6** and **9**, it is evident that coordination of ligand **IV** to an Au(PPh₃)⁺ unit results in Au–N bond lengths comparable to that of an Au(C₆F₅) Lewis acid. As was observed for compound **8**, substitution of a nitrate anion for the ylideneamine ligand goes together with an elongation of the Au–P bond compared to that of [Au(NO₃)(PPh₃)]. This observation is symptomatic of a labilising *trans* influence. The C–N and C=N bond lengths [1.359(9) Å and 1.289(9) Å] do not testify of any substantial electron delocalisation over the N–C–N bonds. The limited electron delocalisation possibly arises from an enhanced charged neutralisation through hydrogen bonding between the imine hydrogen atom and the oxygen atom of the nitrate

counterion (N–H \cdots O, 2.02 Å). This efficient neutralisation may result in a reduced need for charge stabilisation by means of electron delocalisation.

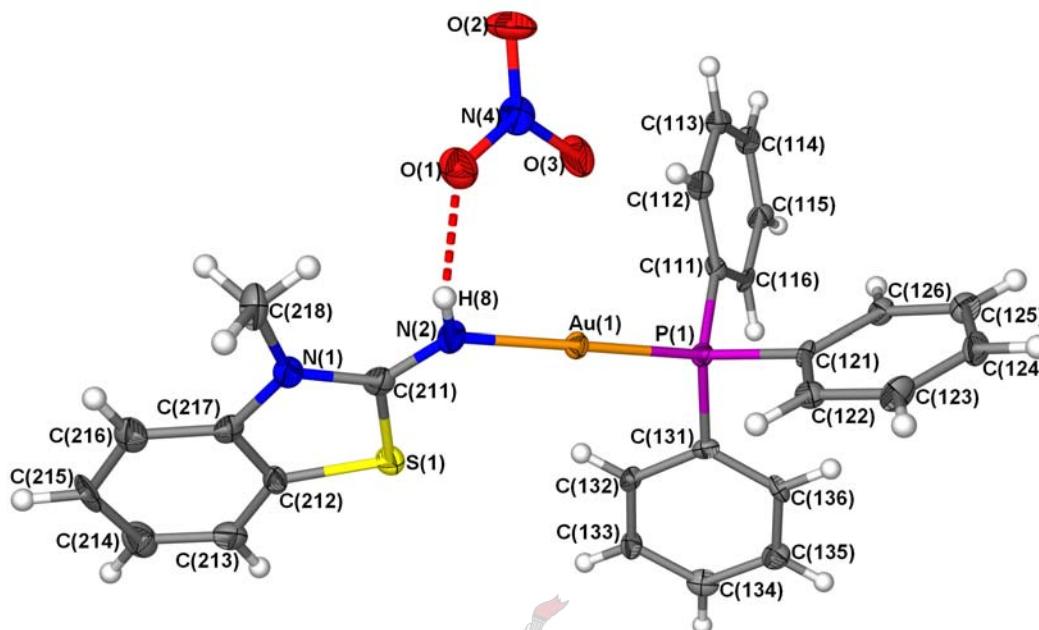


Figure 4.7 Molecular structure of **9** showing the numbering scheme; thermal ellipsoids are set at 50% probability.

The crystal lattice of **9** displays a molecular arrangement similar to that of compound **8**, with like ligands from adjacent molecules directed towards each other (Figure 4.8).

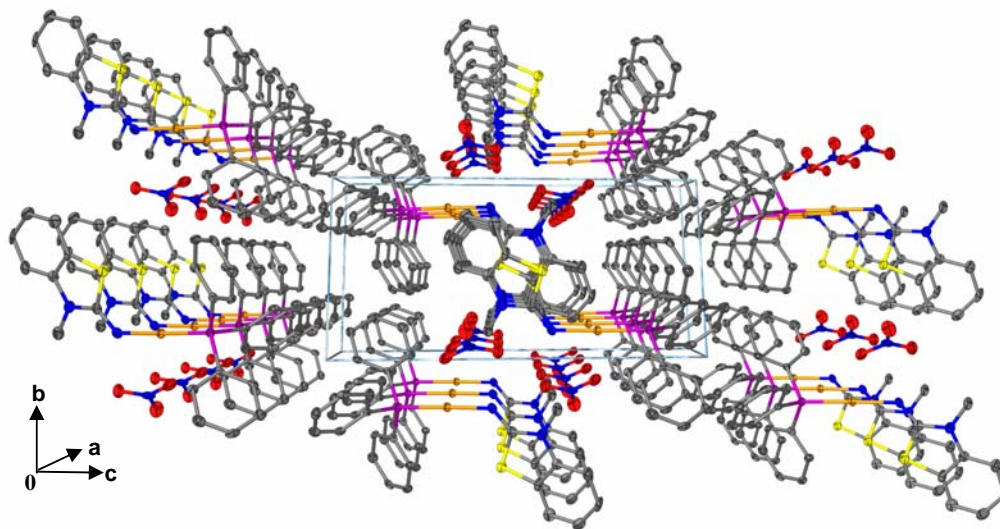


Figure 4.8 Perspective drawing of the molecular packing of **9** viewed along the a-axis. Hydrogen atoms are omitted for clarity.

Only two distinct layers exist and no noteworthy intermolecular forces, apart from the hydrogen bonding between the imine protons and the oxygen atoms of the nitrate anions, are observed. The smallest gold-gold separations observed in the crystal lattice are 7.131 Å and do not qualify as aurophilic interactions. Furthermore, large separations between adjacent ligand rings exist and the molecular packing does not display any significant π - π interactions between neighbouring molecules.

Table 4.9 Selected bond lengths (Å) and angles (°) of **9** with estimated standard deviations in parenthesis.

<i>Bond lengths (Å)</i>			
Au(1)–P(1)	2.225(2)	S(1)–C(212)	1.755(7)
Au(1)–N(2)	2.028(6)	N(1)–C(218)	1.421(9)
N(1)–C(211)	1.359(9)	C(212)–C(217)	1.39(1)
N(2)–C(211)	1.289(9)	P(1)–C(111)	1.812(7)
S(1)–C(211)	1.770(8)	P(1)–C(121)	1.827(7)
N(1)–C(217)	1.403(9)	P(1)–C(131)	1.816(7)
<i>Bond angles (°)</i>			
N(2)–Au(1)–P(1)	178.4(2)	N(1)–C(217)–C(212)	113.3(7)
C(211)–N(2)–Au(1)	127.3(5)	S(1)–C(212)–C(217)	111.0(6)
N(1)–C(211)–S(1)	111.5(5)	C(111)–P(1)–Au(1)	113.1(2)
N(1)–C(211)–N(2)	128.6(7)	C(121)–P(1)–Au(1)	114.6(2)
S(1)–C(211)–N(2)	120.0(6)	C(131)–P(1)–Au(1)	111.9(2)
C(211)–N(1)–C(217)	113.8(6)	C(111)–P(1)–C(121)	103.0(3)
C(211)–S(1)–C(212)	90.4(4)	C(111)–P(1)–C(131)	107.0(3)
C(211)–N(1)–C(218)	123.4(6)	C(121)–P(1)–C(131)	106.4(3)

4.2.3.3 Structure determination of compound **11**

Single crystals of the carbene-ylideneamine compound **11** were obtained as colourless cubes from a dichloromethane solution of **11** and were subjected to X-ray diffraction study. Apart from these colourless cubic crystals, a second type of crystal (colourless needles) could be isolated from the crystallisation mixture. These crystals were however too fine for X-ray structure determination. Since initial NMR analysis did not show any sign of impurities, these crystals may correspond to the homoleptic biscarbene rearrangement product, which could have formed during prolonged storage of **11** in solution. Compound **11** crystallises, together with one solvent molecule, in the triclinic space group $P\bar{1}$ with $Z = 2$ molecules in the unit cell. Figure 4.9 depicts the molecular structure of **11**, showing the numbering scheme, and selected bond lengths and angles are summarised in Table 4.10. In view of the fact that the included dichloromethane

molecules are disordered over an inversion centre, hydrogen atoms of these dichloromethane molecules were not included in the refinement. The geometry about the gold centre deviates from linearity with a C–Au–N angle of $174.8(1)^\circ$. Furthermore, in order to minimize steric interactions between the two ligands, the planar ring of the NHC ligand is approximately perpendicular to the plane formed by the benzimidazol-2-ylideneamine ligand rings. No appreciable difference exists between the Au–N bond lengths of compounds **8** [$2.029(10)\text{Å}$], **9** [$2.028(6)\text{Å}$] and **11** [$2.028(4)\text{Å}$], again emphasizing the electronic similarities between the triphenylphosphine and NHC ligand. The Au–C distance of $1.993(4)\text{Å}$ is, however, significantly shorter than the Au–P distance [$2.226(3)\text{Å}$] measured for compound **8**. Furthermore, the Au–C bond length [$1.993(4)\text{Å}$] observed for (1,3-*tert*-butylimidazolin-2-ylidene)gold(I) nitrate [$1.973(4)\text{Å}$]²⁰ remains relatively unaltered by substitution of a nitrate ligand for the ylideneamine ligand **III**. This indicates that this ligand class has a less pronounced *trans* influence on an NHC ligand than on triphenylphosphine. The bond lengths and angles of the coordinated ligand **III** are comparable to those of compound **8** and the free ligand, and no noteworthy disparities exist.

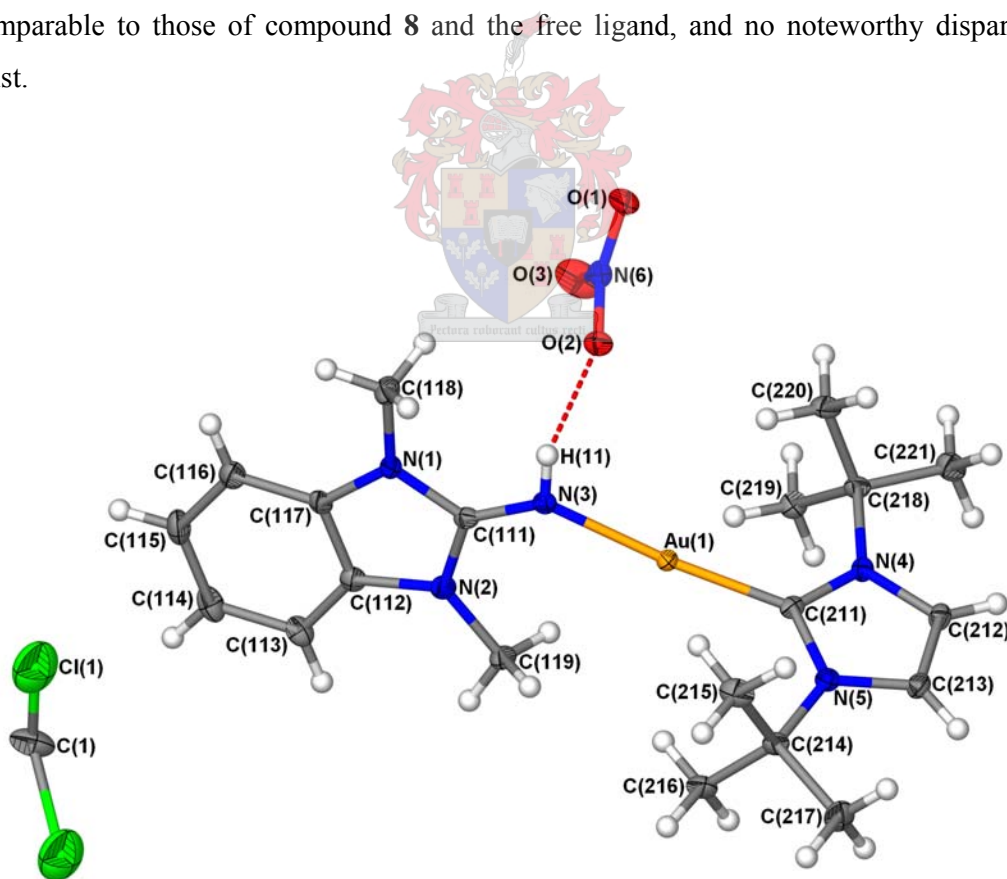


Figure 4.9 Molecular structure of **11** showing the numbering scheme. Thermal ellipsoids are set at 50% probability.

Table 4.10 Selected bond lengths (Å) and angles (°) of **11** with estimated standard deviations in parenthesis.

<i>Bond lengths (Å)</i>			
Au(1)–C(211)	1.993(4)	N(4)–C(212)	1.378(5)
Au(1)–N(3)	2.028(4)	N(5)–C(213)	1.384(5)
N(1)–C(111)	1.372(5)	N(4)–C(218)	1.507(5)
N(2)–C(111)	1.377(5)	N(5)–C(214)	1.504(5)
N(3)–C(111)	1.299(6)	C(212)–C(213)	1.345(6)
N(1)–C(117)	1.386(5)	C(214)–C(215)	1.531(6)
N(2)–C(112)	1.399(5)	C(214)–C(216)	1.527(6)
N(1)–C(118)	1.460(5)	C(214)–C(217)	1.528(6)
N(2)–C(119)	1.454(5)	C(218)–C(219)	1.529(6)
C(112)–C(117)	1.401(6)	C(218)–C(220)	1.536(6)
N(4)–C(211)	1.363(5)	C(218)–C(221)	1.535(6)
N(5)–C(211)	1.364(5)		
<i>Bond angles (°)</i>			
N(3)–Au(1)–C(211)	174.8(1)	N(2)–C(112)–C(117)	106.8(4)
C(111)–N(3)–Au(1)	134.5(3)	N(4)–C(211)–Au(1)	126.3(3)
N(1)–C(111)–N(2)	107.0(3)	N(5)–C(211)–Au(1)	128.2(3)
N(1)–C(111)–N(3)	126.0(4)	N(4)–C(211)–N(5)	105.4(3)
N(2)–C(111)–N(3)	127.0(4)	C(211)–N(4)–C(218)	125.5(3)
C(111)–N(1)–C(117)	110.0(3)	C(211)–N(5)–C(214)	125.4(3)
C(111)–N(2)–C(112)	109.3(3)	C(211)–N(4)–C(212)	109.8(3)
C(111)–N(1)–C(118)	123.1(4)	C(211)–N(5)–C(213)	110.0(3)
C(111)–N(2)–C(119)	125.8(3)	N(4)–C(212)–C(213)	107.8(4)
N(1)–C(117)–C(112)	107.0(4)	N(5)–C(213)–C(212)	107.0(4)

In the crystal lattice of compound **11**, due to the steric demands of the bulky ^tBu substituents together with the inclusion of dichloromethane molecules, small intermolecular separations and hence aurophilic interactions between adjacent molecules are prohibited. The smallest gold-gold separations present in the crystal lattice are 7.18 Å and may therefore not be regarded as aurophilic interactions. Hydrogen bonding between the imine protons and the oxygen atoms of the anionic nitrate counterions are observed [N–H ··· O, 2.18 Å]. In addition, weak π - π interactions between neighbouring benzimidazole rings (centroid to centroid distance: 3.47 Å) are observed. To ensure efficient π - π interactions, the molecules assemble in a head to head and tail to tail fashion (Figure 4.10). No other intermolecular forces are observed, and the solid state packing of **11** is therefore solely directed by the hydrogen bonding and π -stacking interactions.

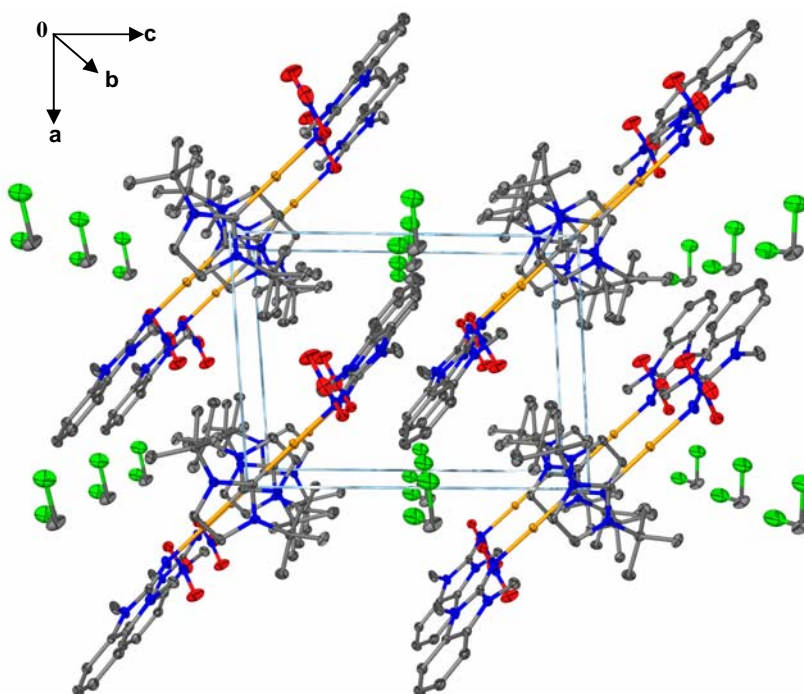


Figure 4.10 Perspective drawing of the molecular packing of **11** viewed along the b-axis. Hydrogen atoms are omitted for clarity.

4.2.4 Cytotoxicity assays of compounds **8** – **11**

The *in vitro* cytotoxicity of compounds **8** – **11** at different concentrations were determined, using cervical carcinoma cells (HeLa)(CCL-2) as the target cell line. Identical assays were also performed on ligands **III** – **V** to serve as control experiments for ensuring that any growth inhibition observed is indeed the result of auration and not due to an inherent activity of the free ligands. The results obtained for these preliminary studies are summarised in Table 4.11. In addition, the IC_{50} , lymphocyte resting and lymphocyte stimulation values for cisplatin, the main transition metal-based drug currently employed in the treatment of cancer, are also listed to represent the goal values. Compounds with minimum inhibitory concentrations (IC_{50}) greater than 30 μ M were not subjected to any further testing. Regrettably, none of the tested compounds showed remarkable cytotoxic potential, with the free ligands **III**, **IV** and **V** resulting in the least growth inhibition having IC_{50} values greater than 30 μ M. Note however that the lack of cytotoxicity observed for these compounds may also be reflective of a low degree of cellular uptake which is determined by the hydrophilicity of the compounds. Although all of complexes **8** – **11** showed a significant increase in growth inhibition with respect to the free ligands, the measured IC_{50} values were not nearly comparable to that of cisplatin. However, it can be

concluded that coordination to an Au(PPh₃)⁺ moiety has the greatest effect on ligand **III** with the IC₅₀ value changing from greater than 50 μM to 10.169 μM. Furthermore, gold(I) coordination of ligand **IV** to afford complex **9** does not bring about any significant changes in the cytotoxic potency; however, the tumour specificity is decreased drastically. Although complex **10** displayed the greatest growth inhibition as well as tumour specificity, the measured lymphocyte resting and stimulation values were of intermediate nature in the series. From a comparison of complex **8** and **11** it is evident that the triphenylphosphine ancillary ligand imparts much greater cytotoxicity and tumour specificity on the complex than its NHC counterpart – a result not expected owing to the already mentioned activity results obtained by Baker and co-workers. Overall, the anti-tumour properties of the various gold(I) complexes discussed here appears to be of little consequence and whether cellular uptake is the determining factor in this limited anti-tumour activity remains unclear.

Table 4.11 Results obtained for preliminary cytotoxicity studies of compounds **III** – **V** and **8** – **11** against (HeLa)(CCL-2) cells.

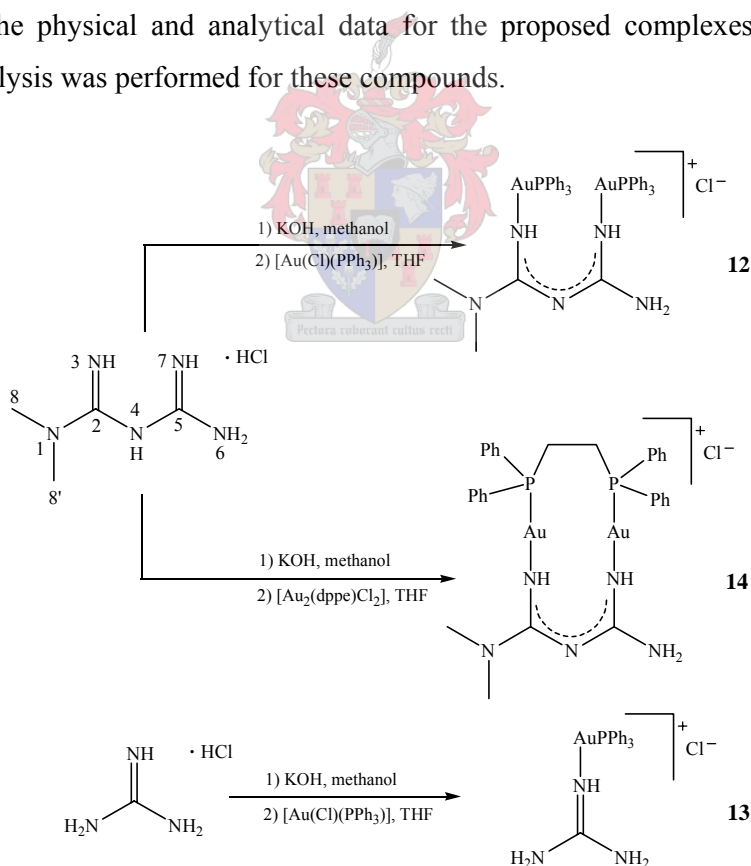
Compound	HeLa IC ₅₀ [*] (μM)	Lymphocyte resting (μM)	Lymphocyte stimulation (μM)	Tumour specificity
III	> 50	not performed	not performed	not performed
IV	32.188 ± 2.990	not performed	not performed	not performed
V	> 50	not performed	not performed	not performed
8	10.169 ± 0.418	6.368 ± 1.317	3.345 ± 1.969	0.478
9	27.344 ± 4.014	3.596 ± 0.275	3.963 ± 0.337	0.075
10	9.131 ± 0.268	6.112 ± 1.175	4.328 ± 0.706	0.572
11	19.191 ± 0.274	6.504 ± 0.159	6.76 ± 0.981	0.346
Cisplatin	0.639	30.363 ± 6.696	2.203 ± 0.316	

* IC₅₀ values refer to the minimum concentration required to effect growth inhibition in 50% of the cells.

4.2.5 Deprotonation studies: preparation of 1,1-dimethylbiguanidinobis-[(triphenylphosphine)gold(I)], **12**, guanidine(triphenylphosphine)-gold(I), **13**, 1,1-dimethylbiguanidinato[1,2-bis(diphenylphosphino)-ethane]digold(I), **14**

Several attempts to prepare ylideneamide gold(I) complexes derived from deprotonated ylideneamine ligand precursors were made. In the first attempts we endeavoured

deprotonation of the =NH functionalities of biguanidine and guanidine type ligands using KOH as base. This was done by treating methanol solutions of either 1,1-dimethylbiguanidine hydrochloride or guanidine hydrochloride with $[\text{Au}(\text{Cl})(\text{PPh}_3)]$ or $[\text{Au}_2(\text{Cl})_2(\text{dppe})]$ in the presence of ground KOH (Scheme 4.4). Although it is not certain from spectroscopic and spectrometric analysis (to be discussed in section 4.2.6) of the reaction products (**12** – **14**) whether deprotonation of the =NH functionalities were successful, it is evident that coordination of these ligands to gold(I) had indeed occurred. We, however, firmly believe that deprotonation of the =NH functionalities does not occur and that deprotonation of the central N^4 of 1,1-dimethylbiguanidine (see Scheme 4.4 for numbering format) takes place instead. This belief is based on several literature reports of similar successful deprotonations on related compounds.^{24,25} Again, this assumption could not be confirmed by spectroscopic techniques. Furthermore, despite several crystallisation attempts, single crystals suitable for X-ray analysis eluded us and the matter could therefore not be clarified by means of crystal structure determinations. Table 4.12 summarises the physical and analytical data for the proposed complexes **12** – **14**. No elemental analysis was performed for these compounds.

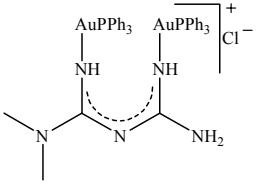
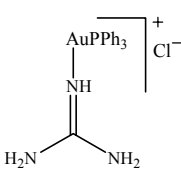
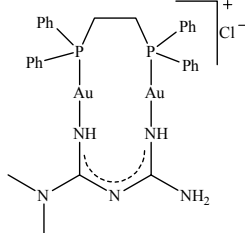


Scheme 4.4 Reaction scheme for the preparation of complexes, **12** - **14**.

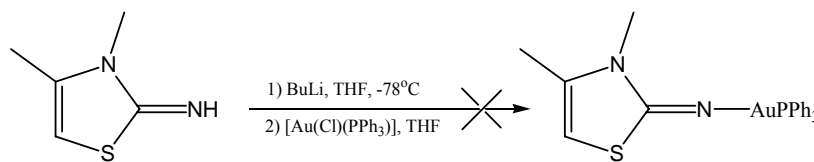
²⁴ A. Marchi, L. Marvelli, M. Cattabriga, R. Rossi, M. Neves, V. Bertolasi, V. Ferretti, *J. Chem. Soc., Dalton Trans.* **1999**, 1937-1943.

²⁵ M. Zhu, L. Lu, P. Yang, X. Jin, *Acta Crystallogr. Sect. E* **2002**, 58, m272-m274.

Table 4.12 Analytical data of complexes **12**, **13** and **14**.

Complex			
	12	13	14
M.p (°C)	80-85	153-156(decomp.)	161-167(decomp.)
Colour	off-white	white	off-white
Yield (%)	95	91	59
M_r	1082.18	553.78	955.96
M_f	$C_{40}H_{40}Au_2ClN_5P_2$	$C_{19}H_{20}AuClN_3P$	$C_{30}H_{34}Au_2ClN_5P_2$

In related attempts, deprotonation of ylideneamine-functionalised heterocyclic ligands were considered. It is known that the pK_a values of ligand **IV** (7.96) and the 4*H* analogue of ligand **V**, 3-methyl-3*H*-thiazol-2-ylideneamine (9.50), display lesser and greater basicity respectively compared to ammonia (9.26).²⁶ Deprotonation using a stronger base, such as *n*-BuLi, was thus explored in an attempt to prepare the neutral complex, 3,4-dimethyl-3*H*-thiazol-2-ylideneamide(triphenylphosphine)gold(I) (Scheme 4.5). ¹H NMR analysis of the product isolated from this reaction mixture, revealed the presence of almost equal amounts of unreacted and modified ligand. However the ³¹P NMR spectrum, contains a sharp singlet resonance at δ 33.5 assigned to unreacted [Au(Cl)(PPh₃)]. Kuhn and co-workers²⁷ isolated polymeric products when related ligands were treated with strong bases such as BuLi, MeLi, NaH, KH and KMe. The modified ligand resonances identified in the ¹H NMR spectrum may therefore be the result of such reactions.

**Scheme 4.5** Proposed preparation of 3,4-dimethyl-3*H*-thiazol-2-ylideneamide(triphenylphosphine)gold(I).²⁶ R. G. Button, J. P. Cairns, P. J. Taylor, *J. Chem. Soc., Perkin Trans. II* **1985**, 1555-1558.²⁷ N. Kuhn, M. Göhner, M. Grathwohl, J. Wiethoff, G. Frenking, Y. Chen, *Z. Anorg. Allg. Chem.* **2003**, 629, 793-802.

From the above mentioned reaction mixture, a single crystal of compound 3-methyl-3*H*-thiazol-2-ylideneaminegold(I) triflate, **15** (Figure 4.5), was isolated and subjected to single crystal X-ray analysis. The crystal and molecular structure of this compound will be discussed in section 4.2.6.

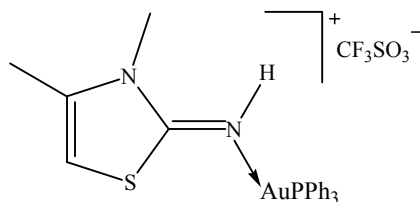


Figure 4.5 3-Methyl-3*H*-thiazol-2-ylideneamine(triphenyl-phosphine)gold(I) triflate, **15**.

From the discussion in section 4.2.2.1, it is evident that coordination of ligands **III** – **V** to a gold(I) centre has a significant effect on the electronic nature of the imine protons. This finding prompted further deprotonation attempts on ylideneamine ligands after gold(I) coordination. Deprotonation of complexes **8** – **11** (Figure 4.6), which represent possibly more acidic precursors, was therefore attempted using KH as base. The bulk material from these reaction mixtures, however, revealed the presence of unmodified substrates, as was shown by the isolation of crystalline starting complexes **8** – **11** and a solvate variant of **8**, **8b**. The elucidation of structure **8b** is discussed in section 4.2.6.1. Furthermore, NMR spectra still contained the diagnostic =NH resonances, confirming the resistance of the =NH functionality towards deprotonation.

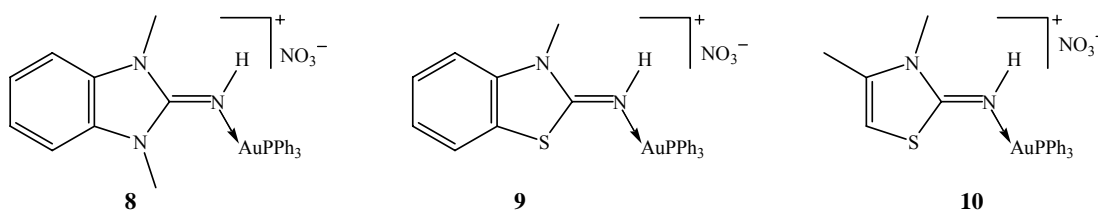


Figure 4.6 Compounds **8** – **10**.

4.2.6 Spectroscopic characterisation of compounds **12** – **14**

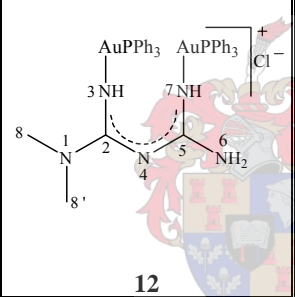
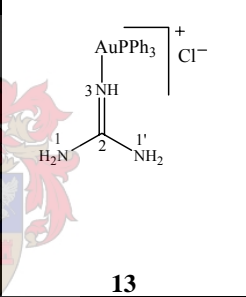
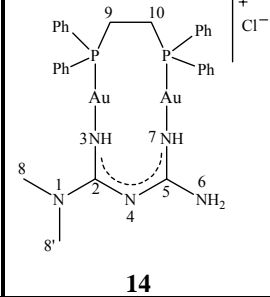
4.2.6.1 Nuclear magnetic resonance spectroscopy

The ^1H , ^{13}C and ^{31}P NMR spectroscopic data obtained for dichloromethane- d_2 or methanol- d_4 solutions of complexes **12** – **14** are summarised in Table 4.13. The ^1H and ^{13}C NMR spectra of complexes **12** – **14**, as was mentioned in section 4.2.5, do not provide

unambiguous proof as to their precise constitution. Furthermore, extensive overlap of the NH₂, NH and =NH resonances, which are observed as broad singlets in the ¹H NMR spectra of compounds **12** and **14**, preclude easy observation of deprotonation. Although a decrease in the intensity of these signals, with respect to the corresponding signals in the free ligand spectra, are observed, the broad nature of these signals prevent accurate measurement and whether deprotonation of the N⁴ atoms has taken place therefore remains unclear.

In the ¹³C NMR spectra of complexes **12** – **14** the ylidene carbon atoms show a consistent downfield shift of δΔ 12 (**12**), δΔ 8 (**13**) and δΔ 10 (**14**) compared to the free ligand resonances. Note however, that in the instance of complexes **12** and **14**, different solvent systems were used for analysis.

Table 4.13 ¹H, ¹³C, ¹⁵N and ³¹P NMR spectroscopic data of complexes **12**, **13** and **14**.

Complex			
Solvent	Dichloromethane-d ₂	Methanol-d ₄	Dichloromethane-d ₂
Temperature (°C)	25	25	25
Assignment	Chemical shift (ppm)		
¹ H NMR (300 MHz)	4.86 (s, 5H)		
H ¹ , H ^{1'}			
H ³ , H ⁶ , H ⁷	2.73 (bs, 4H)		4.65 (bs, 4H)
H ⁸ , H ^{8'}	2.87 (s, 6H)		2.95 (bs, 6H)
H ⁹ , H ^{10'}			2.86 (bs, 4H)
¹³ C NMR (75 MHz)	7.50-7.60 (m, 15H)		
PPh	7.35-7.66 (m, 15H)	7.50-7.60 (m, 15H)	7.16-7.74 (m, 20H)
C ²	172.9 (s)	168.9 (s)	172.3 (s)
C ⁵	172.9 (s)		172.4 (s)
C ⁸ , C ^{8'}	38.1 (s)		38.1 (s)
C ⁹ , C ¹⁰			25.5 (s)
PPh-C ^{ipso}	130.3 (d, ¹ J = 55.8 Hz)	131.2 (d, ¹ J = 60.1 Hz)	133.4 (d, ¹ J = 64.4 Hz)
PPh-C ^{ortho}	134.4 (d, ² J = 13.7 Hz)	135.3 (d, ² J = 13.3 Hz)	133.8 (m), 132.4 (m)
PPh-C ^{meta}	129.3 (d, ³ J = 11.2 Hz)	130.4 (d, ³ J = 11.2 Hz)	129.2 (m), 129.6 (m)
PPh-C ^{para}	131.7 (bs)	132.8 (bs)	130.8 (s), 132.3 (s)
³¹ P NMR (121MHz)	33.8 (s)		
P	30.5 (bs)	33.8 (s)	21.5 (s) and 30.3 (s)

The ^{31}P NMR spectrum compound **12**, displays a broad singlet at δ 30.5. The broadness of this signal is attributable to overlap of the phosphorus atom resonances of the two coordinated $\text{Au}(\text{PPh}_3)^+$ groups. In contrast, in the ^{31}P NMR spectrum of compound **14**, these two phosphorus atoms give rise to two sharp singlets of more or less equal intensities at δ 21.5 and δ 30.3. A sharp singlet resonance at δ 33.8 in the ^{31}P NMR spectrum of **13** confirms the formation of a single phosphorus containing product.

4.2.6.2 Mass spectrometry

The FAB-MS spectrometric data of compounds **12** – **14** is summarised in Table 4.14. In the MS spectra of **12** and **13**, signals for the rearrangement and the fragmentation entities $[\text{Au}(\text{PPh}_3)_2]^+$ and $[\text{Au}(\text{PPh}_3)]^+$ are detected at m/z 721 and m/z 459 respectively. Further loss of a phenyl group from the latter fragment results in a signal at m/z 382. In addition to these characteristic fragmentation patterns, peaks that correspond to the cations of the molecules are observed at m/z 1046 for compound **12** and m/z 518 for compound **13**, confirming the formation of the gold(I) coordinated compounds.

Loss of an $\text{Au}(\text{PPh}_3)^+$ unit from the cation of **12** is observed as a peak at m/z 588 and in the spectrum of **13**, the loss of three phenyl groups from the cation results in a signal at m/z 289. Very little fragmentation is observed in the spectrum of compound **14**. Apart from the peak that corresponds to the cation of the molecule (m/z 921), additional diagnostic peaks can be assigned to the fragments resulting from the loss of a $(\text{CH}_3)_2\text{N}(\text{C})=\text{NH}(\text{N})$ or $(\text{C}=\text{N})\text{Au}(\text{PPh}_2)$ moiety from the cation (m/z 833 and m/z 409, respectively).

Table 4.14 Mass spectrometric data of complexes **12**, **13** and **14**.

Fragment	m/z (I in %)		
	12	13	14
$\{[\text{M}]-\text{Cl}\}^+$	1046 (35)	518 (29)	921(25)
$\{[\text{M}]-\text{Cl}-(\text{CH}_3)_2\text{NC}=\text{NH}(\text{N})\}^+$	—	—	833 (12)
$\{[\text{M}]-\text{Cl}-3\text{Ph}\}^+$	—	289 (23)	—
$\{[\text{M}]-\text{Cl}-\text{Au}(\text{PPh}_3)\}^+$	588 (66)	—	—
$\{\text{Au}(\text{PPh}_3)\}^+$	459 (100)	459 (48)	—
$\{\text{Au}(\text{PPh}_2)\}^+$	382 (5)	382 (3)	—
$\{\text{Au}(\text{PPh}_3)_2\}^+$	721 (31)	721 (5)	—
$\{(\text{C}=\text{NH})\text{Au}(\text{PPh}_2)\}^+$	—	—	409

4.2.6.2 Infrared spectroscopy

Table 4.15 summarises the solid state ATR FT-IR spectroscopic data obtained for compounds **12** – **14**. All spectra show very broad bands of medium to high intensity in the range 3316-3346 cm^{-1} , assignable to the stretching vibrations of the =NH and NH_2 groups. It is probable that, apart from broadening caused by overlap of the =NH and NH_2 absorption bands, inter and intramolecular hydrogen bonding contribute to band broadening. In all of the complexes, the mentioned bands were of lower intensity than those observed in the spectra of the parent ligands. Furthermore, these bands were shifted appreciably towards higher wavenumbers, symptomatic of metal coordination. Although successful deprotonation may be a plausible explanation for the decreased band intensity, it is also possible that coordination is the sole root of this effect.

In the spectrum of compound **12**, weak bands detected in the region 1631-1573 cm^{-1} were assigned to the C=N stretching vibrations while the strong bands in the region 1479-1434 cm^{-1} signify the presence of the phenyl ring $\nu(\text{C}=\text{C})$. Furthermore, out of plane aromatic C=C bending vibrations are observed in the form of an absorption band at 745 cm^{-1} .

The FT-IR spectrum of **13** shows, apart from the mentioned NH and NH_2 absorption bands, strong bands in the region 1621-1539 cm^{-1} attributable to the C=N vibrations. No significant change exists between the frequencies of the C=N absorption bands in **13** and the free ligand. The intensity of these bands however decreased dramatically with coordination to the gold(I) centre. The absorption frequencies of the C=C stretching and bending vibrations, confirming the presence of phenyl rings, are also observed in the region 1479-1434 cm^{-1} and at 746 cm^{-1} , as was the case for **12**.

Table 4.15 Infrared spectroscopic data of complexes **12**, **13** and **14**.

Functional group	Wavenumber (cm^{-1})		
	12	13	14
$\nu(\text{=N-H})$	3290 (w, br)	3195 (m, br)	3215(w, br)
$\text{sp}^3 \nu(\text{N-H})$	3316 (m, br)	3317 (st, br)	3346 (st, br)
Ar $\nu(\text{C-H})$	3051(w)	3051 (w)	3051 (m)
$\text{sp}^3 \nu(\text{C-H})$	n.o.	n.a.	2933 (w)
$\nu(\text{C=N})$	1631-1573 (w)	1621-1539 (st)	1614-1564 (st)
Ar $\nu(\text{C=C})$	1479-1434 (st)	1479-1434 (m)	1481-1435 (st)
Ar $\delta_{\text{oop}}^{\text{b}}(\text{C=C})$	745 (m)	746 (m)	744 (m)

An absorption band, attributable to the sp^3 C–H bonds of the Me groups are observed at 2933 cm^{-1} in the FT-IR spectrum of compound **14**. Furthermore, the C=N stretching vibrations, detected in the region $1614\text{--}1564\text{ cm}^{-1}$, appear at the same absorption frequency as was observed in the free ligand spectrum. Other diagnostic absorption bands include the aromatic $\nu(\text{C}=\text{C})$ and $\delta_{\text{oop}}^{\text{b}}(\text{C}=\text{C})$ bands in the range $1481\text{--}1435\text{ cm}^{-1}$ and at 744 cm^{-1} respectively.

4.2.7 Structure determination of compounds **8b** and **15**

The crystal and molecular structures of compounds **8b** and **15** (Figure 4.7) were determined by single crystal X-ray diffraction. Crystals suitable for X-ray structure determination were obtained by vapour diffusion of pentane into a solution of the crude reaction mixtures in dichloromethane. All crystallisation mixtures were stored under argon at $-22\text{ }^\circ\text{C}$.

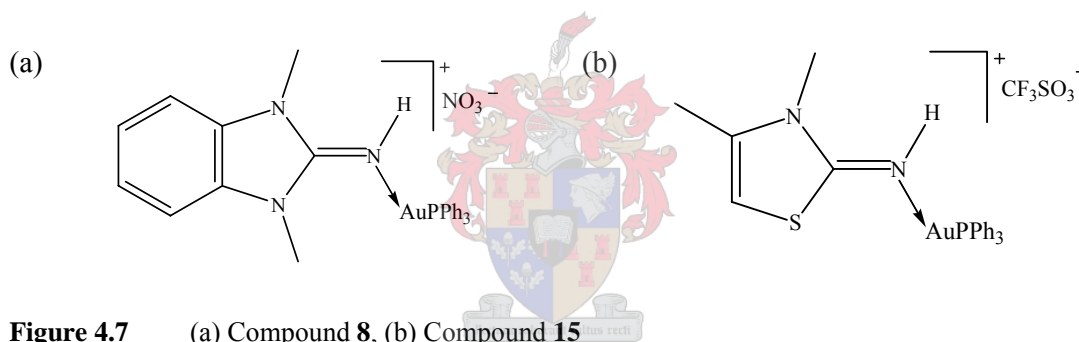


Figure 4.7 (a) Compound **8**, (b) Compound **15**

4.2.7.1 Crystal and molecular structure of compound **8b**

In the absence of included solvent molecules compound **8** crystallises as colourless rectangles from a dichloromethane solution in the monoclinic space group $P2_1/c$ with only one unique molecule in the asymmetric unit and $Z = 4$ molecules in the unit cell. Devoid of any disorder as a result of solvent inclusion, this crystal structure refinement is of superior quality and the bond lengths and angles listed in Table 4.16 are therefore more reliable than those in the previously described structure **8a** that contained included solvent. As could be expected, apart from the insignificant changes resulting from an improved data set, no discrepancies exist between the bond lengths and angles of structures **8a** and **8b**. Figure 4.11 depicts the molecular structure of **8b** indicating the numbering scheme while Figure 4.12 shows a perspective representation of the solid state packing of compound **8a** when viewed along the a-axis.

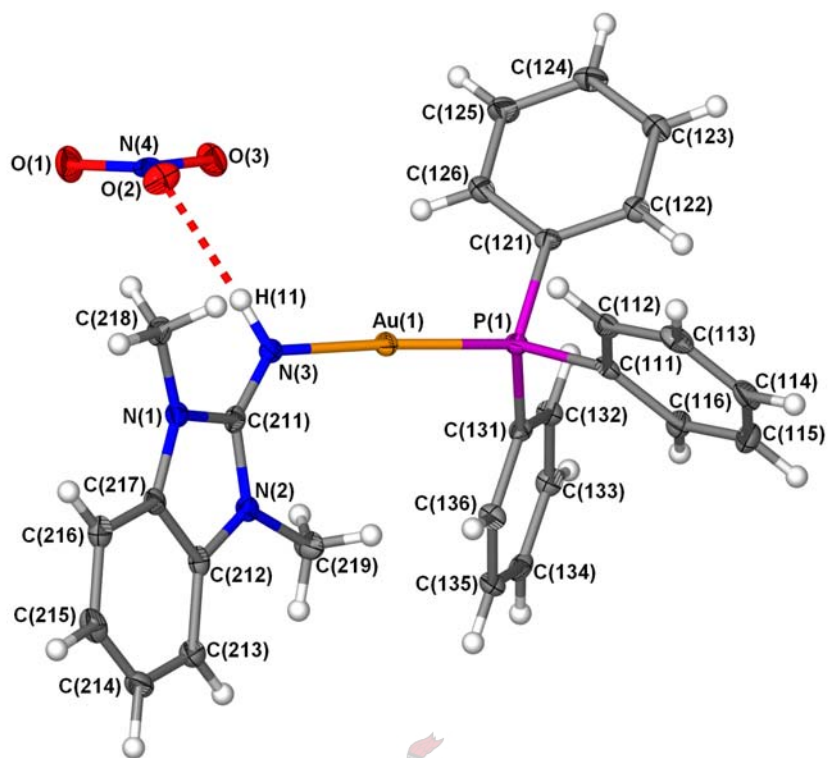


Figure 4.11 Molecular structure of **8b** showing the numbering scheme. Thermal ellipsoids are set at 50% probability.

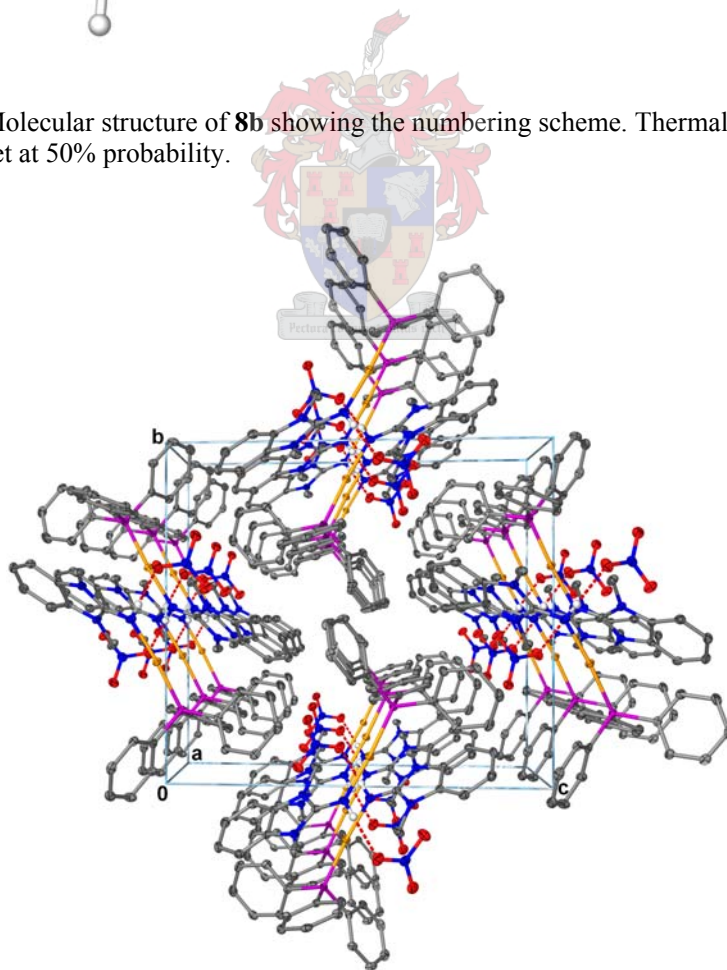


Figure 4.12 Perspective drawing of the molecular packing of **8b** viewed along the a-axis; all hydrogen atoms, except imine hydrogen atoms, are omitted for clarity.

Unlike the solid state packing of **8a**, molecules of **8b** do not assemble with like ligands aligned; instead molecules are arranged in an alternating head to tail manner with the bulky phenyl rings preventing molecular separations smaller than 5.863 Å (Figure 4.12). No intermolecular interactions, other than hydrogen bonding of the imine hydrogen atoms to the nitrate counterions, are observed (N–H ··· O, 2.15 Å). The smallest gold-gold separation present in the crystal lattice is 5.863 Å and does not qualify as an aurophilic interaction.

Table 4.16 Selected bond lengths (Å) and angles (°) of **8b** with estimated standard deviations in parenthesis.

<i>Bond lengths (Å)</i>			
Au(1)–P(1)	2.230(1)	N(1)–C(218)	1.458(5)
Au(1)–N(3)	2.040(3)	N(2)–C(219)	1.460(5)
N(1)–C(211)	1.374(5)	C(212)–C(217)	1.397(5)
N(2)–C(211)	1.364(4)	P(1)–C(111)	1.815(4)
N(3)–C(211)	1.309(4)	P(1)–C(121)	1.811(4)
N(1)–C(217)	1.393(4)	P(1)–C(131)	1.809(4)
N(2)–C(212)	1.391(4)		
<i>Bond angles (°)</i>			
N(3)–Au(1)–P(1)	175.59(9)	N(1)–C(217)–C(212)	107.0(3)
C(211)–N(3)–Au(1)	129.8(3)	N(2)–C(212)–C(217)	106.8(3)
N(1)–C(211)–N(2)	107.4(3)	C(111)–P(1)–Au(1)	110.4(1)
N(1)–C(211)–N(3)	125.9(3)	C(121)–P(1)–Au(1)	116.5(1)
N(2)–C(211)–N(3)	126.7(3)	C(131)–P(1)–Au(1)	112.0(1)
C(211)–N(1)–C(217)	109.1(3)	C(111)–P(1)–C(121)	104.6(2)
C(211)–N(2)–C(212)	109.6(3)	C(111)–P(1)–C(131)	106.3(2)
C(211)–N(1)–C(218)	123.5(3)	C(121)–P(1)–C(131)	106.3(2)
C(211)–N(2)–C(219)	126.0(3)		

4.2.7.2 Crystal and molecular structure of compound 15

The thiazol-2-ylideneamine coordinated (triphenylphosphine)gold(I) compound **15** crystallises, together with one solvent molecule, from a dichloromethane solution as colourless rectangles in the triclinic space group $P\bar{1}$, with three unique molecules in the asymmetric unit and $Z = 2$ molecules in the unit cell. Figure 4.13 depicts the arrangement of the three symmetrically unique molecules present in the asymmetric unit, viewed along the *a*-axis. The molecular structure of only one of the unique molecules, indicating the numbering scheme, is depicted in Figure 4.14. Selected bond lengths and angles for only one of the molecules are summarised in Table 4.17, since the bond lengths and angles of the unique molecules do not differ significantly. Similar to all of the discussed complexes,

the geometry about the gold(I) centre is best described as linear [177.2(2) Å]. The Au–N distances range from 2.031(7)Å to 2.040(7)Å, and are comparable to those of compounds **8** – **11** and the literature values mentioned previously.¹⁹ Furthermore, the *trans* influence of ligand **V** appears to be in the same order of magnitudes as those displayed by ligands **III** and **IV**, with Au–P distance [2.233(2) Å] comparable to those of compounds **8** and **9**. No verdict concerning the significance of electron delocalisation over the N–C=N bonds could be reached with certainty, owing to the rather large standard deviations associated with the C=N and C–N bond lengths. As was noted for complexes **8** – **11**, coordination to an Au(PPh₃)⁺ moiety does not result in any noteworthy changes in the bond lengths and angles of ligand **V**.

In the solid state packing of compound **15**, the molecules are assembled in groups of six stabilised by a relatively strong hydrogen bonding system involving the imine hydrogen atoms and oxygen atoms of the triflate anion (N–H ··· O, 2.06-2.08 Å). This arrangement, when viewed along the a-axis, bestows a beautiful flower-like appearance upon the crystal lattice (Figure 4.15). The core of the flower motif consists of six triflate counterions arranged about a central dichloromethane molecule whilst the “petals” comprise of six molecules of **15**, connected to the inner part *via* hydrogen bonding.

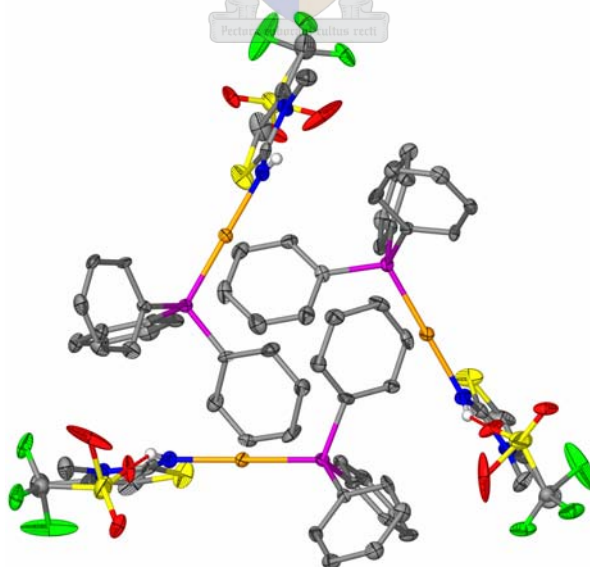


Figure 4.13 Depiction of the three symmetrically unique molecules in the unit cell of **15**; Hydrogen atoms, excluding imine hydrogens, as well as the solvent molecule are omitted for clarity. Thermal ellipsoids of the triflate counterions are set at 35% probability and non-positive definite atoms are shown as spheres; all other thermal ellipsoids are set at 50% probability.

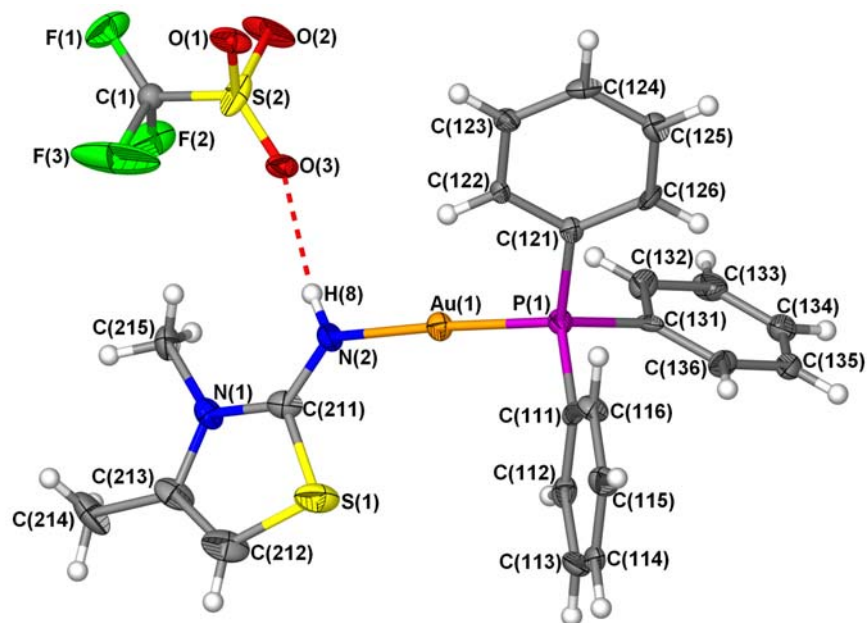


Figure 4.14 The molecular structure of only one of the unique molecules in the unit cell of **15** showing the numbering scheme. Thermal ellipsoids are set at 50% probability.

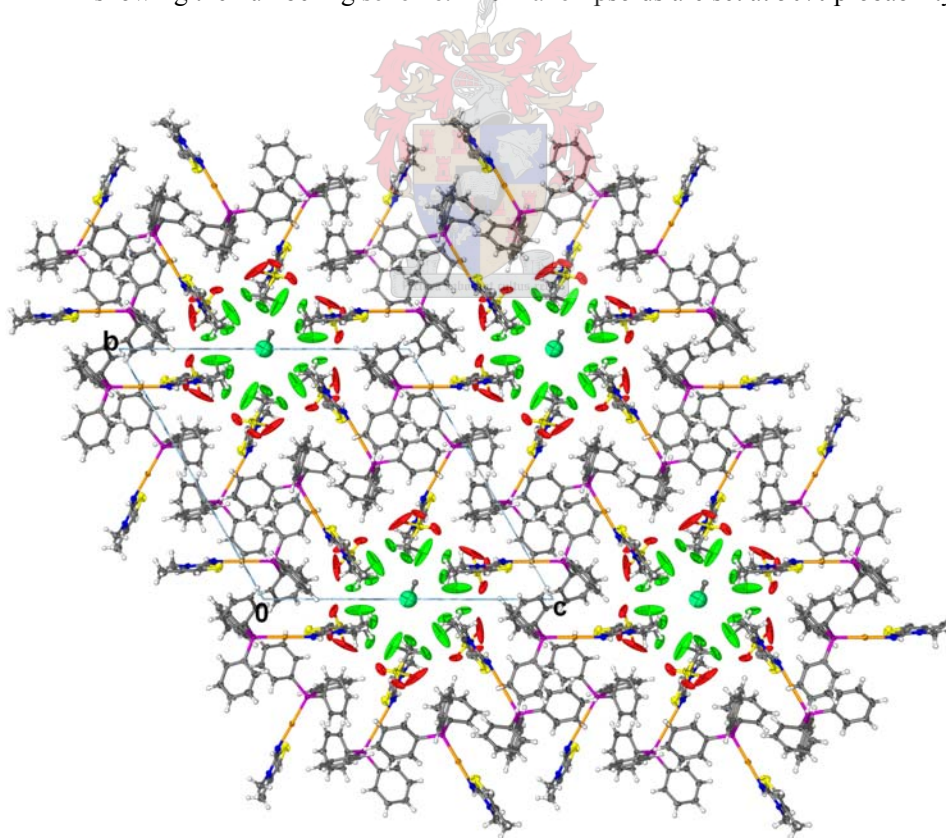


Figure 4.15 Diagram showing the flower-like molecular packing of **15** viewed along the a-axis; all non-positive definite atoms are shown as spheres.

Table 4.17 Selected bond lengths (Å) and angles (°) of only one of the unique molecules in the asymmetric unit of **15** with estimated standard deviations in parenthesis.

<i>Bond lengths (Å)</i>			
Au(1)–P(1)	2.233(2)	N(1)–C(215)	1.45(1)
Au(1)–N(2)	2.031(7)	C(213)–C(214)	1.49(1)
N(1)–C(211)	1.35(1)	C(212)–C(213)	1.34(1)
N(2)–C(211)	1.30(1)	P(1)–C(111)	1.809(8)
S(1)–C(211)	1.732(9)	P(1)–C(121)	1.815(8)
N(1)–C(213)	1.41(1)	P(1)–C(131)	1.824(8)
S(1)–C(212)	1.72(1)		
<i>Bond angles (°)</i>			
N(2)–Au(1)–P(1)	177.2(2)	N(1)–C(213)–C(212)	111.6(9)
C(211)–N(2)–Au(1)	124.7(6)	S(1)–C(212)–C(213)	112.6(8)
N(1)–C(211)–N(2)	127.4(8)	C(111)–P(1)–Au(1)	111.2(3)
N(1)–C(211)–S(1)	110.2(7)	C(121)–P(1)–Au(1)	114.0(3)
N(2)–C(211)–S(1)	122.3(7)	C(131)–P(1)–Au(1)	112.2(3)
C(211)–N(1)–C(213)	114.7(8)	C(111)–P(1)–C(121)	107.7(4)
C(211)–S(1)–C(212)	91.0(5)	C(111)–P(1)–C(131)	104.3(4)
C(211)–N(1)–C(215)	120.6(8)	C(121)–P(1)–C(131)	106.9(4)

4.3 Conclusions

As an extension of the series of gold(I) complexes derived from ylideneamine-functionalised heterocyclic ligands discussed in Chapter 3, a further complement to this novel class of compound was presented. These lipophilic cationic compounds, which contain phosphine or NHC ancillary ligands, showed marked stability which rendered them potentially suitable for biological testing.

From NMR studies, especially from the ^{13}C NMR chemical shift of C^2 , it could be concluded that the benzimidazol-2-ylideneamine ligand allows more sufficient stabilisation of the charge on the complex through delocalisation over the N–C–N unit, than its thiazol-2-ylideneamine counterparts. This result was supported by the ^1H NMR observation that coordination of gold(I) centre to thiazol-2-ylideneamine ligands has a more pronounced effect on the NH chemical shifts, than coordination to benzimidazol-2-ylideneamine ligand. Such differences in behaviour can be explained in terms of anisotropic and hybridisation effects. Coordination of ligand **III** to an $\text{Au}(\text{PPh}_3)^+$ moiety resulted in a marked downfield shift of the N^1 and N^3 resonances in the ^{15}N NMR spectra of **8**.

From FT-IR spectroscopy it was evident that coordination of the ligands **III** – **V** to a $\text{Au}(\text{PPh}_3)^+$ entity results in increased electron delocalisation over the carbon-nitrogen bonds since $\nu(\text{=NH})$ absorption bands were observed at lower wavenumbers. Furthermore, from comparative studies it could be concluded that coordination of a 2-ylideneamine ligand to a neutral $\text{Au}(\text{C}_6\text{F}_5)$ entity has a more pronounced effect on the =NH and C=N stretching vibrations than coordination to a positively charged $\text{Au}(\text{PPh}_3)^+$ or $\text{Au}(\text{NHC})^+$ unit.

The FAB-MS spectra of all complexes displayed peaks that corresponded to the cation of the molecules and diagnostic fragmentation patterns confirmed all proposed structures.

A comprehensive structural comparison of the linear complexes **8** – **11** revealed classical bonding characteristics. The C=N and C-N bond lengths in complexes **8** – **11** are typical and reflect limited delocalisation over the N-C-N units in the solid state. An elongation of the Au-P bonds in complexes **8**, **9** and **15**, when the nitrate ligand is substituted for a 2-ylideneamine ligand, representing a labilising *trans* effect, was observed. In contrast, this effect was not noted where a NHC was employed as an ancillary ligand. The well-documented electronic similarities that exist between phosphine and NHC ligands were further substantiated by the negligible difference between the Au-N bonds of complexes **9** and **11**. From an evaluation of the Au-N bond lengths of compounds **8** – **11** and **5** – **7** it is evident that coordination of ligand **III** – **IV** to a cationic $\text{Au}(\text{PPh}_3)^+$ unit results in Au-N bond lengths comparable to those of the $\text{Au}(\text{C}_6\text{F}_5)$ coordinated complexes. In the molecular structures of complexes **8** – **11** and **15** the charges on the complexes are neutralised by anionic nitrate or triflate counterions which participate in the formation of hydrogen bonds between the imine hydrogen atoms and the oxygen atoms of the counterions.

Despite the acidic character indicated by both NMR and solid state analysis, deprotonation of both gold(I) coordinated and free ylideneamines proved less facile than that of the secondary amine functionalities in biguanide ligands. No unambiguous evidence for the deprotonation was observed but FAB-MS results warrant further investigation.

From cytotoxicity studies of complexes **9** – **11** and free ligands **III** – **V** in HeLa cells, it became clear that the anti-tumour potential of these complexes is limited. Complexation to

a gold(I) centre resulted in a significant increase in the cytotoxic potency of the free ligands.

4.4 Experimental

4.4.1 General procedures and instruments

All reactions were carried out under argon using standard Schlenk and vacuum-line techniques. All solvents were predried on ground KOH or molecular sieves and freshly distilled prior to use. Tetrahydrofuran (THF), *n*-hexane, *n*-pentane and diethyl ether were distilled under N₂ from sodium benzophenone ketyl, acetone from 3 Å molecular sieves, dichloromethane and methanol from CaH₂ and ethanol from magnesium. Guanidine hydrochloride, Ag₂O, AgNO₃ and KH were purchased from Fluka, and 1,1-dimethylbiguanidine hydrochloride from Aldrich. Literature methods were used to prepare [Au(Cl)(PPh₃)]²⁸ from [HAuCl₄]²⁹ and [Au(PPh₃)(NO₃)]³⁰ from [Au(Cl)(PPh₃)]. [Au(Cl)(SMe₂)] was prepared from [HAuCl₄] following the same method as reported in the literature for the preparation of [Au(Cl)(tbt)].³¹ Literature procedures were employed to prepare [Au(NO₃)(1,3-^tBuIm-2-ylidene)]²⁰ from 1,3-^tBuIm.^{32,33}

Melting points were determined on a Stuart SMP3 apparatus and are uncorrected. Mass spectra were recorded on a VG 70 SEQ (FAB, 70 eV) instrument. NMR spectra were recorded on a Varian 300/400 FT or INOVA 600 MHz spectrometer (¹H NMR at 300/400/600 MHz, ¹³C NMR at 75/100/150 MHz, ¹⁵N NMR at 60.8 MHz and ³¹P NMR at 121/161 MHz) with chemical shifts reported relative to the solvent resonance or external reference of 85 % H₃PO₄ (³¹P) or NH₃NO₂ (¹⁵N). Infrared spectra were recorded on a Thermo Nicolet Avatar 330FT-IR with Smart OMNI ATR (attenuated total reflectance) sampler. Elemental analysis was carried out at the School of Chemistry, University of the Witwatersrand. For elemental analysis, products were evacuated under high vacuum for

²⁸ M. I. Bruce, B. K. Nicholson, O. Bin Shawkataly, *Inorg. Synth.* **1989**, 324.

²⁹ A. Haas, J. Helmbrecht, U. Nieman in *Handbuch der Präparativen Anorganischen Chemie*, Vol 2 (Ed. G. Brauer) 3rd edition, Ferdinand Enke, Stuttgart, **1978**, p1014.

³⁰ L. Malatesta, L. Naldini, G. Simonetta, F. Cariati, *Coord. Chem. Rev.* **1966**, 1, 255-262.

³¹ R. Usò and A. Laguna in: *Organometallic Synthesis*, Vol 3 (Eds. R. B. Lang, J. J. Eisch) Elsevier, Amsterdam, **1986**, p325.

³² W. A. Hermann, V. P. W. Bohm, C. W. K. Gstottmayr, M. Grosche, C.P. Reisinger, T. Weskamp, *J. Organomet. Chem.* **2001**, 617-618, 616-628.

³³ W. A. Hermann, L. J. Goossen, C. Koecher, G. R. J. Artus, *Angew. Chem. Int. Ed. Engl.* **1996**, 35, 2805-2807.

10h. Cytotoxicity assays were performed by Margo Nell at the Department of Pharmacology at the University of Pretoria.

4.4.2 Preparations and procedures

4.4.2.1 Preparation of 1,3-dimethyl-1,3-dihydro-benzimidazol-2-ylideneamine-(triphenylphosphine)gold(I) nitrate, 8

A suspension of [Au(NO₃)(PPh₃)] (0.45 g, 0.81 mmol) in ether (10 ml) was added to a stirring solution of **III** (0.13 g, 0.83 mmol) in ether (20 ml). The reaction mixture was allowed to stir for three days at room temperature. During this period, the light yellow solution had become colourless and a new suspension formed. The mixture was filtered, the remaining solid washed with ether (2 × 20 ml), extracted with CH₂Cl₂ and reduced to dryness *in vacuo* to yield the pure product as a colourless solid (0.49 g, 87.9 %).

4.4.2.2 Preparation of 3-methyl-3H-benzothiazol-2-ylideneamine(triphenylphosphine)gold(I) nitrate, 9

A suspension of [Au(NO₃)(PPh₃)] (0.45 g, 0.81 mmol) in ether (10 ml) was added to a stirring solution of **IV** (0.14 g, 0.82 mmol) in ether (20 ml). The reaction mixture was allowed to stir for three days at room temperature. During this period, the yellow solution had become colourless and a new suspension was visible. The mixture was filtered, the remaining solid washed with ether (2 × 20 ml) and dried *in vacuo* to yield the pure product as a colourless solid (0.50 g, 89 %).

4.4.2.3 Preparation of 3,4-dimethyl-3H-thiazol-2-ylideneamine(triphenylphosphine)gold(I) nitrate, 10

A suspension of [Au(NO₃)(PPh₃)] (0.36 g, 0.69 mmol) in ether (10 ml) was added to a stirring solution of **V** (0.09 g, 0.69 mmol) in ether (10 ml). The reaction mixture was allowed to stir for two days at room temperature. During this period, the yellow solution had become colourless and a new suspension formed. The mixture was filtered, the remaining solid washed with ether (2 × 20 ml) and dried *in vacuo* to yield the pure product as a colourless solid (0.38 g, 84 %).³⁴

³⁴ Note: Product undergoes a colour change when dissolved in chlorinated solvents. It may be sensitive towards oxidation, see H. H. Murray, J. P. Fackler, Jr., *Inorg. Chim. Acta* **1986**, *115*, 207-209.

4.4.2.4 Preparation of 1,3-dimethyl-1,3-dihydro-benzimidazol-2-ylideneamine-(1,3-di-tert-butylimidazol-2-ylidene)gold(I) nitrate, 11

A solution of $[\text{Au}(\text{NO}_3)(1,3\text{-}^t\text{BuIm-2-ylidene})]$ (0.17 g, 0.39 mmol) in THF (10 ml) was added to a stirring solution of **III** (0.06 g, 0.39 mmol) in THF (20 ml). Upon addition a white suspension formed. The mixture was allowed to stir overnight at room temperature. The brownish solution was stripped of solvent *in vacuo* and the remaining residue was extracted with CH_2Cl_2 , filtered through MgSO_4 and reduced to dryness to yield the product as an off-white solid (0.23 g, 96 %).

4.4.2.5 Preparation of 1,1-dimethylbiguanidinebis[(triphenylphosphine)gold(I)], 12

Powdered KOH (0.08 g, 1.50 mmol) was added to a stirring solution of 1,1-dimethylbiguanidine hydrochloride (0.08 g, 0.50 mmol) in methanol (30 ml) at room temperature. After a 2h stirring period, a solution of $[\text{Au}(\text{Cl})(\text{PPh}_3)]$ (0.50 g, 1.00 mmol) in THF (15 ml) was added to the reaction mixture. Upon the addition, $[\text{Au}(\text{Cl})(\text{PPh}_3)]$ precipitated from the solution. The suspension was decreased by the addition of more THF. The colourless mixture was allowed to stir for 7 days after which the mixture was reduced to dryness, extracted with THF and filtered through Na_2SO_4 to achieve a light yellow solution. The solvent was removed *in vacuo* and the remaining residue was washed with ether (2×20 ml) to afford the pure product as an off-white solid (0.50 g, 95 %).

4.4.2.6 Preparation of guanidine(triphenylphosphine)gold(I), 13

Powdered KOH (0.07 g, 1.19 mmol) was added to a stirring solution of guanidine hydrochloride (0.06 g, 0.60 mmol) in methanol (30 ml) at room temperature. After a 2h stirring period, a solution of $[\text{Au}(\text{Cl})(\text{PPh}_3)]$ (0.30 g, 0.60 mmol) in THF (30 ml) was added to the reaction mixture. The colourless mixture was allowed to stir for 7 days after which the mixture was reduced to dryness to yield an oily off-white residue. The residue was washed with THF (30 ml) and the remaining solid was dried *in vacuo* to afford the product as a colourless solid (0.28 g, 91 %).

4.4.2.7 Preparation of 1,1-dimethylbiguanidine[1,2-bis(diphenylphosphino)ethane]digold(I), **14**

Powdered KOH (0.08 g, 1.50 mmol) was added to a stirring solution of 1,1-dimethylbiguanidine hydrochloride (0.08 g, 0.50 mmol) in methanol (30 ml) at room temperature. After a 2h stirring period, a suspension of $[\text{Au}_2(\text{Ph}_2\text{PCH}_2\text{CH}_2\text{PPh}_2)\text{Cl}_2]$ (0.50 g, 1.0 mmol) in THF (15 ml) was added to the reaction mixture. After 7 days of stirring, the mixture was reduced to dryness, extracted with CH_2Cl_2 and filtered through Na_2SO_4 to achieve a colourless solution. The solvent was removed *in vacuo* and the remaining residue was washed with ether (2×20 ml) to afford the pure product as an off-white solid (0.27 g, 59 %).

4.4.3 X-ray structure determinations

Crystal data collection and refinement details of compounds **8**, **8b**, **9**, **11** and **15** are summarised in Tables 4.18 - 4.20. Data sets were collected on a Bruker SMART Apex CCD diffractometer with graphite monochromated $\text{MoK}\alpha$ radiation ($\lambda = 0.71073 \text{ \AA}$).³⁵ Data reduction was carried out with standard methods using the software package Bruker SAINT and data were treated with SADABS.^{36,37,38} All the structures were solved using direct methods or interpretation of a Patterson synthesis, which yielded the position of the metal atoms, and conventional difference Fourier methods. All non-hydrogen atoms were refined anisotropically by full-matrix least squares calculations on F^2 using SHELX-97³⁹ within an X-seed environment.^{40,41} The hydrogen atoms were fixed in calculated positions. Figures were generated with X-seed⁴⁰ and POV Ray for Windows, with the displacement ellipsoids at 50% probability level unless stated otherwise. Further information is available from Dr. S. Cronje at the Department of Chemistry and Polymer Science, Stellenbosch University.

³⁵ SMART Data Collection Software (version 5.629), Bruker AXS Inc. (Madison), WI, **2003**.

³⁶ SAINT, Data Reduction Software (version 6.45), Bruker AXS Inc. (Madison), WI, **2003**.

³⁷ R. H. Blessing, *Acta Crystallogr., Sect. A*, **1995**, *51*, 33-38.

³⁸ SADABS (version 2.05), Bruker AXS Inc. (Madison), WI, **2002**.

³⁹ G. M. Shelrick, SHELX-97. Program for Crystal Structure Analysis, University of Göttingen (Germany), **1997**.

⁴⁰ L. J. Barbour, *J. Supramol. Chem.* **2003**, *1*, 189-191.

⁴¹ J. L. Atwood, L. J. Barbour, *Cryst. Growth Des.* **2003**, *3*, 3-8.

Table 4.18 Crystallographic data of compounds **8a** and **8b**.

	8a	8b
Empirical formula	[C ₂₇ H ₂₆ AuN ₄ O ₃ P]·2[C ₃ H ₆ O]	C ₂₇ H ₂₆ AuN ₄ O ₃ P
<i>M_r</i>	798.61	682.45
Temp. (K)	100 (2)	100(2)
Wavelength (Å)	0.71073	0.71073
Crystal system	Triclinic	Monoclinic
Crystal dimensions (mm)	0.05 × 0.05 × 0.03	0.15 × 0.07 × 0.05
Crystal shape and colour	cube, colourless	rectangles, colourless
Space group	<i>P</i> $\bar{1}$ (No. 2)	<i>P</i> 2 ₁ / <i>c</i> (No. 14)
<i>a</i> (Å)	9.043(3)	9.322(2)
<i>b</i> (Å)	14.043(4)	15.499(3)
<i>c</i> (Å)	14.902(4)	17.446(3)
α (°)	63.333(4)	90
β (°)	85.257(4)	96.825(3)
γ (°)	84.437(4)	90
Volume (Å ³)	1681.5(8)	2502.7(8)
<i>Z</i>	2	4
<i>d</i> _{calcd} (g/cm ³)	1.577	1.811
μ (Mo–K α) (mm ⁻¹)	4.467	5.979
Absorption correction	Semi-empirical from equivalents (SADABS)	Semi-empirical from equivalents (SADABS)
F(000)	796	1336
θ -range for data collection (°)	1.63 to 28.32	1.76 to 26.40
Index range	-12 ≤ <i>h</i> ≤ 11, -17 ≤ <i>k</i> ≤ 17, -19 ≤ <i>l</i> ≤ 19	-9 ≤ <i>h</i> ≤ 11, -19 ≤ <i>k</i> ≤ 19, -20 ≤ <i>l</i> ≤ 21
No. of reflections collected	18792	13611
No. of unique reflections	7601 (<i>R</i> _{int} = 0.0876)	4950 (<i>R</i> _{int} = 0.0269)
Max. and min. transmission	0.875 and 0.795	0.7542 and 0.4674
Refinement parameters / restraints	403 / 0	327 / 0
Goodness of fit on <i>F</i> ²	1.138	1.092
Final <i>R</i> -indices [<i>I</i> > 2 σ (>(<i>I</i>))]	<i>R</i> ₁ = 0.0867 <i>wR</i> ₂ = 0.1696	<i>R</i> ₁ = 0.0256 <i>wR</i> ₂ = 0.0576
<i>R</i> indices (all data)	<i>R</i> ₁ = 0.1189 <i>wR</i> ₂ = 0.1823	<i>R</i> ₁ = 0.0335 <i>wR</i> ₂ = 0.0623
Largest diff. peak and hole (e·Å ⁻³)	5.496 and -3.854	1.557 and -0.567
Weighing scheme ^a	<i>a</i> = 0.0830 / <i>b</i> = 0	<i>a</i> = 0.0303 / <i>b</i> = 0.4643

^a $wR_2 = \{\sum[w(F_o^2 - F_c^2)^2] / \sum[w(F_o^2)^2]\}^{1/2}$; $w = 1/[\sigma^2(F_o^2) + (aP)^2 + bP + d + e \sin \theta]$; $P = [f(\text{Max}(0 \text{ or } F_o^2)) + (1-f) F_c^2]$

Table 4.19 Crystallographic data of compounds **9** and **11**.

	9	11
Empirical formula	0.50[C ₂₆ H ₂₃ Au ₁ N ₃ O ₃ P ₁ S ₁]	[C ₂₀ H ₃₁ AuN ₆ O ₃]·0.50[CH ₂ Cl ₂]
<i>M</i> _r	342.74	642.93
Temp. (K)	100 (2)	100 (2)
Wavelength (Å)	0.71073	0.71073
Crystal system	Triclinic	Triclinic
Crystal dimensions (mm)	0.10 × 0.07 × 0.02	0.07 × 0.07 × 0.05
Crystal shape and colour	needle, colourless	cubes, colourless
Space group	<i>P</i> $\bar{1}$ (No. 2)	<i>P</i> $\bar{1}$ (No. 2)
a (Å)	8.1497(7)	9.109(1)
b (Å)	9.462(1)	10.968(2)
c (Å)	17.913(2)	12.293(2)
α (°)	86.292(2)	86.931(2)
β (°)	80.051(2)	85.686(2)
γ (°)	64.497(2)	82.015(2)
Volume (Å ³)	1227.9(2)	1211.6(3)
Z	4	2
<i>d</i> _{calcd} (g/cm ³)	1.854	1.760
μ (Mo–Kα) (mm ⁻¹)	6.175	6.215
Absorption correction	Semi-empirical from equivalents (SADABS)	Semi-empirical from equivalents (SADABS)
F(000)	668	632
θ-range for data collection (°)	2.31 to 25.71	1.66 to 26.40
Index range	-9 ≤ h ≤ 9, -11 ≤ k ≤ 11, -21 ≤ l ≤ 21	-11 ≤ h ≤ 11, -13 ≤ k ≤ 13, -15 ≤ l ≤ 15
No. of reflections collected	11163	12698
No. of unique reflections	4614 (R _{int} = 0.0505)	4930 (R _{int} = 0.0294)
Max. and min. transmission	0.884 and 0.603	0.733 and 0.639
Refinement parameters / restraints	317 / 0	301 / 0
Goodness of fit on F ²	1.036	1.111
Final R-indices [I > 2σ >(I)]	R ₁ = 0.0445 wR ₂ = 0.0839	R ₁ = 0.0275 wR ₂ = 0.0675
R indices (all data)	R ₁ = 0.0574 wR ₂ = 0.0897	R ₁ = 0.0285 wR ₂ = 0.0681
Largest diff. peak and hole (e.Å ⁻³)	1.418 and -0.897	2.297 and -1.135
Weighing scheme ^a	a = 0.0402 / b = 0	a = 0.0335 / b = 2.1327

^a $wR_2 = \{\sum[w(F_o^2 - F_c^2)^2] / \sum[w(F_o^2)^2]\}^{1/2}$; $w = 1/[\sigma^2(F_o^2) + (aP)^2 + bP + d + e \sin \theta]$; $P = [f(\text{Max}(0 \text{ or } F_o^2)) + (1-f) F_c^2]$

Table 4.20 Crystallographic data of compound **15**.

	15
Empirical formula	C ₇₃ H ₆₉ Au ₃ ClF ₉ N ₆ O ₉ P ₃ S ₆
<i>M_r</i>	2256.96
Temp. (K)	100 (2)
Wavelength (Å)	0.71073
Crystal system	Triclinic
Crystal dimensions (mm)	0.14 × 0.09 × 0.05
Crystal shape and colour	rectangles, colourless
Space group	<i>P</i> $\bar{1}$ (No. 2)
<i>a</i> (Å)	11.178(1)
<i>b</i> (Å)	20.713(2)
<i>c</i> (Å)	20.733(2)
α (°)	116.694(2)
β (°)	100.345(2)
γ (°)	100.324(2)
Volume (Å ³)	4030.2
<i>Z</i>	2
<i>d</i> _{calcd} (g/cm ³)	1.860
μ (Mo–K α) (mm ⁻¹)	5.774
Absorption correction	Semi-empirical from equivalents (SADABS)
F(000)	2194
θ -range for data collection (°)	1.94 to 25.74
Index range	-13 ≤ <i>h</i> ≤ 13, -19 ≤ <i>k</i> ≤ 25, -25 ≤ <i>l</i> ≤ 25
No. of reflections collected	22204
No. of unique reflections	14984 (<i>R</i> _{int} = 0.0333)
Max. and min. transmission	0.7611 and 0.4986
Refinement parameters / restraints	997 / 0
Goodness of fit on <i>F</i> ²	1.012
Final <i>R</i> -indices [<i>I</i> > 2 σ (>(<i>I</i>))]	<i>R</i> ₁ = 0.0496 <i>wR</i> ₂ = 0.1037
<i>R</i> indices (all data)	<i>R</i> ₁ = 0.0798 <i>wR</i> ₂ = 0.1156
Largest diff. peak and hole (e.Å ⁻³)	1.722 and -1.469
Weighing scheme ^a	<i>a</i> = 0.0558 / <i>b</i> = 0.4408

$$^a wR_2 = \{ \Sigma [w(F_o^2 - F_c^2)^2] / \Sigma [w(F_o^2)^2] \}^{1/2}; w = 1 / [\sigma^2(F_o^2) + (aP)^2 + bP + d + e \sin \theta];$$

$$P = [f(\text{Max}(0 \text{ or } F_o^2))] + (1-f) F_c^2$$